Order Number 9015522

A study of the transient behavior during start-up of residential heat pumps

Katipamula, Srinivas, Ph.D.

Texas A&M University, 1989

U·M·I
300 N. Zeeb Rd.
Ann Arbor, MI 48106

A STUDY OF THE TRANSIENT BEHAVIOR DURING START-UP OF RESIDENTIAL HEAT PUMPS

A Dissertation

by

SRINIVAS KATIPAMULA

Submitted to Office of the Graduate College of
Texas A&M University
in partial fulfillment of the requirements for the degree of

DOCTOR OF PHILOSOPHY

December 1989

Major Subject: Mechanical Engineering

A STUDY OF THE TRANSIENT BEHAVIOR DURING

START-UP OF RESIDENTIAL HEAT PUMPS

A Dissertation

by

SRINIVAS KATIPAMULA

Approved as to style and content by:

D.L. O'Neal
(Chair of Committee)

W.D. Turner
(Member)

S. Somasundaram
(Member)

B.A. Stout
(Member)

for W.L. Bradley
(Head of Department)

December 1989

ABSTRACT

A Study of Transient Behavior During
Start-Up of Residential Heat Pumps. (December 1989)
Srinivas Katipamula, B.S., Osmania University
M.S., Texas A&M University
Chairman of Advisory Committee: D.L. O'Neal

An experimental and analytical study concerned with the transient performance of heat pumps is presented. A series of tests were performed to study and characterize the transient sensible and dehumidification performance of a heat pump in the cooling mode. All the tests were conducted according to the ASHRAE Standard [1983]. The effects of indoor dry-bulb temperature (72 to 80 F), indoor relative humidity (20 to 67%), outdoor dry-bulb temperature (82 to 100 F), cycling rate (0.8 to 10 cph) and percent ON-time (20 to 95%) on the transient performance (sensible and latent capacity, efficiency and sensible heat ratio) are addressed in this study. The results indicated that part load factor (PLF) can be as low as 0.65 at low percent ON-times and high cycling rates. The combination of low percent ON-times and high cycling rates produced maximum cyclic losses. The dehumidification process usually started between 60 to 150 seconds after start-up depending on the indoor ambient conditions, percent ON-time and cycling rate. The sensible and latent capacity response and part load efficiency of the heat pump increased with an increase in indoor relative humidity. There was a slight increase in PLF with indoor dry-bulb temperature. The outdoor dry-bulb temperature did not have any effect on the transient performance. Based on the functional relationship of PLF and coefficient of degradation (C_D) with the five independent variables a

multiple linear regression analysis was performed on the experimental data. The analysis yielded two general equations to predict PLF and C_D.

A lumped parameter heat pump transient analysis computer model was developed, which drew upon methodologies from the earlier models by Chi and Didion [1982] and Oak Ridge National Laboratory [1981]. The model was capable of simulating the transient response of a vapor compression air-to-air heat pump commonly used in residential applications. The simulated results were in good agreement with the laboratory results at high percent ON-times (> 20) and high relative humidities (> 45).

ACKNOWLEDGMENTS

I gratefully acknowledge Dr. D.L. O'Neal for his outstanding guidance, invaluable help and encouragement during the course of this study.

I thank Dr. S. Somasundaram, and Dr. W.D. Turner for their constant support, encouragement and helpful suggestions. I also want to thank Dr. B.A. Stout for serving on my committee and Dr. D.R. Anderson for being my graduate council representative. I would like to acknowledge the partial financial support provided by the Center for Energy and Mineral Research.

I would like to thank my fellow graduate students Steve and Kurt for doing a wonderful job in constructing and instrumenting the test heat pump. I appreciate the help given by Ray, Frank and Chris, technicians at the Energy Systems Lab, in the Department of Mechanical Engineering. I would also thank all those who have given me intangible help during my stay here at Texas A&M Unversity.

Finally, I would like to express special thanks to my parents for their understanding and constant encouragement during the course of my graduate studies.

DEDICATION

To My Dear Parents

TABLE OF CONTENTS

CHAPTER		Page
I	INTRODUCTION	1
II	LITERATURE REVIEW	8
	FIELD MEASUREMENTS	8
	LABORATORY MEASUREMENTS OF TRANSIENT RESPONSE	10
	STUDY OF REFRIGERANT DYNAMICS	12
	MODELING OF TRANSIENT BEHAVIOR IN HEAT PUMPS	14
	SUMMARY OF LITERATURE REVIEW	20
III	TEST FACILITY	22
	PSYCHROMETRIC ROOMS	22
	TEST HEAT PUMP	23
	HEAT EXCHANGER TEST SECTIONS	33
	DATA ACQUISITION AND REDUCTION	36
IV	MODEL DEVELOPMENT	37
	MOTOR/SHAFT/COMPRESSOR	38
	HEAT EXCHANGER MODULES	41
	EXPANSION DEVICE	57
	MODELING METHODOLOGY	59
	SUMMARY OF MODIFICATIONS TO TRPUMP MODEL	66
V	EXPERIMENTAL METHODOLOGY	67
	TESTING PROCEDURE	67
	EXPERIMENTAL TESTS	70
	DEFINITION OF TERMINOLOGY	75

TABLE OF CONTENTS (Continued)

CHAPTER		Page
VI	BASE-CASE STEADY-STATE AND CYCLIC TESTS	78
	STEADY-STATE TEST RESULTS	78
	CHARACTERISTICS OF TRANSIENT RESPONSE	80
VII	EXPERIMENTAL RESULTS	91
	EFFECTS OF CYCLING RATE AND PERCENT ON-TIME ON CYCLIC LOSSES	93
	EFFECTS OF INDOOR HUMIDITY ON CYCLIC LOSSES	102
	EFFECTS OF INDOOR ROOM DRY-BULB TEMPERATURE ON CYCLIC LOSSES	111
	EFFECTS OF OUTDOOR DRY-BULB TEMPERATURE ON CYCLIC LOSSES	117
	DEVELOPMENT OF A GENERAL EQUATION TO ESTIMATE PLF AND C_D	121
	SUMMARY OF TRANSIENT BEHAVIOR	133
VIII	MODEL RESULTS	137
	SIMULATION OF TRANSIENT CHARACTERISTICS	137
	COMPARISON OF RESULTS AT VARIOUS INDOOR RELATIVE HUMIDITIES	142
	COMPARISON OF RESULTS AT VARIOUS INDOOR DRY-BULB TEMPERATURES	146
	COMPARISON OF RESULTS AT VARIOUS OUTDOOR DRY-BULB TEMPERATURES	152
	SUMMARY OF COMPARISON OF SIMULATED RESULTS WITH MEASURED RESULTS	152
IX	CONCLUSIONS AND RECOMMENDATIONS	156
	CONCLUSIONS	156
	RECOMMENDATIONS	158

TABLE OF CONTENTS (Continued)

CHAPTER Page

REFERENCES 161

APPENDIX A 166

APPENDIX B 171

APPENDIX C 174

VITA 175

LIST OF TABLES

Table		Page
3.1	Characteristics of the Cooling Mode Thermostatic Expansion Valve.	27
3.2	Description of Test Points Used in the Heat Pump Set-Up.	30
5.1	Tests with Varying Percent ON-Times and Cycling Rates.	71
5.2	Test with Varying Indoor Relative Humidity.	72
5.3	Tests with Varying Indoor Dry-Bulb Temperature and Constant Indoor Relative Humidity.	73
5.4	Tests with Varying Indoor Dry-Bulb Temperature and Constant Indoor Dew-Point Temperature.	73
5.5	Tests with Varying Outdoor Dry-Bulb Temperature.	75
6.1	Average Performance Characteristics for Base-Case Steady-State Test A.	80
6.2	Integrated Average Room Conditions for the Typical Cyclic Test.	82
6.3	Cyclic Performance Characteristics for T9M10.	90
6.4	Deviation of Cyclic Performance From the Steady-State.	90
7.1	Time Constants at Various Indoor Temperatures.	117
7.2	Percent ON-Times and Cycling Rates at a Given Outdoor Dry-Bulb Temperature.	120
7.3	Summary of Statistical Analysis.	130
8.1	Affect of Time-Step on Selected Variables.	138
8.2	Initial Temperatures for Selected Components.	139

LIST OF FIGURES

Figure		Page
1.1	Schematic of a Split System Heat Pump. (Arrows indicate flow path for heating application)	2
1.2	Typical Transient Capacity Response: (Mulroy and Didion, [1985])	5
2.1	Part-Load Cooling Performance Results: (Parken, et al., 1977)	11
2.2	Part-Load Heating Performance Results: (Parken, et al., 1977; Miller, 1985)	13
3.1	Schematic of Psychrometric Rooms	24
3.2	Schematic of Outdoor Coil Refrigerant Circuit	26
3.3	Heat Pump System Schematic	29
3.4	Refrigerant Line Temperature Probe	31
3.5	Schematic of Indoor Test Section Set-Up	34
4.1	Tube-and-Fin Heat Exchanger	42
4.2	Schematic of Computational Sequence	60
4.3	Flow Chart of the Heat Exchanger Module	63
4.4	Flow Chart of the Refrigerant-Side Heat Transfer	64
5.1	Typical Residential Thermostat Cycling Rate (NEMA)	74
5.2	Heat Pump Cycling Rate and Outdoor Temperature vs Percent ON-Time	74
6.1	Psychrometric Room Characteristics for a Steady-State Test	79
6.2	Comparison of Air-Side and Refrigerant-Side Capacities	79
6.3	Psychrometric Room Characterisitics for a Cyclic Test	81
6.4	Compressor Suction and Discharge Pressure and Temperature	81
6.5	Sensible Capacity and Moisture Removal Across the Evaporator Coil	83
6.6	Accumulator and Compressor Surface Temperatures	83

LIST OF FIGURES (Continued)

Figure		Page
6.7	Refrigerant Mass Flow Rate and Power Consumption.	85
6.8	Air-Side Sensible, Latent, and Total Capacities.	85
6.9	Air-Side Sensible, Latent and Total Capacities 0–70 Minutes.	86
6.10	Evaporator Exit, Compressor Suction and Saturation Temperatures.	86
6.11	Superheating and Sub-Cooling Characteristics.	89
6.12	Pressure Drop Across the Expansion Device and Pressure Loss in Evaporator and Condenser Coils.	89
7.1	Change in Part Load Factor with Cooling Load Factor for Various Cycling Rates and Percent ON-Times.	94
7.2	Change in Part Load Factor with Cooling Load Factor for Constant Cycling Rate.	94
7.3	Change of Normalized Sensible and Latent Capacities at Various Cycling Rates and Percent ON-Times.	96
7.4	Loss in Cooling Capacity at Various Cycling Rates.	96
7.5	Change in Normalized Energy Consumption with CLF at Various Cycling Rates and Percent ON-Times.	98
7.6	Change in Coefficient of Degradation at Various Cycling Rates and Percent ON-Times.	98
7.7	Relationship Between (1 - PLF) and (1 - CLF) with Percent ON-Time.	99
7.8	Constant Coefficient of Degradation Curves at Various Cycling Rates and CLFs.	99
7.9	Constant Coefficient of Degradation Curves at Various Cycling Rates and PLFs.	101
7.10	Change in Cyclic EER with Unit Run Time for Three Different Percent ON-Times.	101
7.11	Response of Cyclic Sensible Capacity at Various Indoor Relative Humidities (80% ON-Time).	103
7.12	Response of Moisture Removal Across the Evaporator Coil at Various Indoor Relative Humidities (80% ON-Time).	103

LIST OF FIGURES (Continued)

Figure		Page
7.13	Response of Cyclic Sensible Capacity at Various Indoor Relative Humidities (20% ON-Time).	105
7.14	Response of Moisture Removal Across the Evaporator Coil at Various Indoor Relative Humidities (20% ON-Time).	105
7.15	Change in Cyclic Sensible Capacity with Indoor Relative Humidity.	106
7.16	Change in Cyclic Latent Capacity with Indoor Relative Humidity.	106
7.17	Change in Part Load Factor with Indoor Relative Humidity.	108
7.18	Change of Coefficient of Degradation with Indoor Relative Humidity.	108
7.19	Change in PLF with CLF for Various Indoor Relative Humidities and Percent ON-Times.	109
7.20	Change in Cyclic Sensible Capacity with CLF at Various Indoor Relative Humidities.	109
7.21	Change in Normalized Latent Capacity with CLF at Various Indoor Relative Humidities.	110
7.22	Change in Coefficient of Degradation with CLF at Various Indoor Relative Humidities.	110
7.23	Response of Cyclic Sensible Capacity at Various Indoor Temperatures and Constant Relative Humidity (50% ON-Time).	112
7.24	Response of Moisture Removal Rate at Various Indoor Temperatures and Constant Relative Humidity (50% ON-Time).	112
7.25	Change in Normalized Sensible Capacity with Indoor Dry-Bulb Temperature and Constant Indoor Relative Humidity.	114
7.26	Change in Normalized Latent Capacity with Indoor Dry-Bulb Temperature and Constant Indoor Relative Humidity.	114
7.27	Change in Part Load Factor with Indoor Dry-Bulb Temperature and Constant Indoor Relative Humidity.	115
7.28	Change in Coefficient of Degradation with Indoor Dry-Bulb Temperature and Constant Indoor Relative Humidity.	115
7.29	Change in Normalized Sensible Capacity with Indoor Dry-Bulb Temperature and Constant Indoor Dew-Point Temperature.	118
7.30	Change in Normalized Latent Capacity with Indoor Dry-Bulb Temperature and Constant Indoor Dew-Point Temperature.	118

LIST OF FIGURES (Continued)

Figure		Page
7.31	Change in Part Load Factor with Indoor Dry-Bulb Temperature at Constant Dew-Point Temperature. . . .	119
7.32	Change in Coefficient of Degradation with Indoor Dry-Bulb Temperature at Constant Dew-Point Temperature. . . .	119
7.33	Response of Cyclic Sensible Capacity at Various Outdoor Dry-Bulb Temperatures.	122
7.34	Response of Moisture Removal Across the Evaporator Coil at Various Outdoor Dry-Bulb Temperatures. . .	122
7.35	Change in Normalized Sensible Capacity with Outdoor Dry-Bulb Temperature.	123
7.36	Change in Normalized Latent Capacity with Outdoor Dry-Bulb Temperature.	123
7.37	Change in Part Load Factor with Outdoor Dry-Bulb Temperature.	124
7.38	Change in Coefficient of Degradation with Outdoor Dry-Bulb Temperature.	124
7.39	Change in (1-PLF) and (1-CLF) with Outdoor Dry-Bulb Temperature.	125
7.40	Relationship of PLF with Percent ON-Time.	125
7.41	PLF vs Percent ON-Time at Various Cycling Rate and Constant Indoor and Outdoor Conditions.	127
7.42	Relationship of PLF with Cycling Rate at Constant Indoor and Outdoor Conditions.	127
7.43	Measured vs Predicted Part Load Factor.	129
7.44	Measured vs Predicted Coefficient of Degradation.	129
8.1	Comparison of Compressor Suction and Discharge Pressure.	140
8.2	Comparison of Compressor Suction and Discharge Temperature.	140
8.3	Comparison of Refrigerant Mass Flow Rate and Power Consumption.	141
8.4	Comparison of Air-Side Latent, Sensible, and Total Capacities.	141

LIST OF FIGURES (Continued)

Figure		Page
8.5	Comparison of Cyclic Sensible and Latent Response at 20 % Indoor Relative Humidity and 20 Percent ON-Time. . . .	143
8.6	Comparison of Cyclic Sensible and Latent Response at 67 % Indoor Relative Humidity and 20 Percent ON-Time. . . .	143
8.7	Comparison of Normalized Sensible and Latent Capacities at Various Indoor Relative Humidities and 80 Percent ON-Time. . .	144
8.8	Comparison of Normalized Sensible and Latent Capacities at Various Indoor Relative Humidities and 20 Percent ON-Time. . .	144
8.9	Comparison of Part Load Factors at Various Indoor Relative Humidities and 80 Percent ON-Time.	145
8.10	Comparison of Part Load Factors at Various Indoor Relative Humidities and 20 Percent ON-Time.	145
8.11	Comparison of Cyclic Sensible and Latent Response at 80 F Indoor Dry-Bulb Temperature and 80 Percent ON-Time. . .	147
8.12	Comparison of Cyclic Sensible and Latent Response at 76 F Indoor Dry-Bulb Temperature and 80 Percent ON-Time. . .	147
8.13	Comparison of Normalized Sensible and Latent Capacities at Various Indoor Temperatures, 50 % Rh and 80 Percent ON-Time.	148
8.14	Comparison of Normalized Sensible and Latent Capacities at Various Indoor Temperatures, 50 % Rh and 50 Percent ON-Time.	148
8.15	Comparison of Part Load Factors at Various Indoor Dry-Bulb Temperatures, 50 % Rh and 80 Percent ON-Time. . .	149
8.16	Comparison of Part Load Factors at Various Indoor Dry-Bulb Temperatures, 50 % Rh and 20 Percent ON-Time. . .	149
8.17	Comparison of Cyclic Sensible and Latent Response at 78 F Indoor Dry-Bulb Temperature and 80 Percent ON-Time.	150
8.18	Comparison of Cyclic Sensible and Latent Response at 72 F Indoor Dry-Bulb Temperature and 80 Percent ON-Time.	150
8.19	Comparison of Normalized Sensible and Latent Capacities at Various Indoor Temperatures, 58 F Dew-Point and 80 % ON-Time.	151
8.20	Comparison of Normalized Sensible and Latent Capacities at Various Indoor Temperatures, 58 F Dew-Point and 50 % ON-Time.	151
8.21	Comparison of Part Load Factors at Various Indoor Dry-Bulb Temperatures, 58 F Dew-Point and 80 Percent ON-Time.	153
8.22	Comparison of Part Load Factors at Various Indoor Dry-Bulb Temperatures, 58 F Dew-Point and 80 Percent ON-Time.	153

LIST OF FIGURES (Continued)

Figure		Page
8.23	Comparison of Normalized Sensible and Latent Capacities at Various Outdoor Dry-Bulb Temperatures.	154
8.24	Comparison of Part Load Factors at Various Outdoor Dry-Bulb Temperatures.	154

NOMENCLATURE

A	Area, ft^2
C_{fac}	ratio of humidity gradient to temperature gradient
c_p	specific heat at constant pressure, Btu/lb-F
C_i	compressor inlet valve P coefficient, psi-sec^2/lb^2
C_o	compressor outlet valve P coefficient, psi-sec^2/lb^2
C_{TXV}	general orifice flow coefficient
f	volumetric fraction
G	mass flow rate per unit volume, lbm/min-ft^2
h	specific enthalpy, Btu/lb
$\bar{h}$	convective heat transfer coefficient, Btu/ft^2-hr-F
$\bar{h}'$	mass transfer coefficient, lbm/ft^2-hr
I	moment of inertia, lb-ft^2
J	joules constant,
k	Thermal conductivity, Btu/hr-ft-F
L	perimeter, ft
Le	Lewis number
$\dot{m}$	mass flow rate, lbm/min
M	Total mass lbm
n	polytropic compression coefficient
N	shaft speed, rpm
N_{PR}	Prandtl number
N_{Re}	Reynolds number
P	pressure, psia
p	pressure, psia

p_c	discharge pressure, psia
p_s	suction pressure, psia
qac	air-side heat transfer rate in the condenser, Btu/hr
qae	air-side heat transfer rate in the evaporator, Btu/hr
$\dot{q}$	heat transfer rate, Btu/hr
t	time, sec
T	temperature, F or R
u	specific internal energy, Btu/lbm
v	specific volume, ft^3/lbm
V	total volume, ft^3
V_s	swept volume, ft^3
w	specific humidity, (lbm moist air)/(lbm dry air)
x	quality of refrigerant, (dimensionless)

Greek Symbols

δ	fin thickness, ft
Δp_{rated}	rated pressure drop across the expansion device
Δp_{TXV}	available pressure drop across the expansion device
ΔT_{oper}	actual operating superheat
ΔT_{static}	static superheat (superheat at which the valve is just barely open)
ϵ	heat exchanger effectiveness
ϵ^*	modified heat exchanger effectiveness
η	efficiency, fraction
μ	kinematic viscocity, ft^2/sec
ρ	mass density, lbm/ft^3
$\rho_{r,rated}$	refrigerant density at rated liquid line temperature, lbm/ft^3
σ_{xx}	stress
τ^o	torque, lbf-ft
∞	free stream conditions

Subscripts

a	air or ambient
B	braking
c	compression
D	driving
f	fluid, fin
ft	fin-and-tube
fg	latent
g	gas
i	inside, inlet
l	liquid
o	outside, outlet
p	polytropic
r	refrigerant
s	saturated, sensible
t	total, tube
tp	two-phase
v	volumetric, vapor
w	wall
wet	wetted surface

CHAPTER I

INTRODUCTION

In recent years, heat pumps have become a popular choice for space conditioning in new residences. In the heating season, the heat pump is used to extract heat from the cold outside air and to release heat into the conditioned space. In the cooling mode, the heat pump absorbs heat from the air inside a residence and rejects it to the outside air. In the process it performs two functions: sensible cooling and dehumidification.

A split system air-to-air heat pump comes with an outdoor and indoor section (Figure 1.1). The outdoor section contains the heat exchanger, the compressor, reversing valve, suction line accumulator and a fan. The indoor section contains a heat exchanger and a fan. The fans located at the heat exchanger coils circulate air to facilitate the exchange of heat between the air and the refrigerant. A four-way valve controls the refrigerant flow, reversing it when the unit is operated as an air conditioner instead of a heat pump.

In the cooling mode, cool two-phase refrigerant entering the indoor heat exchanger is evaporated by warmer indoor air blowing across the heat exchanger surface. As the indoor air cools, heat and moisture are removed from it After leaving the indoor coil, refrigerant vapor is pulled through the suction port of the compressor into the compression chamber. In the chamber, the refrigerant is compressed to a higher pressure and a temperature 20 to 30 F above the outdoor ambient air temperature. After being compressed, the refrigerant is discharged from the compressor to the outdoor heat exchanger

---

The format of this dissertation conforms to that of the Transactions of the American Society of Heating, Refrigeration and Air–Conditioning Engineers.

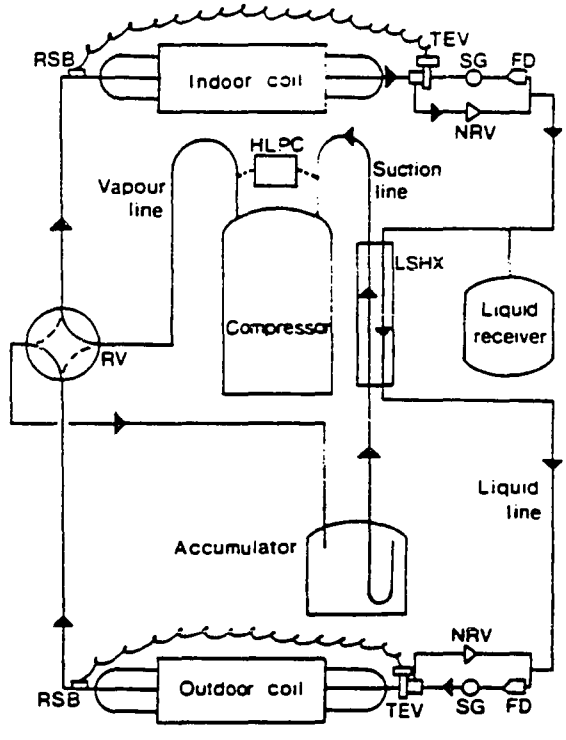

TEV	thermostatic expansion valve (refrigerant flow controller)
RSB	remote sensing bulb
SG	sight glass
FD	filter dryer
NRV	non-return valve
HLPC	high and low pressure cut-outs
LSHX	liquid/suction heat exchanger

Figure 1.1 – Schematic of a Split System Heat Pump.
(Arrows indicate flow path for heating application)

coil. Ambient air forced across the outdoor coil surface is cooler than the refrigerant within it. Thus, heat is transferred from the refrigerant to the ambient air and the refrigerant condenses to liquid. The refrigerant is then metered through the cooling mode expansion device where it is returned to a low pressure two-phase state before entering the evaporator again.

Because of increasing Federal regulations, one of the primary objectives of a heat pump design during the past 10 years has been to improve the heating and cooling efficiencies. The steady-state cooling efficiency is described by Energy Efficiency Ratio (EER):

$$\text{EER} = \frac{HCC}{HPP} \times 3.413 \frac{Btu}{W\ hr} \tag{1.1}$$

where, HCC is heat pump cooling capacity (W), and HPP is heat pump power (W). In the heating mode, the performance is described by a coefficient of performance (COP):

$$\text{COP} = \frac{HHC}{HPP} \tag{1.2}$$

where, HHC is heat pump heating capacity. One method of improving the heat pump efficiency is to increase the surface area of the heat exchanger on both the indoor and the outdoor coil sides. Such a strategy allows the heat pump to run at higher refrigerant temperatures in the evaporator and lower refrigerant temperatures in the condenser. As the temperature of the refrigerant in the evaporator is increased, the ability of the heat pump to dehumidify is reduced. The amount of dehumidification is measured in terms

of the sensible heat ratio (SHR):

$$\text{SHR} = \frac{\text{Sensible Heat Transfer}}{\text{Total Heat Transfer}} \tag{1.3}$$

In climates such as in Houston, where summers are both warm and humid, the dehumidification capabilities of the heat pump are as important as the sensible cooling achieved to maintain comfort in the conditioned space [Katipamula et al. 1987, 1988]. Manufacturers are required by federal legislation to label the heat pump with seasonal energy usage. Many manufacturers provide detailed steady-state performance data. However, much of the seasonal operation of a heat pump occurs at part-load conditions. Upon compressor start-up, the cooling capacity of a heat pump increases to steady-state over several minutes (Figure 1.2). The slow response leads to average capacities and efficiencies which are lower than the steady-state values. Since heat pumps operate at a part-load condition for long periods of time, understanding their transient behavior is essential if both comfort and efficiency are to be improved.

The transient operation of a heat pump affects: (i) the response of the sensible and the latent capacities, (ii) the efficiency and (iii) the seasonal efficiency. Major influences on the transient losses are the refrigerant dynamics, the thermal mass of the heat exchangers, and the expansion device.

To gain a better understanding of heat pump operation and efficiency under transient conditions, experimental and analytical investigation was initiated. The main objectives of this study were to quantify and model the transient sensible and dehumidification response of heat pumps during the

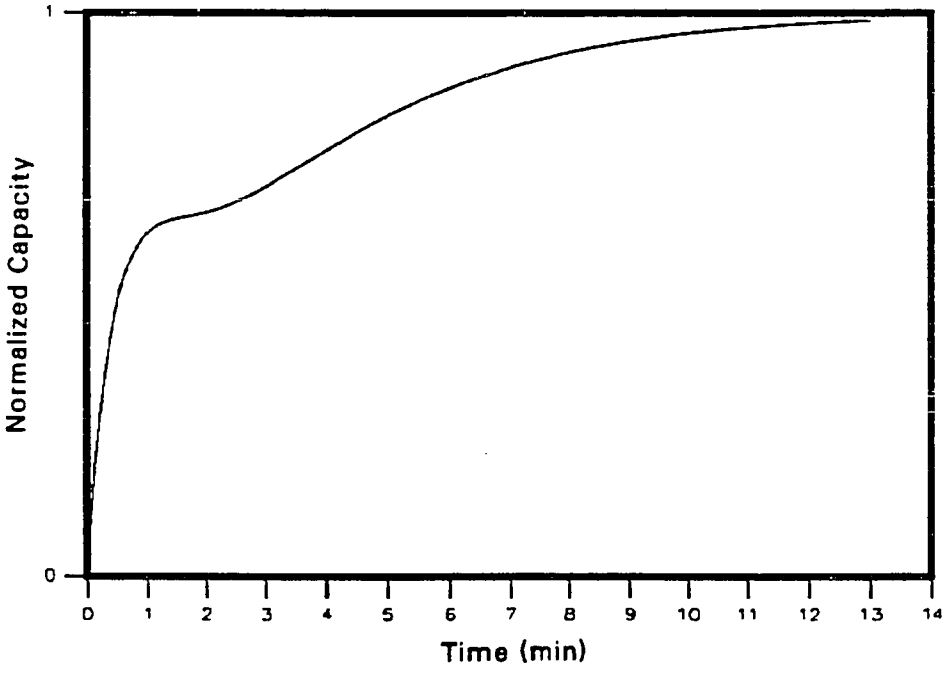

Figure 1.2 - Typical Transient Capacity Response: (Mulroy and Didion, [1985]).

cooling operation. The effects of indoor temperature and humidity, outdoor temperature, cycling rate and percent ON-times on the transient performance are addressed in this study.

Although a general characterization of the transient performance is needed to better understand the heat pump operation, it is limited to the resources and practicality of the tests. However, this study will illuminate certain trends required to characterize and model the transient performance of the air-to-air residential heat pumps in the cooling mode. Also, a cycling test required by the American Refrigeration Institute (ARI) only provides performance degradation for a specific outdoor and indoor condition. Since it is not practical to test all the manufactured units at various off-design conditions, the proposed model would estimate the performance of heat pumps at various off-design conditions and predict their seasonal performance as well.

This study includes a review of the relevant literature, discussion of the experimental test results, model development and analysis. Chapter II summarizes the literature reviewed for the research. The review was done to determine the current state of knowledge of transient heat pump operation and to justify the need for additional research. Chapter III provides details of the experimental test facility. Since it is not practical to test all the manufactured units for various indoor and outdoor conditions, a good theoretical model is needed to predict the off-design performance. Therefore, a model, TRPUMP (TRansient PUMP), developed at the National Bureau of Standards (NBS) was modified and used to predict the transient sensible and dehumidification performance of a heat pump. The modifications made to the model are described in Chapter IV. The methodology developed for studying

the heat pump transient performance is discussed in Chapter V. Chapters VI and VII are discussions of the experimental test results. Chapter VII compares of the simulated results with the experimental results. Conclusions and recommendations for future research are provided in Chapter IX.

CHAPTER II

LITERATURE REVIEW

In 1976, the National Bureau of Standards (NBS) identified that cycling operation degrades the seasonal performance of heat pumps [Kelly and Bean, 1976]. Since then, a number of researchers have recognized the significance of the transient losses in capacity and efficiency at start-up [Kelly and Bean 1977; Parken et al., 1977; Bullock and Reedy, 1978; Murphy and Goldschmidt, 1979; Hart and Goldschmidt, 1980; Baxter and Moyers 1985; Miller, 1985]. These studies on transient heat pump performance can be classified into four major areas: (i) field measurements of transient response, (ii) laboratory measurements of the transient response, (iii) experimental study of refrigerant distribution in the heat pump system and its effects on the transient response and (iv) modeling of transient response of a heat pump.

FIELD MEASUREMENTS

Kelly and Bean [1976], tested a 5-ton heat pump installed in a residence in Washington D.C. When the heat pump operated at outdoor temperatures below 40 F, the measured performance was about 10% below that specified by the manufacturer. In cooling, the effect of part-load operation on performance was found to be as high as 18%.

In 1979, the National Bureau of Standards (NBS) proposed a new rating procedure for seasonal performance of heat pumps which included part-load cyclic and frost tests in addition to traditional steady-state tests [Didion and Kelly, 1979]. With the change in rating procedures, many attempts were made to understand the heat pump operation under actual field conditions. In

a test performed on an unoccupied single-family house near Knoxville, TN, it was reported that the transient start-up losses in heating and cooling modes were 9% and 3%, respectively. The unit took 4 min. to reach steady-state conditions. The degradation coefficient, C_D (which is defined in Chapter V), for the heating season was 0.26 and 0.11 for the cooling season.

A study of the effects of duty cycling was conducted by Hart and Goldschmidt [1980] with a 3–ton heat pump installed in a mobile home. The transient response measured by the temperature difference (ΔT) between the supply and return air exhibited three characteristics: (i) the ΔT at time, $t = 0$, was approximately half the value at steady state, (ii) the response could be approximated by a first order system, and (iii) the ratio of $\Delta T/\Delta T_{ss}$ was independent of the operating conditions.

Goldschmidt et al., [1980], suggested that the transient response is not a simple function of the thermal mass of the heat exchanger coils and that the degradation of performance was different for the heating and cooling modes of a heat pump. Their analysis also suggests that the transient response could be sufficiently described by a simple time constant.

Murphy and Goldschmidt [1979], noted that the losses in performance due to transient effects is most likely attributed to refrigerant dynamics rather than the thermal mass of the heat exchanger coils. They also calculated the degradation of a self-contained 3-ton air-conditioner installed in a mobile home. They concluded that the degradation coefficient is not unique but depends on the transient response under a fixed set of test conditions. A relationship was obtained from experimental data between ON-time and cycle time:

$$\frac{t_{on}}{t_{cyc}} = 1 - \frac{\alpha}{t_{on}}$$

where $\alpha = 5.3$ for that particular mobile home. They suggested that α depends on the thermostat dead band, thermal mass of the building and the cooling capacity.

LABORATORY MEASUREMENTS OF TRANSIENT RESPONSE

Studying transient response in controlled environmental chambers can contribute to better understanding of heat pump operation and modeling its performance. Numerous researchers have attempted to study the transient response of heat pumps: Parken et al., [1977], Murphy and Goldschmidt [1984], Miller [1985], Bullock and Reedy [1978].

Parken et al., [1977] studied the transient performance of a 3–ton heat pump in a laboratory for both heating and cooling at different cycling rates and loads. The steady–state cooling capacity and coefficient of performance agreed with the manufacturers' published data within 5%. The part–load cooling capacity was substantially lower than the steady–state value. At 20% ON–time, the decrement of the part-load cooling capacity from the steady-state cooling capacity changed from 10% at a cycling rate of 0.8 cycles per hour (cph) to 35% at 4 cph (Figure 2.1). For an ON–time of 80% (i.e the ON-time to total time ratio is 0.8), the decrement in cooling capacity ranged from 4% at 0.8 cph to 8% at 4 cph. The compressor power was relatively unaffected by the cycling rate.

All the part–load tests were performed at a single indoor and outdoor dry–bulb temperature. Although the tests showed the effect of part–load operations

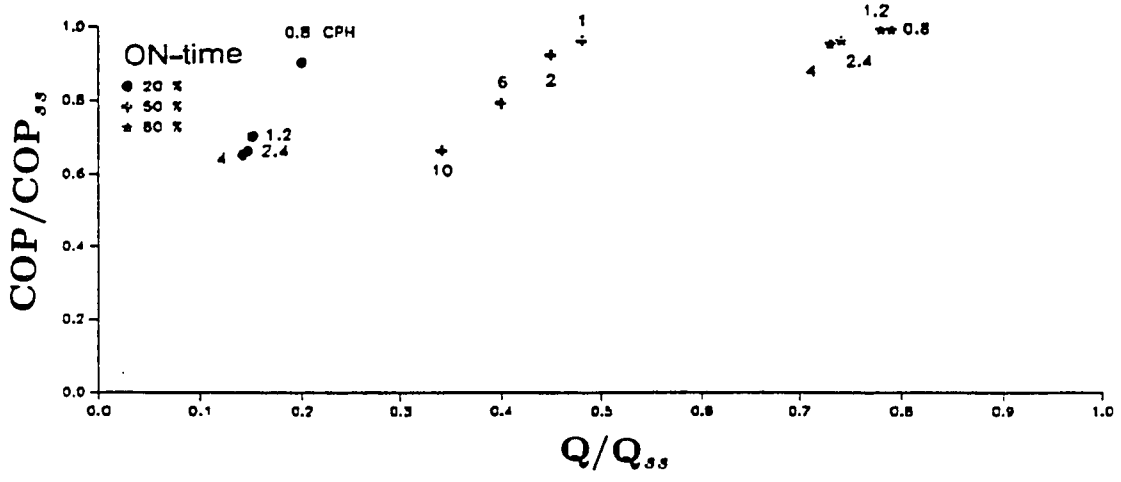

Figure 2.1 - Part-Load Cooling Performance Results: (Parken, et al., 1977).

on the performance, it is not clear how the part-load performance would be affected by the change in indoor and outdoor temperatures.

Murphy and Goldschmidt [1984] reported that certain start-up losses are the result of OFF-cycle phenomena. The migration of refrigerant from condenser to evaporator caused noticeable power differences and capacity losses immediately after start-up and some of these occurred due to a direct exchange of heat between the condenser and the evaporator.

Miller [1985] studied the transient heating performance of a 3-ton air-to-air heat pump. His results indicated that the cycling COP of the heat pump decreased with ON-time. At 50 F outdoor temperature, the degradation in COP varied from 7% to 30% (Figure 2.2). The study revealed the dependence of the part load factor, PLF (which is defined in Chapter V), on outdoor temperatures. Prior studies had only studied the performance at a single indoor and outdoor temperature and had not detected this trend. To better understand the relationship between the outdoor temperature and the part-load efficiency (PLE), the tests should be performed at more than two temperatures.

As evident from the literature reviewed, no attempt has yet been made to understand, in detail, the transient dehumidification performance of the heat pumps. The study of transient dehumidification performance should provide a better understanding of, and its contribution to, the cyclic inefficiency of the heat pumps.

STUDY OF REFRIGERANT DYNAMICS

Tanaka, et al. [1982], and Mulroy and Didion [1985] investigated the distribution of refrigerant and variation of temperature and pressure for steady-

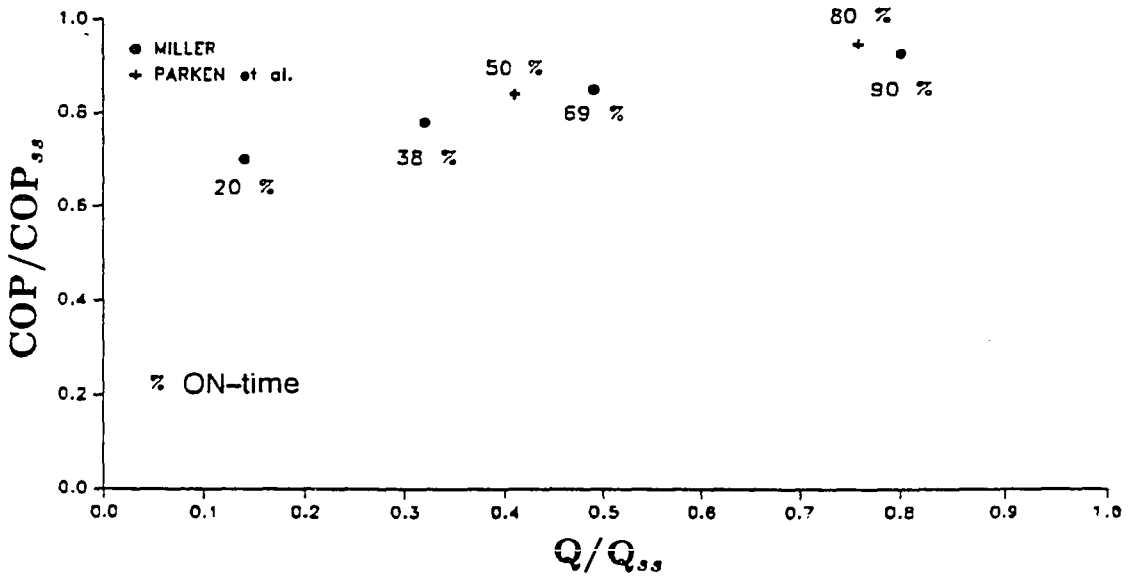

Figure 2.2 – Part-Load Heating Performance Results:
(Parken, et al., 1977; Miller, 1985).

state and start-up conditions. The test results in the cooling mode indicated that, at start-up, more than half of the refrigerant was in the evaporator and almost all of it was liquid. Tanaka et al., reported that a lot of wet refrigerant was found in the compressor sections after about 40 seconds from start-up; however, Mulroy and Didion reported that there was no evidence of substantial liquid refrigerant in the compressor or accumulator at start-up.

Both the studies showed that it takes almost 10 minutes to achieve steady state. The large time to steady-state was due to unequal refrigerant distribution in the heat pump coupled with larger heat inertia (due to the mass of the heat exchanger coils); and the efficiency of the heat pump was reduced in transient mode.

Miller [1985] also studied refrigerant migration in a heat pump in the heating mode. The results indicated that the indoor coil (condenser) had only 0.5 lb (the heat pump total charge was 12.5 lb) of refrigerant vapor at start-up; therefore, a high quality saturated mixture was throttled by the outdoor capillary for approximately 2 minutes of compressor operation. The unit reached steady-state in approximately 15 minutes when the outdoor temperature was 50 F.

MODELING OF TRANSIENT BEHAVIOR IN HEAT PUMPS

A cycling test required by the American Refrigeration Institute (ARI) only provides performance degradation for one set of outdoor and indoor conditions. Testing units at multiple sets of outdoor and indoor conditions is probably not practical. However, a good model should adequately predict the performance of the units at various off-design conditions. Although dynamic

response modeling is complicated and requires extensive computations, several investigators have attempted to model such behavior. Existing models can be classified into three groups: (i) Mathematical models based on empirical correlation of field and laboratory data or time constant approach [Groff and Bullock, 1976; Murphy and Goldschmidt, 1979; Mulroy and Didion, 1985; Tree and Wiess, 1986]. (ii) Mathematical models based on single-node or a lumped parameter approach [Dhar and Soedel, 1979; Chi and Didion, 1982; Murphy and Goldschmidt, 1985; and Sami et al., 1987]. (iii) Finally, mathematical models based on multi-node or distributed approach [Brasz and Koenig; MacArthur, 1984].

Mathematical Models Based on Time-Constant Approach

Groff and Bullock [1976] reported that the transient temperature response of the evaporator can be modeled as a first order system. Murphy and Goldschmidt [1979] reported that the experimental data for the temperature drop across the evaporator and capacity closely satisfied a first order relation of the form:

$$Q = Q_{ss}(1 - e^{-t/\tau}) \tag{2.1}$$

where, Q is the transient capacity, Q_{ss} is the steady state capacity and, τ the time constant. For the unit tested, τ was about 28 seconds. Mulroy and Didion [1985] found that a two time constant model provided a better fit to the data than a first order fit as described in Eq. 2.1. With a single time constant (τ = 3 minutes) the curve matched the transient data values well after 4 minutes. However, before that time the predicted capacity was much too low. They introduced a two time constant (τ_1 and τ_2) equation of the form:

$$Q = Q_{ss}(1 - e^{-t/\tau_1})(1 + Ae^{-t/\tau_2}) \qquad (2.2)$$

to simulate the very high, but rapidly decaying initial capacity. This equation, when fitted to the data, provided a very good fit of the transient phenomena observed. The experimental results from the shut-down transients were successfully fitted with a first order exponential system. Tree and Wiess [1986] also achieved favorable results with a two time constant model. One constant was based on the mass of the coil, while the second was based on the time required to get the excess refrigerant from the evaporator into the rest of the system.

Mathematical Models Based on Single-Node or a Lumped Parameter Approach

Modeling of the dynamic response of a heat pump system is complicated by the of continuous interactions of various system components with each other, rapidly changing pressures and temperatures, and capacitance effects of heat exchangers. A lumped parameter or a single-node approach is relatively simple as compared to a multi-node approach; however, it requires extensive computer time. In this approach, each component in the system is considered as a single-node or a "tank" with constant properties. A number of researchers have successfully modelled the dynamic response using the single-node approach [Dhar and Soedel, 1979; Chi and Didion, 1982; and Sami et al., 1987]. The mathematical formulations are based on conservation of mass, momentum and energy. However, the models based on a single-node approach assume spatial independence. Therefore, the solution of the conservation of momentum equation becomes simple and the partial differential

equations governing conservation of mass and energy are converted into ordinary differential equations. In addition to various component modules (such as heat exchangers, compressor, accumulator, expansion device, fan etc.), these models employ several routines to estimate single-phase and two-phase fluid flow and heat transfer coefficient, as well as the refrigerant and air properties.

One of the first transient models was developed by Dhar and Soedel [1979]. Their model calculated the heat pump thermal dynamics using the fluid dynamic equations based on quasi-steady-state theory. Chi and Didion at NBS [1982] developed a model treating the fluid, thermal and mechanical dynamics of the heat pump simultaneously. The mass and energy conservation equations and the heat exchanger dynamic response are calculated from the following equations:

$$\frac{d}{dt}(\rho A) + \frac{d}{dx}(\rho A v) = 0 \tag{2.3}$$

$$\frac{d}{dt}(\rho A u) + \frac{d}{dx}(\rho A v h) = \frac{\bar{h} A_w}{L}(T_w - T_r) \tag{2.4}$$

$$(c_p M)_w \frac{dT_w}{dt} = \overbrace{\dot{m}_r(h_{i,r} - h_{o,r})}^{\text{Ref. side H.T.}} + \overbrace{(\bar{h}A_w)_o(T_o - T_w)\epsilon}^{\text{Air side H.T.}} \tag{2.5}$$

In addition to the conservation equations, the equations of state is also used to describe the inlet and outlet conditions at each component. The heat exchanger was modelled as three tanks, one each for the vapor, two-phase

and sub-cooled liquid regions. The refrigerant pressure ($p_i(\rho_i, u_i)$) at the inlet of any component was estimated from the property rule for the refrigerant. The first order ordinary differential equations (2.3 and 2.4) describing the component states are solved using Euler method which employs a Taylor series expansion truncated after the first derivative. Since the solution procedure is approximate, the time step had to be small for the difference equation to be stable. Lockhart and Martinelli's correlation is used to calculate the condensation flow pressure drop coefficient, and Traviss, Baron and Rohsenow [1973] correlation is used for the condensation heat transfer coefficient. Pierre's correlation [1964] is used for pressure drop calculation and Chaddock's correlation [1966] for heat transfer in the evaporator. The results obtained from the model were in good agreement comparison with the experimental results.

Murphy and Goldschmidt [1985,1986] modeled both transient start-up and shut-down of a typical 3-ton residential air-conditioner. Their models were limited to compressor, condenser and throttling device for the start-up model and the compressor and evaporator for the shut-down model. The results from the model were in good agreement with the test data. However, a lack of an evaporator model restricts its generality.

Sami, et al. [1987] used a similar approach to that of Chi and Didion to solve the mass and energy conservation equations for each component. However, they solved the governing equations for both vapor phase and liquid phase separately in the heat exchangers. A transient two-phase velocity difference model was used for calculation of the slip at the evaporator, capillary tube, and condenser. The compressor pressure drop calculations in the suction and discharge manifolds are more rigorous. They accounted for the

solubility of oil-refrigerant mixtures. The pressure drop calculation within the two-phase region of the heat exchangers was calculated in terms of the friction, gravity, and change in the momentum. The authors have reported that special correlations were used for heat transfer calculations if the refrigerant quality was over 20% at the inlet of the evaporator. One-dimensional heat conduction across the condensate frost film was considered in this model. The model is capable of simulating both the thermostatic expansion valve and the capillary tube. The estimated results from the model indicated that the heat pump stabilized after a period of 300 seconds from start-up and compared well with the results from their laboratory tests.

Models Base on Multi-Node Approach

Although the idea behind the simplified approach has been to reduce the computational complexity of spatial dependence, it cannot predict the mass distribution of the refrigerant in the system. The models based on the multi-node approach or models which account for spatial dependence are required for predicting the mass distribution accurately. Because the solution methodology is complex very few researchers have attempted it [MacArthur, 1984; and MacArthur and Grald, 1987]. MacArthur [1984] modelled the heat exchangers as multi-node components and the rest of the components in the system with lumped parameters. The conservation equations for mass and energy are:

$$\frac{\partial}{\partial t}(\rho) + \frac{\partial}{\partial x}(\rho u) = 0 \qquad (2.6)$$

$$\frac{\partial}{\partial t}(\rho h) + \frac{\partial}{\partial x}(\rho u h) + \frac{\bar{h}P}{A}(T_r - T_w) = 0 \qquad (2.7)$$

The flow field was assumed to be uniform and one-dimensional along the length of the heat exchanger. The energy equation for the evaporator model is solved for single- and two-phase regions. The solution for the energy equation is obtained by separating it into series of control volumes and integrating over appropriate control volume with respect to time and distance. The resulting equations are a set of fully implicit coupled equations defining the response of the control volumes. The solution of the implicit coupled equations is accomplished by using an iterative line-by-line search for the temperature and enthalpy field at each time step. The heat exchanger wall response is also evaluated in a similar manner. The pressure in the condenser is evaluated explicitly.

MacArthur and Grald [1987] used a similar approach. Instead of assuming a flow field, Eq. 2.5 was integrated with respect to time to get the actual flow field. Also a void fraction model was used to calculate the density field in the two-phase region.

SUMMARY OF LITERATURE REVIEW

A number of conclusions can be drawn from the literature reviewed:

(i) The losses due to transient effects can be as much as 20%.

(ii) It takes 5 - 10 minutes to achieve steady-state after start-up.

(iii) The transient response is not first order in nature.

(iv) The transient response is affected by the number of ON-OFF cycles and percent ON-time during each cycle.

(v) The mass of the heat exchangers affects transient losses.

(vi) The OFF–cycle migration of the refrigerant from the condenser to the evaporator causes significant losses in capacity.

(vii) The transient response can be modeled adequately.

Although a number of researchers have recognized the importance of transient losses in heat pump operations, mostly it has been for a few indoor and outdoor temperatures. Therefore, a general characterization of the transient phenomena of heat pumps has yet to be achieved. Some of the major issues that have to addressed to achieve the goal include:

(i) The effects of indoor and outdoor temperatures on transient behavior.

(ii) The effects of indoor relative humidity on the transient behavior.

(iii) The effects of transient behavior on the dehumidification performance.

(iv) The effects of ON–OFF cycling and percent ON-time on the dehumidification performance.

(v) Although the start–up and shut–down transients have been successfully modeled, they have been modeled separately.

(vi) The physical meaning of the time constants for the empirical correlations is not fully understood.

In light of the above, and to gain a better understanding of the transient phenomena in heat pumps, further studies are required. Furthermore, the reviewed literature did not address the issue of transient dehumidification. Therefore, the present study was initiated to look at both the transient sensible and dehumidification cooling performance of heat pumps, and also to model their behavior.

CHAPTER III

TEST FACILITY

To characterize the transient response of heat pumps, a series of experiments with a heat pump was devised. The experiments provide a comprehensive cyclic characterization by taking performance data from a series of experimental tests on the heat pump. However, the experimentation was limited by the avaiable resources and practicality of the tests on a single base-case configuration. The tests should illustrate certain trends required to characterize and model the performance of the air-to-air residential heat pumps.

The experiments required recording of rapidly changing parameters such as: flow rate, temperature, pressure and humidity of air across the heat exchangers and flow rate, temperature and pressure of the refrigerant at various locations in the heat pump and power consumption of compressor and fans. To achieve the experimental objectives, a test facility was established that consisted of: (i) psychrometric rooms, (ii) a test heat pump, (iii) heat exchanger test sections and (iv) a data acquisition and reduction system.

PSYCHROMETRIC ROOMS

The psychrometric test facility consists of two environmentally controlled test chambers at the Energy Systems Laboratory (ESL) of the Department of Mechanical Engineering, Texas A&M University. This facility is located at the Texas A&M Riverside Campus Research Center. These rooms were constructed and maintained according to the American Society of Heating Refrigeration and Air-Conditioning Engineers (ASHRAE) specifications

[ASHRAE Standard, 1983]. The basic schematic of the environmental chambers is shown in Figure 3.1. The rooms can simulate both indoor and outdoor conditions required for the heat pump performance testing. The rooms are large insulated refrigeration rooms with blowers to circulate room air through control ducts in the ceiling of each room. The control of the test conditions in the rooms was achieved with a TI 550 programmable controller which monitored conditions in each room with thermocouple grids and dew point sensors. A 75-ton chiller and a 300 gallon chilled water storage tank provided the chilled water for the cooling coils. Four banks of 9900 Watt electric heaters in the control air ducts in each room provided resistance heating. Dehumidification of the rooms was achieved by circulating additional chilled water though dehumidification coils in the air control ducts.

TEST HEAT PUMP

A nominal three-ton capacity split-system residential air-to-air heat pump was selected for use in characterizing transient dehumidification performance. The indoor heat exchanger was installed in a galvanized steel air duct in the indoor psychrometric room. The outdoor coil (Carrier Model 544A) was a free-standing, horseshoe-shaped, vertical coil placed in the outdoor room. Other heat pump components such as the compressor, accumulator, reversing valve, and electronic controls were also placed in the outdoor room. The expansion device was placed down-stream of the indoor coil in the indoor room.

The indoor heat exchanger was a four-row, four-circuit vertical coil. Refrigerant tubing in the coil was 3/8 inch nominal diameter copper tubing. Vertical extended surfaces were placed on the tubing at twelve fins per inch. These fins were wavy and are commonly used in the air-conditioning industry.

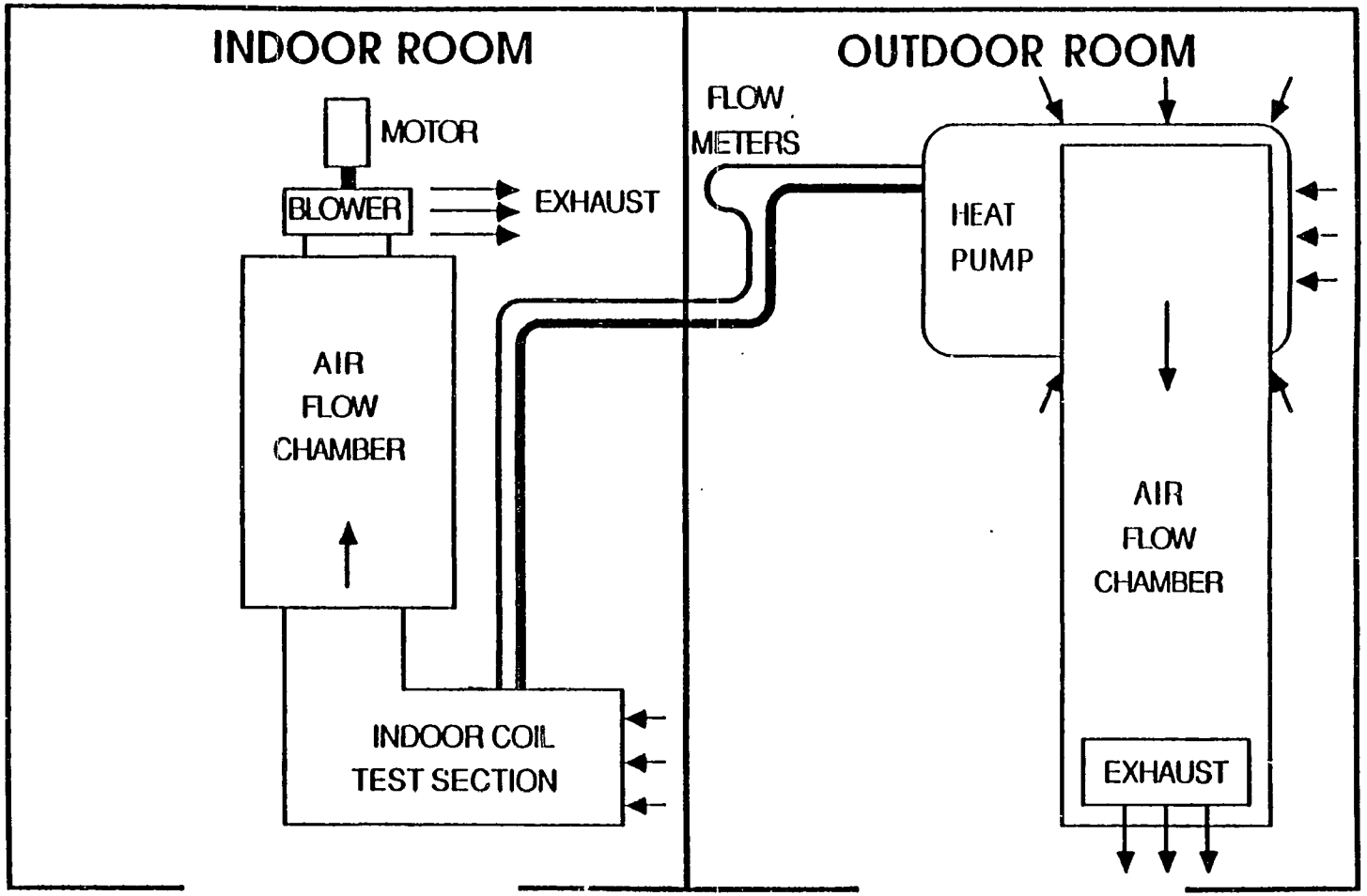

Figure 3.1 -- Schematic of Psychrometric Rooms.

Each row of the coil had seventeen total passes of the horizontal refrigerant tubing. The coil was 30 inches wide, 18 inches high, and was rated at three tons capacity. Typical air flow across the coil during test runs was 1250 cfm.

The outdoor heat exchanger was a two-row, four-circuit vertical coil. Refrigerant tubing in the coil ran horizontally through vertical wavy fins spaced twenty fins per inch. The tubing was 3/8 inch nominal diameter copper tubing. Each row of the coil consisted of thirty passes of refrigerant tubing. Figure 3.2 depicts the circuit arrangement for the outdoor coil. The coil had a frontal dimension of 30 inches high by 84 inches measured around the U shape. A three-blade propeller fan was used to pull air through the coil. The rated flow rate of the fan was 1900 cfm. Air pulled through the coil was exhausted above the unit.

The refrigerant tubing between the coils was 3/8 inch nominal diameter and 39.3 feet long. This section of the refrigerant circuit is referred to as the liquid line and contained the expansion device in the indoor room. The expansion device used for base case test runs was a thermostatic expansion valve (TXV) rated at 2.5 ton capacity and designed to maintain a 10 F superheat at steady state condition. Table 3.1 provides additional details of the TXV. Other equipment in the liquid line included a filter-drier and two parallel refrigerant mass flow meters.

The other major section of refrigerant tubing was the vapor line and included 33 feet of tubing connecting the indoor coil to the reversing valve and 2 feet of tubing connecting the outdoor coil to the reversing valve. This copper tubing was 5/8 inch nominal diameter. The four-way reversing valve also included ports for the suction and discharge lines of the compressor.

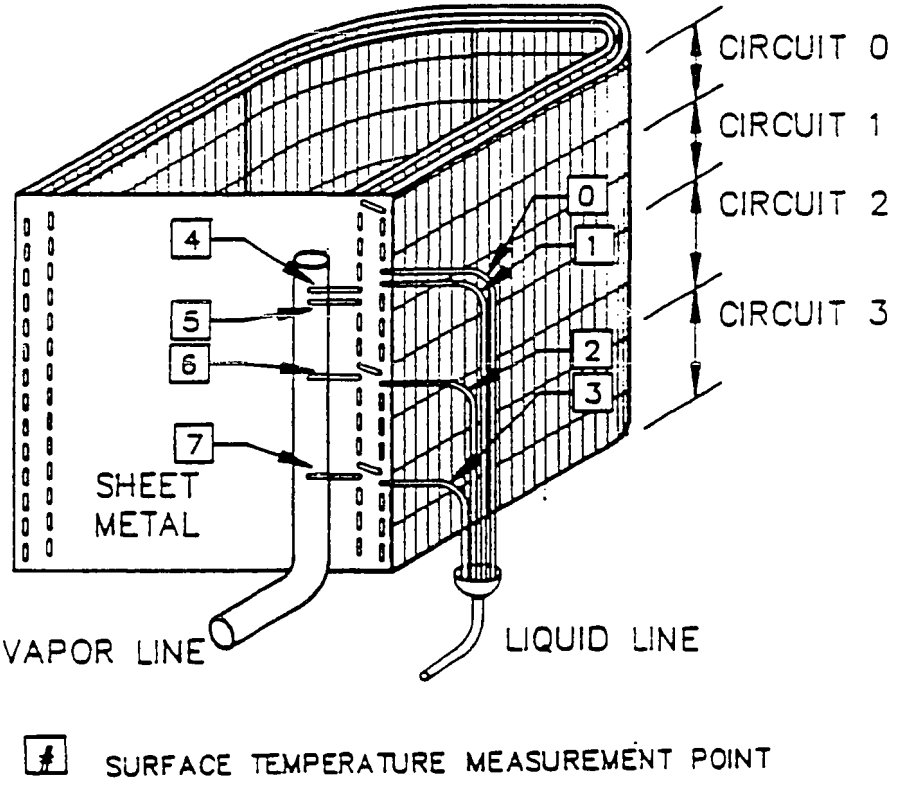

Figure 3.2 - Schematic of Outdoor Coil Refrigerant Circuit.

Table 3.1 - Characteristics of the Cooling Mode Thermostatic Expansion Valve.

ITEM ANEB $2\frac{1}{2}$ HW (ALCO)	TYPE or VALUE
Nominal Capacity	$2\frac{1}{2}$ Ton
Static Superheat	6 F
System Superheat	10 F
Inlet	3/8 in. SAE
Outlet	1/2 in. SAE
Bulb/TXV Line	5 Feet
Bulb Fill	Standard Residential A/C and Heat Pump
Pressure Equalization	Bleed Type
Configuration	Straight
Maximum Opening	0.0059 $in.^2$
Stroke	0.024 in.

This arrangement allowed high pressure refrigerant vapor discharged from the compressor to be directed into the outdoor coil during cooling mode operation.

The test heat pump had a three-ton capacity reciprocating compressor (Tecumseh Model AV5532E) to circulate refrigerant through the heat exchanger coils. The compressor was equipped with a suction line accumulator (Tecumseh Model TA1607) to minimize liquid flow to the compressor during start-up and transient operation periods. This accumulator had two sight glasses: one at the top and other at the bottom. When supplied by the manufacturer, the outdoor coil and compressor section of the test pump were charged with 11.5 pounds of refrigerant.

Electronic controls for the heat pump were attached to a cart upon which the outdoor coil stood. Remote switches placed in the control room of the

psychrometric test facility allowed switching of the heat pump reversing valve. An additional switch permitted independent control of power to the outdoor fan.

To provide necessary data for transient performance characterization, the refrigerant circuit of the heat pump was instrumented with flow meters, temperature probes, pressure taps, and surface temperature thermocouples. Figure 3.3 depicts the placement of these instruments in the refrigerant circuit. Table 3.2 provides description of each of the test points in the refrigerant circuit as well as a description of test points in the heat exchanger test sections which will be discussed later.

Refrigerant line pressure was measured at the ten points (as indicated in Figure 3.3) with 0 – 300 psig pressure transducers (Foxboro Model 1225). These integrated circuit diaphragm-style pressure transducers had a stated total accuracy of 1 % of full scale output (FSO). Temperature probes were placed near the pressure transducer taps in the refrigerant circuit to measure refrigerant temperature at these points. The 1/16 inch diameter probes were constructed as shown in Figure 3.4. The probe tips were far enough into the flow of the refrigerant (approximately eight diameters) to minimize conduction effects with the tube surface. Thermocouple wires were placed in the probe wells and surrounded by an oil bath to maintain a uniform temperature through the probe tip section. Thermocouples were made with wire taken from a common spool and were cut to a uniform length to minimize output variation caused by differences in wire composition or length.

Refrigerant mass flow rate was measured in the liquid line with two parallel mass flow meters (Micro Motion Model D). The mass flow rate of the refrigerant

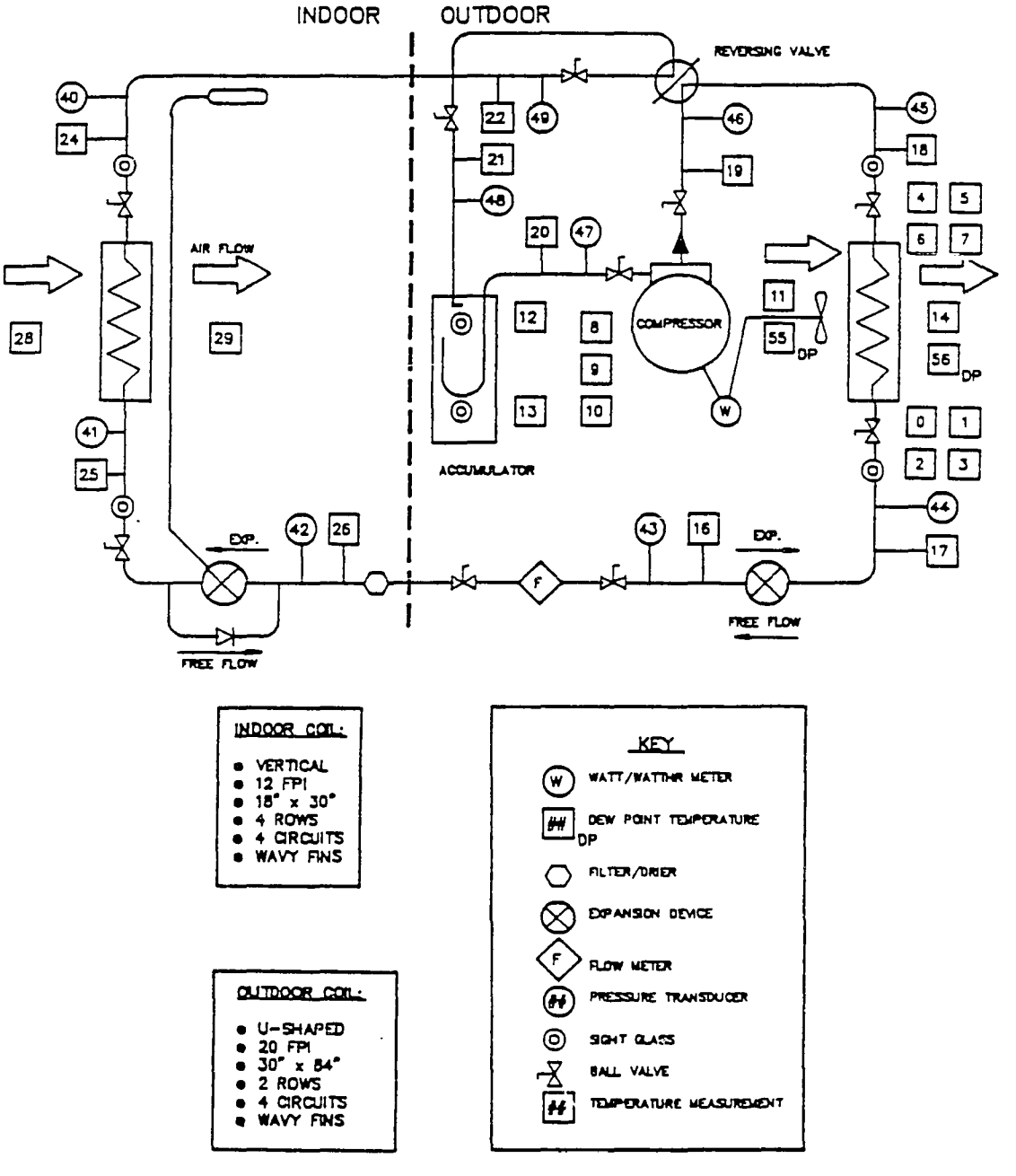

Figure 3.3 - Heat Pump System Schematic.

Table 3.2 – Description of Test Points Used in the Heat Pump Set-Up.

CHANNEL	TYPE	LOCATION
00 - 03	Thermocouple	Outdoor Coil - Inlet (T to B)
04 - 07	Thermocouple	Outdoor Coil - Outlet (T to B)
08 - 10	Thermocouple	Compressor - Surface (T to B)
11	TC - Grid	Outdoor Room
12 - 13	Thermocouple	Accumulator - Surface
14	TC - Grid	Outdoor Air Chamber
15	Thermocouple	Chilled Water Temperature
16 - 19	TC - Probe	Probe in Refrigerant Line
20 - 22	TC - Probe	Probe in Refrigernat Line
24 - 26	TC - Probe	Probe in Refrigerant Line
28	TC - Grid	Up Stream of Indoor Coil (16 pt)
29	TC - Grid	Down Stream of Indoor Coil (16 pt)
40 - 49	Pressure Tran.	Refrigerant Lines
50	Watt Tran.	208 VAC - Single Phase
51	Flowmeter	Refrigerant Liquid Line
52	Diff. Pressure	Indoor Air Chamber
53 - 54	–	– Not Used –
55	Dew Point Sensor	Up Stream Indoor Coil
56	Dew Point Sensor	Down Stream Outdoor Coil
57	Flow Meter	In Parallel with # 51
58	Watthour Tran.	Compressor/Outdoor Fan

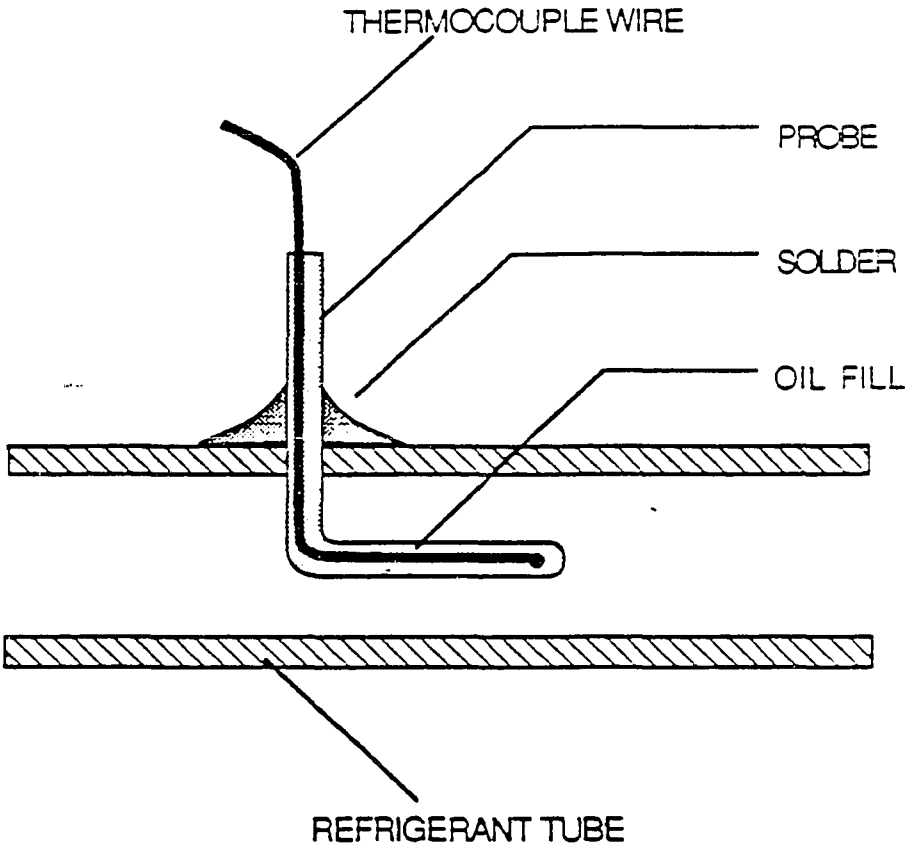

Figure 3.4 - Refrigerant Line Temperature Probe.

through vibrating U-shaped tubes in each meter was determined by Coriolis acceleration and deceleration effects sensed by the meters' electronics. Two flow meters were used to limit pressure losses across the measurement section to a maximum of 10 psi (for a 10 pounds per minute flow rate). This pressure drop was less than the 12 psi pressure drop acceptable by ASHRAE Standard [1983] (12 psi is the equivalent pressure drop for the refrigerant at the test conditions experiencing the maximum allowed temperature drop of 3 F).

Valves shown in the refrigerant circuit diagram were lever-actuated shut-off valves. These valves permitted isolation of sections of the heat pump refrigerant circuit for leak testing, equipment replacement, and system break-down. The valves proved to be extremely useful to isolate sections, when a specific section of the refrigerant circuit had to be opened, preventing excess refrigerant charge loss. Charging taps in each section of the circuitry allowed purging and charging of the sections independently.

Other points where temperature was measured on the refrigerant circuit include: surface temperature of the accumulator and compressor and surface temperature of the liquid and vapor lines going to each of the four circuits of the outdoor heat exchanger. Surface temperature measurements were made with thermocouples constructed from the same wire used in the refrigerant line probes and cut to the same length. Thermocouple junctions used in the surface temperature measurement were fixed to the surface where a temperature measurement was required. These junctions were covered with foam insulating tape. All thermocouple signals were transmitted through uniform-length extension wires to the data acquisition system.

HEAT EXCHANGER TEST SECTIONS

Test sections were designed and constructed for both the indoor and outdoor heat exchangers to provide air-side performance data for the heat pump tests. The test sections permitted conditioned air from the psychrometric rooms to flow over the respective heat exchanger coils and then return to the rooms. Although the state of the air flowing through the test sections was altered by the heat exchanger coils in the sections, the psychrometric rooms had the capacity to handle these changes and re-condition the exhaust air while maintaining set-point conditions. Both test sections are discussed in detail in the following paragraphs.

Indoor Test Section

The schematic of the indoor test section is shown in Figure 3.5. The conditioned air from the indoor psychrometric room was drawn through the 30 by 20 inch insulated duct which contained the indoor coil. This air entered the test section at a control temperature and was pulled through the test section by a booster fan of the downstream chamber. A damper at the booster fan outlet permitted air flow rate to be adjusted to the level desired for testing.

As air entered the test section, it flowed through flow straighteners. Then it passed over a 16-node thermocouple grid which measured average air temperature across the cross-section. Then the air flowed through the indoor heat exchanger coil. Next, the air flowed through a set of mixers which removed any temperature stratifications caused by non-uniform heat exchange with the indoor coil of the heat pump. At this point, the air again passed

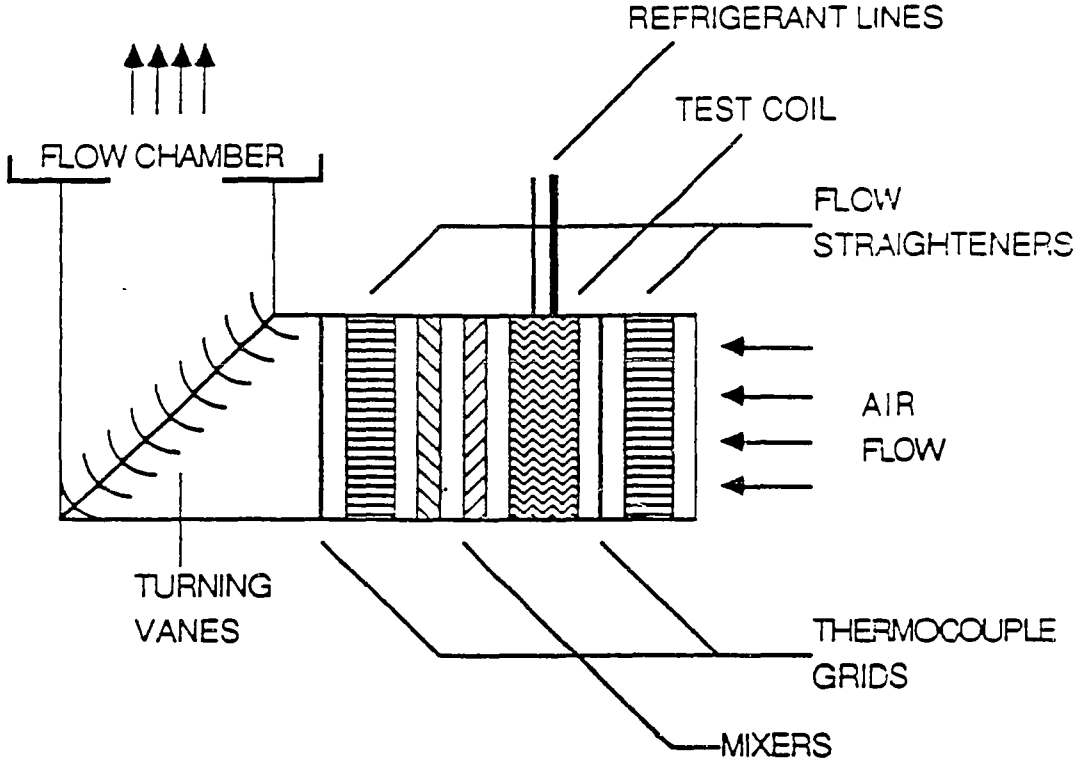

Figure 3.5 – Schematic of Indoor Test Section Set-Up.

through flow straightener. A downstream 16-node thermocouple grid is used to measure air temperature after it is mixed and straightened. Finally, the air entered the flow chamber for flow rate measurement. Flow straighteners, mixers, and thermocouple grids were constructed following ASHRAE Standard 41.1-74 [1974], which specifies procedures for temperature measurement.

An optical mirror dew-point sensor (General Eastern Model DEW-10) placed at the entrance of the indoor test section measured the dew-point temperature of the conditioned air entering the test section and another sensor placed downstream on the indoor coil measured the dew-point temperature of the supply air. In addition to the dew point sensors, a dry/wet bulb thermometer test rig placed in the vicinity to the test section measured the condition of the air entering the test section. The test rig used a small centrifugal fan to pull air across a dry-bulb thermometer and a thermometer whose bulb was wetted with a cotton sock saturated with distilled water.

Air flow rate was measured in the flow chamber located downstream from the test section. This chamber was an AMCA/ANSI Standard 210, flow chamber [1985]. The chamber contained four ASME flow nozzles (one of eight, two of five, and one of three inch diameters) which were used as needed to measure the flow rate with an inclined-tube manometer calibrated to ± 0.01 inches water gauge (inwg) with a micromanometer. For the cooling tests, the two five-inch nozzles were used. Flow was adjusted to give a nozzle pressure drop of 1.3 inwg. This pressure drop approximately corresponded to 1200 cfm of air through the test section.

Outdoor Test Section

The temperature of air entering the outdoor coil was measured with a six-node grid placed in the outdoor chamber. The air flow rate through the outdoor coil was not metered.

DATA ACQUISITION AND REDUCTION

Sensor signals from the test points listed in Table 3.2 were collected and converted to engineering units by an Acurex (Model Autocalc) data logger. The data logger handled milli-volt and milli-amp signals as well as larger voltages and frequency signals. During each transient test of the heat pump, data processed by the data logger was transferred to an IBM compatible personal computer where it was stored on a hard disk drive. The fastest collection and storage rate for the 60 data channels used in the cyclic testing was seven seconds per scan. The scan rate was adjusted such that at start-up the scan rate was seven seconds and gradually increased to a minute after five minutes of start-up for every cyclic test.

Also the data acquisition system was programmed to display the data on the computer screen as it was scanned and stored. This display helped to visually monitor the data continuously during testing. After completion of a test series, all data collected on the hard disk was transferred to the main campus VAX computer system for analysis. Appropriate FORTRAN routines were written and to reduce, analyze and plot the test data.

CHAPTER IV

MODEL DEVELOPMENT

The literature reviewed in Chapter II showed that a number of researchers have successfully modeled the transient performance of the heat pumps. However, modeling of the transient dehumidification performance of heat pumps was not a major concern in the models previously developed. Therefore, a simplified model which would predict the transient dehumidification performance of heat pumps could provide a useful extension to the previous work. The idea behind the simplified approach is to reduce the computational complexity of the spatially distributed model while retaining as much accuracy as possible. The spatial independence in modeling the heat exchangers reduces the three governing partial differential equations (mass, momentum and energy) to two ordinary differential equations (mass and energy). Most models available in the open literature utilize this simplified approach.

The simulation of the transient operation of heat pumps is complicated and requires a significant amount of computation. A heat pump has several components with the performance of each component linked to that of each of other components in the system. The transient performance of the heat pumps can be systematically simulated by logically linking each of its components. The major components in a heat pump include: (i) the motor/compressor, (ii) the condenser, (iii) the evaporator and (iv) the expansion device and (v) the accumulator. Modeling the transient performance of a heat pump requires developing physical models for each of the five components. The computer program developed from the physical model must also include subprograms that describe refrigerant properties and psychrometric properties of air.

The present model has evolved from the models developed by Chi and Didion [1982] and ORNL [1981]. It can predict the transient performance of a conventional, vapor compression, electrically-driven air-to-air heat pump. New condenser, evaporator and expansion device modules were developed. The details of which are modules are discussed in this Chapter. This chapter also includes: (i) A detailed discussion of the physical models for the compressor, condenser, evaporator and the expansion devices. (ii) A description of the computer program, and (iii) summarization of the major differences between the present model and the TRPUMP model of Chi and Didion [1982].

MOTOR/SHAFT/COMPRESSOR

In modeling the compressor, the kinetic and potential energies of the refrigerant vapor are assumed to be negligible. Since the compressor is modeled as a lumped parameter, the specific volume and internal energy of the refrigerant inside the compressor and the compressor wall temperature are sufficient to describe the compressor dynamics. They are estimated by solving the following differential equations:

Continuity,

$$\frac{d\rho_i}{dt} = \frac{1}{V}(\dot{m}_{i,r} - \dot{m}_{o,r}) \tag{4.1}$$

Energy refrigerant side,

$$\frac{du_i}{dt} = \frac{1}{\rho_i V}\left(\dot{m}_{i,r}h_{i,r} - \dot{m}_{o,r}h_{o,r} + (\hbar A)_{i,r}(T_w - T_{i,r}) - u_i(\dot{m}_{i,r} - \dot{m}_{o,r}) + \dot{Q}_{loss}\right) \tag{4.2}$$

Energy air side,

$$\frac{dT_w}{dt} = \frac{1}{(c_p M)_w}\left[(\hbar A)_i(T_{i,r} - T_w) + (\hbar A)_o(T_w - T_{amb})\right] \tag{4.3}$$

The first term in Eq. 4.2 is the change in enthalpy of the control volume, the second term is the heat transfer between the control volume and the compressor walls, the third term is the change in internal energy of the tank and the last term is the motor heating. The first term in Eq. 4.3 is the heat exchange between the control volume and the compressor wall and the second term is the heat exchange between the wall the the ambient air.The three equations (4.1 – 4.3) are solved by a fourth-order Runge Kutta (RK) method. The unknowns in the above equations are the outlet refrigerant flow rate, $\dot{m}_{o,r}$, and the outlet specific enthalpy, $h_{o,r}$. The refrigerant flow rate at the outlet of the compressor is given by:

$$\dot{m}_{o,r} = \rho_s N V_s \eta_v \qquad (4.4)$$

The shaft speed, N, of the compressor motor depends on the motor driving torque, τ_D and the compressor braking torque, τ_B, which is calculated from the following equation:

$$\frac{dN}{dt} = \frac{30(\tau_D - \tau_B)}{\pi I} \qquad (4.5)$$

A table of the motor driving torque versus speed, and motor efficiency versus speed must be provided to the model. The braking torque, τ_B, is calculated from the expression:

$$\tau_B = \frac{\dot{m}_{o,r}\,(h_{o,r} - h_{i,r})\,J}{2\pi N} \qquad (4.6)$$

The volumetric efficiency, η_v, is calculated from:

$$\eta_v = c_1 \left\{ 1 - c_2 \left[\left(\frac{P_c}{P_s} \right)^{\frac{n-1}{n}} - 1 \right] \right\} \tag{4.7}$$

The above equation accounts for the three principal factors which affect compressor volumetric efficiency – re-expansion of clearance vapor, pressure drop in the suction and discharge valves, and heating of the vapor on the intake stroke. The constants, c_1 and c_2, are the leakage fraction and clearance fraction of the swept volume, V_s, respectively. The suction and head pressures in the cylinder are calculated from the following equations:

$$p_s = p_{i,r} - C_i v_i m_{i,r}^2 \tag{4.8}$$

$$p_c = p_{o,r} + C_o v_o m_{o,r}^2 \tag{4.9}$$

where C_i and C_o are the inlet and outlet port pressure drop coefficients. The refrigerant pressure at inlet is calculated from a property relationship for the refrigerant, $p_{i,r} = f(v_i, u_i)$. The specific enthalpy at the outlet is calculated from the following equation:

$$h_{o,r} = h_{i,r} + \frac{(h_{o,s} - h_{i,r})}{\eta_c} \tag{4.10}$$

where, $h_{o,s}$, is calculated from the functional relationship:

$$h_{o,s} = f(v_{o,s}, p_{o,r}) \tag{4.11}$$

The compression efficiency, η_c is given by:

$$\eta_c = \left[\left(\frac{p_c}{p_s}\right)^{\frac{\gamma-1}{\gamma}} - 1\right] / \left[\eta_p\left(\left(\frac{p_c}{p_s}\right)^{\frac{(n-1)}{n}} - 1\right)\right] \tag{4.12}$$

HEAT EXCHANGER MODULES

TRPUMP does not model dehumidification explicitly; therefore, it was decided that a heat exchanger model with dehumidification capabilities was necessary to get a better understanding of both the sensible and the latent heat transfer rates.

Two separate models were developed, one for the condenser and other for the evaporator. The difference between these models is the dehumidification algorithm. Therefore, the models will be discussed together and the differences will be pointed out where they occur. The models are based on a cross-flow heat exchanger design (Figure 4.1).

The refrigerant side heat transfer calculations are separated into superheated, two-phase and sub-cooled regions for the condenser model and two-phase, and superheated regions for the evaporator model. The air side heat transfer calculation is different for both models. The basic governing equations defining the mass, momentum and energy conservation for transient one-dimensional flows of a fluid with heat transfer may be written as:

Mass,

$$\frac{\partial}{\partial t}(\rho A) + \frac{\partial}{\partial x}(\rho A v) = 0 \tag{4.13}$$

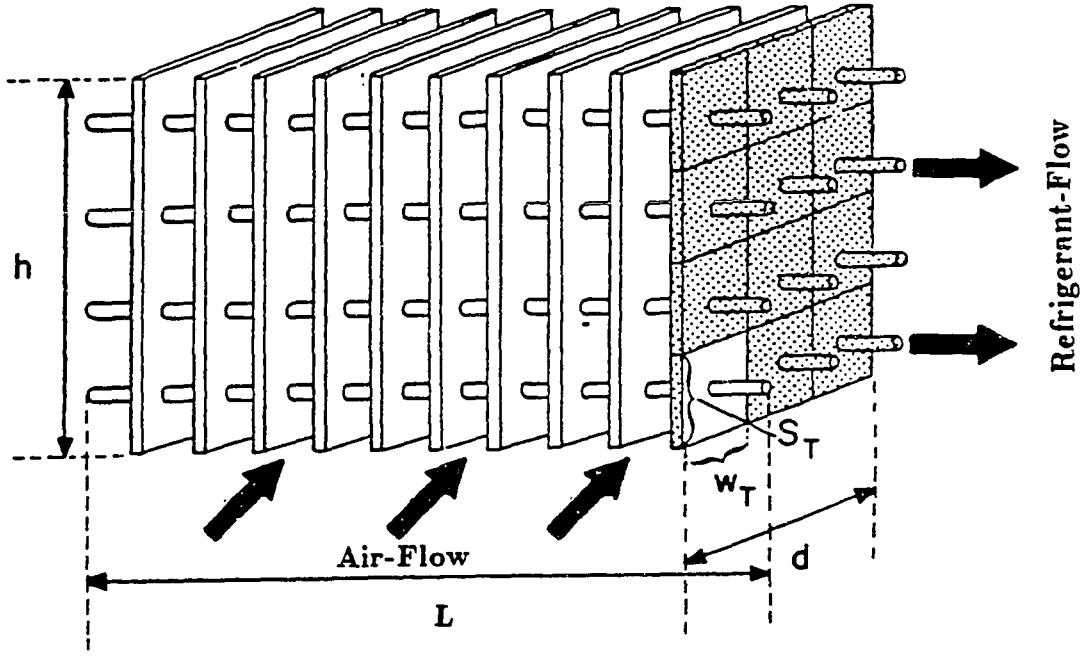

Figure 4.1 - Tube-and-Fin Heat Exchanger.

Momentum,

$$\frac{\partial}{\partial t}(\rho A) + \frac{\partial}{\partial x}(\rho A v^2) = -A\frac{\partial P}{\partial x} + \frac{\partial}{\partial x}\sigma_{xx}A - A\rho sin\theta \tag{4.14}$$

Energy,

$$\frac{\partial}{\partial t}(\rho A u) + \frac{\partial}{\partial x}(\rho A v h) = \frac{\hbar A_w}{L}(T_w - T_r) \tag{4.15}$$

The energy balance at the heat exchanger walls is:

$$(c_p M)_w \frac{\partial T_w}{\partial t} = \overbrace{\dot{m}_r(h_{i,r} - h_{o,r})}^{\text{Ref. side H.T.}} + \overbrace{(\hbar A_w)_o(T_o - T_w)\epsilon}^{\text{Air side H.T.}} \tag{4.16}$$

The spatial variation of pressure and viscous dissipation are small; therefore, they can be neglected. Hence, the momentum equation is no longer necessary, and the partial derivatives can be written as ordinary derivatives. Further, neglecting the compressibility effect (or assuming density to be constant) and the gravity pressure drop, the refrigerant side continuity and energy equations can be rewritten as:

Continuity,

$$\frac{d\rho_{i,r}}{dt} = \frac{1}{V}(\dot{m}_{i,r} - \dot{m}_{o,r}) \tag{4.17}$$

Energy,

$$\frac{du_i}{dt} = \frac{1}{\dot{m}_r}\left[(\dot{m}_{i,r}h_{i,r} - \dot{m}_{o,r}h_{o,r}) + \dot{Q}_{wr} - u_i(\dot{m}_{i,r} - \dot{m}_{o,r})\right] \tag{4.18}$$

where, $\dot{Q}_{wr}$ is the rate of heat transfer between the refrigerant and the heat exchanger walls. The last two differential equations are solved by the fourth-order RK method which is described later in the chapter.

Calculation of Refrigeration Side Heat Transfer Rate

The heat transfer rate for the condenser coil is calculated as the sum of the rates for the superheated, two-phase, and sub-cooled regions. For the evaporator, it is the sum of two-phase and superheated regions. The heat transfer rate in the single phase region is given by:

$$\dot{Q}_{wr} = (c_p \overline{m})_r (T_w - \overline{T}_r)\epsilon \tag{4.19}$$

where, $\overline{T}_r$, is the average refrigerant temperature entering and leaving the single-phase region and ϵ is the heat exchanger effectiveness. For a cross flow heat exchanger, ϵ is given by:

$$\epsilon = 1 - e^{\left(\frac{f\bar{h}A_w}{c_p\overline{m}}\right)_r} \tag{4.20}$$

Single-Phase heat transfer coefficient. The refrigerant side heat transfer coefficient for the superheated region in the condenser is calculated (as reported in ORNL model [1981]) by:

$$\bar{h} = C_1 G_r c_{p,v} N_{pr}^{-2/3} N_{Re}^{C_2} \tag{4.21}$$

where, $N_{Re} = G_r D/\mu$ and

$$C_1 = \begin{cases} 1.10647 & \text{for } N_{Re} < 3500; \\ 3.5194 \times 10^{-7} & \text{for } 3500 \leq N_{Re} < 6000; \\ 0.01080 & \text{for } N_{Re} \geq 6000. \end{cases} \tag{4.22}$$

$$C_2 = \begin{cases} -0.78992 & \text{for } N_{Re} < 3500; \\ 1.03804 \times 10^{-7} & \text{for } 3500 \leq N_{Re} < 6000; \\ -0.13750 & \text{for } N_{Re} \geq 6000. \end{cases} \tag{4.23}$$

The heat transfer coefficient for the sub-cooled region of the condenser and the superheated region in the evaporator are computed using Dittus-Boelter correlation for fully developed flow [ORNL, 1981]:

$$\bar{h} = 0.023 G_r c_p N_{pr}^{(C-1)} N_{Re}^{-0.20} \tag{4.24}$$

where, "C" is 0.3 for cooling and 0.4 for heating.

Two-Phase heat transfer coefficient. The heat transfer in the two-phase region of the evaporator and the condenser is calculated from:

$$\dot{Q}_{wr} = \bar{h}_{r,tp} A_w (T_w - T_{s,r}) \tag{4.25}$$

where, $\bar{h}_{r,tp}$, is the two-phase refrigerant heat transfer coefficient. The two-phase heat transfer coefficient for the condenser and the evaporator are average values obtained by effectively integrating local values over the length of the two-phase region. The actual integration is performed over the range of refrigerant quality [ORNL, 1981] where length of tube dz is related to a change in quality dx by:

$$dz \propto \frac{dx}{\bar{h}(x)\Delta T} \tag{4.26}$$

where, ΔT, is the difference between the refrigerant temperature and the tube wall temperature. For constant ΔT, $\bar{h}_{avg}$ is given by:

$$\bar{h}_{avg} = \frac{\int_{z_i}^{z_o} \bar{h}(x)dz}{\int_{z_i}^{z_o} dz} = \frac{\int_{x_i}^{x_o} dx}{\int_{x_i}^{x_o} \frac{dx}{\bar{h}(x)}} \tag{4.27}$$

$$\bar{h}_{avg} = \frac{\int_{x_i}^{x_o} \frac{dx}{\bar{h}(x)}}{\frac{dx}{(x_i - x_o)}} \tag{4.28}$$

The local heat transfer coefficients, $\bar{h}(x)$, for condenser and evaporator, are calculated from the correlations of Travis, and Chaddock and Noerager, respectively, as reported in the ORNL model [1981].

Air-Side Heat Transfer Calculations

The total air-side heat transfer for the condenser, where no dehumidification occurs, is calculated from the NTU effectiveness method:

$$qac_t = c_p \dot{\bar{m}}_a (T_{i,a} - T_w)\epsilon \tag{4.29}$$

where the heat exchanger effectiveness, ϵ, is calculated from:

$$\epsilon = \left[1 - e^{\left(\frac{\bar{h}A_{tt}}{c_p \dot{\bar{m}}}\right)_a}\right] \tag{4.30}$$

The total air-side heat flux for the evaporator, where dehumidification occurs along with sensible cooling, is calculated from:

$$qae_t'' = \bar{h}(T_{i,a} - T_w) + \frac{\bar{h}}{c_p Le}(w_{i,a} - w_w)(h_g - h_{f,w}) \tag{4.31}$$

The Lewis number, Le, is the ratio of the heat transfer coefficient, $\bar{h}$, to the mass transfer coefficient, $\bar{h}'$, times the specific heat:

$$Le = \frac{\bar{h}}{\bar{h}' c_p} \tag{4.32}$$

The heat flux equation can be written in a more convenient form by defining a pseudo heat transfer coefficient, $\bar{h}^*$, such that:

$$qae_t'' = \bar{h}^*(T_{i,a} - T_w) \tag{4.33}$$

Comparing Eq. 4.31 and 4.33, the pseudo coefficient, $\bar{h}^*$, is:

$$\bar{h}^* = \bar{h}\left[1 + \frac{(h_g - h_{f,w})(w_{i,a} - w_w)}{c_p Le(T_{i,a} - T_w)}\right] \tag{4.34}$$

The Lewis number is assumed to be unity [McQuiston and Parker, 1987]. Hence the total air-side heat transfer in the evaporator with both sensible and latent heat transfer is given by:

$$qae_t = c_p \dot{\bar{m}}_a (T_{i,a} - T_w)\epsilon^* \tag{4.35}$$

where the modified heat exchanger effectiveness, ϵ^*, is given by:

$$\epsilon^* = \left[1 - e^{\left(\frac{\bar{h}^* A_{ft}}{c_p \dot{m}}\right)_a}\right] \tag{4.36}$$

The total air-side heat transfer given by Eq. 4.35 does not separate the sensible and latent heat transfer rates; therefore, an algorithm was developed based on the ORNL model.

Dehumidification Algorithm

The local driving force for the simultaneous heat and mass transfer can be described using simplifying assumptions:

$$d\dot{Q} = \bar{h}'(h_{a,\infty} - h_t) dA_w \eta_{w,ft} \tag{4.37}$$

The above equation contains assumptions that the Colburn analogy given by:

$$\frac{\bar{h}}{c_p \bar{h}'} = Le^{\frac{2}{3}} \tag{4.38}$$

holds and $Le^{\frac{2}{3}} \approx 1$. Also, the energy content of the condensate is neglected and the effect of the water film thickness is assumed to be negligible. The overall wet surface effectiveness, $\eta_{w,ft}$, in Eq. 4.37, as defined by McQuiston and Parker [1987] is:

$$\eta_{w,ft} = 1 - \frac{A_f}{A_{ft}}(1 - \eta_{w,f}) \tag{4.39}$$

$$\eta_{w,f} = tanh(ML)/ML \tag{4.40}$$

where, M is given by:

$$M = \left\{ \frac{2\bar{h}_{wet}}{k_f \delta} \left[1 + \frac{c_{fac} h_{fg}}{c_p m} \right] \right\}^{\frac{1}{2}} = \left[\frac{2\bar{h}^*}{k_f \delta} \right]^{\frac{1}{2}} \tag{4.41}$$

The Eq. 4.37 contains, h_t, the enthalpy of saturated air evaluated at the tube wall temperature. Since the tube surface is only a small portion of the external heat transfer surface, a better variable for use in determining when both the fin and tube start to condense water vapor is the mean temperature of fin-and-tube, $T_{ft,m}$. The effectiveness, $\eta_{w,ft}$, can also be written as shown in ORNL model as:

$$\eta_{w,ft} = \frac{h_{a,\infty} - h_{ft,m}}{h_{a,\infty} - h_t} = \frac{T_{a,\infty} - T_{ft,m}}{T_{a,\infty} - T_t} \tag{4.42}$$

Substituting the above expression in Eq. 4.37 yields:

$$d\dot{Q} = \bar{h}'(h_{a,\infty} - h_{ft,m}) dA_{ft} \tag{4.43}$$

where, $h_{ft,m}$, is the enthalpy of saturated air at mean fin-and-tube temperature. Using the definition of, $\eta_{ft,m}$, the total heat flow can be written in two ways, i.e.,

$$d\dot{Q} = \bar{h}^* \eta_{w,ft} (T_{a,\infty} - T_t) dA_{ft}$$

$$\text{and } d\dot{Q} = \bar{h}^*(T_{a,\infty} - T_{ft,m})dA_{ft} \tag{4.44}$$

Eliminating, $T_{a,\infty}$, in the above expressions yields:

$$d\dot{Q} = \bar{h}^* \eta_{w,ft} \frac{(T_{ft,m} - T_t)dA_{ft}}{1 - \eta_{w,ft}} \tag{4.45}$$

The total heat flow from the refrigerant to the tube is, therefore:

$$d\dot{Q} = \bar{h}_r(T_t - T_r)dA_r \tag{4.46}$$

Eliminating T_t from Eqs. 4.45 and 4.46 yields:

$$d\dot{Q} = \frac{(T_{ft,m} - T_r)}{\left[\frac{1-\eta_{w}ft}{\eta_{w,ft}\bar{h}^* dA_{ft}} + \frac{1}{\bar{h}_r dA_r}\right]} \tag{4.47}$$

Combining Eqs. 4.43 and 4.47, a relationship between, $[h_{a,\infty} - h_{ft,m}]$ and $[T_{ft,m} - T_r]$ is obtained. This relationship is known as the coil characteristics, s, and is given by:

$$s = \frac{T_{ft,m} - T_r}{h_{a,\infty} - h_{ft,m}} = \frac{1}{c_{pm}} \frac{(1 - \eta_{w,ft})}{\eta_{w,ft}} \frac{\bar{h}_{wet}}{\bar{h}^*} + \frac{\bar{h}_{wet} dA_{ft}}{\bar{h}_r dA_r} \tag{4.48}$$

Assuming, $\frac{dA_{ft}}{dA_r} = \frac{A_{ft}}{A_r}$, and using relationship between $\bar{h}^*$ and $\bar{h}_{wet}$, the above equation can be written as:

$$s = \frac{T_{ft,m} - T_r}{h_{a,\infty} - h_{ft,m}} = \frac{(1 - \eta_{w,ft})}{\eta_{w,ft}(c_{pm} + C_{fac}h_{fg})} + \frac{\bar{h}_{wet}}{\bar{h}_r c_{pm}} \frac{A_{ft}}{A_r} \tag{4.49}$$

Now, the change in energy content of the air in the free-stream is given by:

$$\dot{m}_a dh_{a,\infty} = -h'(T_{a,\infty} - T_{ft,m})dA_{ft} \tag{4.50}$$

Differentiating Eq. 4.49 yields:

$$dT_{ft,m} - dT_r = s(dh_{a,\infty} - dh_{ft,m}) \tag{4.51}$$

For a direct expansion coil, $dT_r = 0$,

$$dT_{ft,m} = s(dh_{a,\infty} - dh_{ft,m}) \tag{4.52}$$

Now, it is assumed that $h_{ft,m}$ is related to $T_{ft,m}$ by a quadratic expression (between h and T on the saturation line of the psychrometric chart):

$$h_{ft,m} = a + bT_{ft,m} + cT_{ft,m}^2 \tag{4.53}$$

Differentiating the above equation yields:

$$dh_{ft,m} = dT_{ft,m}(b + 2cT_{ft,m}) \tag{4.54}$$

Solving for $dh_{a,\infty}$ from Eqs. 4.52 and 4.54 yields:

$$dh_{a,\infty} = dT_{ft,m}(\frac{1}{s} + b + 2cT_{ft,m}) \tag{4.55}$$

Again, solving Eqs. 4.49 and 4.50 yields another expression for $dh_{a,\infty}$:

$$dh_{a,\infty} = \frac{-h'}{\dot{m}_a}\frac{(T_{ft,m} - T_r)dA_{ft}}{s} \tag{4.56}$$

Equating, Eqs. 4.55 and 4.56 and collecting like terms:

$$\frac{(u + vT_{ft,m})\,dT_{ft,m}}{T_{ft,m} - T_r} = \frac{-h'}{\dot{m}_a}dA_{ft} \tag{4.57}$$

where, $u = 1 + bs$, and $v = 2cs$.

Eq. 4.57 can be integrated between $T_{ft,m}(i)$ and $T_{ft,m}(o)$, where i and o are the beginning and end of the wet coil region in the air flow direction, to obtain the mean fin-tube surface temperature:

$$\begin{aligned}&(u + vT_r)ln\left[T_{ft,m}(o) - T_r\right] + v\left[T_{ft,m}(o) - T_r\right] = \\ &(u + vT_r)ln\left[T_{ft,m}(i) - T_r\right] + v\left[T_{ft,m}(i) - T_r\right] - \frac{h'A_{ft}F_{moist}}{\dot{m}_a}\end{aligned} \tag{4.58}$$

where F_{moist} is the fraction of the coil depth that is wetted. $T_{ft,m}(i)$ is calculated from Eq. 4.49. Therefore, the only unknown in Eq. 4.58 is $T_{ft,m}(o)$. Once $T_{ft,m}(o)$ is evaluated, Eq. 4.49 is used in conjunction with the psychrometric routine to calculate $h_{a,\infty}(o)$. Therefore, the total heat flow between the air and the refrigerant can then be evaluated from:

$$\dot{Q} = \dot{m}_a \left[T_{i,a} - T_{a,\infty}(i)\right] + \dot{m}_a \left[h_{a,\infty}(i) - h_{a,\infty}(o)\right] \tag{4.59}$$

where the first term on the right hand side represents total heat transfer (sensible) in the dry coil section and the second term is the total heat transfer (sensible and latent) in the wet coil region. However, the expression still does not provide separation of the sensible and latent heat transfer rates. The exit air dry-bulb temperature, $T_{a,\infty}(o)$ is needed to estimate the sensible heat ratio.

The sensible heat transfer from the air to the fin-and-tube surface at a cross-section in the air flow direction can be written as:

$$\begin{aligned} d\dot{Q}_s &= -\bar{h}_w (T_{a,\infty} - T_{ft,m}) dA_{ft} \\ d\dot{Q}_s &= \dot{m}_a c_p dT_{a,\infty} \end{aligned} \tag{4.60}$$

where, $dT_{a,\infty}$, is the change in temperature of the air stream. Eliminating dA_{ft} by using Eq. 4.57 and canceling like terms yields:

$$dT_{a,\infty} = \frac{(T_{a,\infty} - T_{ft,m})}{(T_{ft,m} - T_r)} (u + vT_{ft,m}) dT_{ft,m} \tag{4.61}$$

Since T_r is constant, Eq. 4.61 can be rewritten as:

$$\begin{aligned} \frac{d(T_{a,\infty} - T_r)}{d(T_{ft,m} - T_r)} - \frac{(T_{a,\infty} - T_r)\left[u + v(T_{ft,m} - T_r) + vT_r\right]}{(T_{ft,m} - T_r)} \\ = -\left[u + v(T_{ft,m} - T_r) + vT_r\right] \end{aligned} \tag{4.62}$$

The above equation is solved as shown in the ORNL model. Once $T_{a,\infty}(o)$ has been evaluated, the humidity ratio of the exit air $w_{a,\infty}$ is estimated from:

$$w_{a,\infty}(o) = \frac{[h_{a,\infty}(o) - c_p T_{a,\infty}(o)]}{[1061.2 + 0.444 * T_{a,\infty}(o)]} \tag{4.63}$$

The sensible heat transfer rate $\dot{Q}_s$, and the rate of water condensation on the coil $\dot{m}_w$ are obtained from:

$$\dot{Q}_s = \dot{m}_a \left[T_{a,\infty}(i) - T_{a,\infty}(o)\right] \tag{4.64}$$

$$\dot{m}_w = \dot{m}_a \left[w_{a,\infty}(i) - w_{a,\infty}(o)\right] \tag{4.65}$$

The dehumidification calculations are performed only if the air temperature, T_{aid}, at which dehumidification would occur at the fin-tube surface is greater than the exit air temperature $T_{a,\infty,sens}(o)$ from the two-phase region that is calculated assuming only sensible heat transfer. If this condition occurs, T_{aid} is then compared to the evaporator inlet air temperature, $T_{i,a}$. If $T_{i,a}$ is greater than T_{aid}, moisture removal does not occur on the leading edge of the coil and the fraction of the coil depth which has only sensible heat transfer, F_{sens}, is computed from:

$$F_{sens} = ln\left[(T_{i,a} - T_r)/(T_{aid} - T_r)\right]/\epsilon_{tp} \tag{4.66}$$

If dehumidification does not occur on the leading edge of the coil, then the effective surface temperature, $T_{ft,m}$, at the transition point from dry to wet coil is equal to the dew point temperature of the entering air. Also $w_{ft,m}(i) = w_{a,\infty}$, $C_{fac}(i) = 0$, and $\eta_{m,ft}(i) = \eta_{dry,ft}$. However, if T_{aid} is greater than $T_{i,a}$ dehumidification occurs on the leading edge of the coil. In this case, the temperature $T_{ft,m}$ is less than the dew point temperature of the entering air. The value of $T_{ft,m}$ at the leading edge is evaluated iteratively using the coil characteristics Eq. 4.49. Initially, s is unknown because C_{fac} at the leading edge is also unknown. However, for the first iteration s is calculated assuming dry conditions at the leading edge. Next, the psychrometric routine which relates $h_{ft,m}$ to $T_{ft,m}$ at the leading edge is used to solve for $T_{ft,m}$. Once an initial value for $T_{ft,m}(i)$ at the leading edge is estimated, $C_{fac}(i)$, $h_{fg}(i)$, and $h_{fg}(o)$ are calculated, and a new value for $T_{ft,m}$ is computed. This process is repeated until the difference in the value of $T_{ft,m}$ from one iteration to the next is smaller than the prescribed tolerance. Once $T_{ft,m}(i)$ has been evaluated at the leading edge of the coil or at the transition point from dry to wet condition, the fraction of the coil depth that is wetted, F_{moist}, and the enthalpy of the air, $h_{a,\infty}(i)$, are evaluated.

To evaluate the trailing edge fin-tube temperature, $T_{ft,m}(o)$, and the exit air free stream temperature, $T_{a,\infty}(o)$, the coefficients of the quadratic fit are needed. However, to estimate them $T_{ft,m}(o)$ is required. Therefore, an estimate of $T_{ft,m}(o)$ is made on the first attempt and the coefficients are then evaluated. These coefficients are used to evaluate the new $T_{ft,m}(o)$ and the new value of $T_{ft,m}(o)$ is used to update the values of the coefficients. This process is repeated until convergence on $T_{ft,m}(o)$ is achieved. Once $T_{ft,m}(o)$ is calculated, the psychrometric routines are used to obtain $h_{ft,m}(o)$ and an

estimate of $s(o)$ is used to obtain a value for $h_{a,\infty}(o)$. The exit air dry-bulb temperature, $T_{a,\infty}(o)$, is computed next using the values of $T_{ft,m}(o)$, T_r, $s(o)$, b, and c. After $T_{a,\infty}(o)$ and $h_{a,\infty}(o)$ are evaluated, the humidity ratio of the exit air, $w_{a,\infty}(o)$, is evaluated. Values of $C_{fac}(o)$, $h_{ft,m}(o)$, and $s(o)$ are updated using the exit surface and air conditions. The new estimate of $s(o)$ are used to calculate the new exit conditions from the coil. This iteration continues until convergence is obtained on $T_{a,\infty}(o)$.

Specific Enthalpy

The specific enthalpy of the refrigerant at the evaporator outlet is estimated from:

$$h_{o,r} = h_{i,r} + \frac{\bar{h}_r A_o f_{tp}}{\dot{m}_r}(T_w - T_{tp}) \tag{4.67}$$

If, $h_{o,r}$, is greater than, $h_{r,fg}$, then:

$$h_{o,r} = h_{r,fg} + c_{p,v}(T_w - T_{r,fg})\epsilon_v \tag{4.68}$$

At the condenser outlet, the specific enthalpy is estimated from:

$$h_{o,r} = h_{i,r} + c_{p,v}(T_w - T_{in})\epsilon_v \tag{4.69}$$

where,

$$T_{in} = T_{r,fg} + \frac{(h_{i,r} - h_{r,fg})}{c_{p,v}}$$

If, $h_{o,r}$, is less than, $h_{r,fg}$, then:

$$h_{o,r} = h_{r,fg} + \frac{\bar{h}_r A_o f_{tp}}{\dot{m}_r}(T_w - T_{r,fg}) \tag{4.70}$$

If, $h_{o,r}$, is less than, h_f, then:

$$h_{o,r} = h_f + c_{f,v}(T_w - T_{r,fg})\epsilon_f \tag{4.71}$$

Refrigerant Flow Rate at Outlet

The refrigerant flow rate at the outlet of the heat exchanger is estimated from the expression:

$$\dot{m}_{o,r} = \frac{3600 \times vel \times A_c}{v_s} \tag{4.72}$$

where the velocity of the refrigerant, vel, is estimated from:

$$vel = C\sqrt{abs\,(h_i - h_s)} \tag{4.73}$$

where, C, is a constant.

EXPANSION DEVICE

The present model is capable of modeling the transient dehumidification performance of the heat pump with a TXV, a short-tube orifice, or a capillary tube as its expansion device.

TXV Model

The general model of a cross-flow TXV is a form of the equation used in ORNL model:

$$\dot{m}_r = C_{TXV}\left(\Delta T_{oper} - \Delta T_{static}\right)\left(\rho_r \Delta p_{TXV}\right)^{1/2} \tag{4.74}$$

For a cross-charged TXV valve, a given ΔT_{oper}, at a given, ρ_r, and Δp_{TXV}, will provide a certain valve opening that is independent of evaporator pressure. Most TXV valves used in high efficiency heat pumps are of the cross-charge type since such valves tend to maintain a relatively constant superheat over a range of operating conditions [ORNL, 1981]. If the actual operating superheat is greater than the maximum effective superheat, $\Delta T_{max,eff}$, where

$$\Delta T_{max,eff} = \Delta T_{static} + 1.33\left(\Delta T_{rated} - \Delta T_{static}\right) \tag{4.75}$$

then $\Delta T_{max,eff}$ is used in place of ΔT_{oper} in Eq. 4.74.

The flow coefficient, C_{TXV}, and the available pressure drop across the TXV valve, Δp_{TXV}, are estimated from:

$$C_{TXV} = \frac{\dot{m}_{r,rated}}{\left(\Delta T_{rated} - \Delta T_{static}\right)\left(\rho_{r,rated}\Delta p_{rated}\right)^{1/2}} \tag{4.76}$$

$$\Delta p_{TXV} = p_{in,TXV} - p_{in,evap} \tag{4.77}$$

Short-Tube Orifice Model

The short-tube orifice model is based on standard orifice relation given by:

$$G_r = \frac{\dot{m}_r}{A_{orifice}} = C(2g_c\rho\Delta p)^{1/2} \tag{4.78}$$

The orifice coefficient, C, is from the correlations of Mei (as reported in ORNL model [1981]). The correlations obtained were for five 0.5 in long Carrier Accurators with diameter from 0.0420 to 0.0667 in (L/D ratios from 7.5 to 11.9) using R-22 refrigerant. He observed pressure drops between 90 and 220 psi across the restrictor and levels of sub-cooling from 0 to 50 F at the inlet. The observed mass flow rates ranged from 150 to 450 lbm/hr. The correlated values of, C, with both the pressure drop across the short-tube orifice, ΔP, and the level of sub-cooling at the inlet, ΔT, is given by:

$$C_{TXV} = \begin{cases} [0.63683 - 0.019337 * (p_{in} - p_{in,evap}) + 0.06 * \Delta T] & \text{for } \Delta T \leq 40 \\ [0.9175 - 0.00325 * \Delta T] & \text{for } \Delta T > 40 \end{cases} \tag{4.79}$$

MODELING METHODOLOGY

The present model which is a modified version of the TRPUMP is programmed in FORTRAN 77 language on a digital computer. Some heat transfer subroutines from the ORNL steady state model [1981] have been adopted. The basic computational sequence will be similar to the TRPUMP model as shown in Figure 4.2. The present model as modified allows the user to specify:

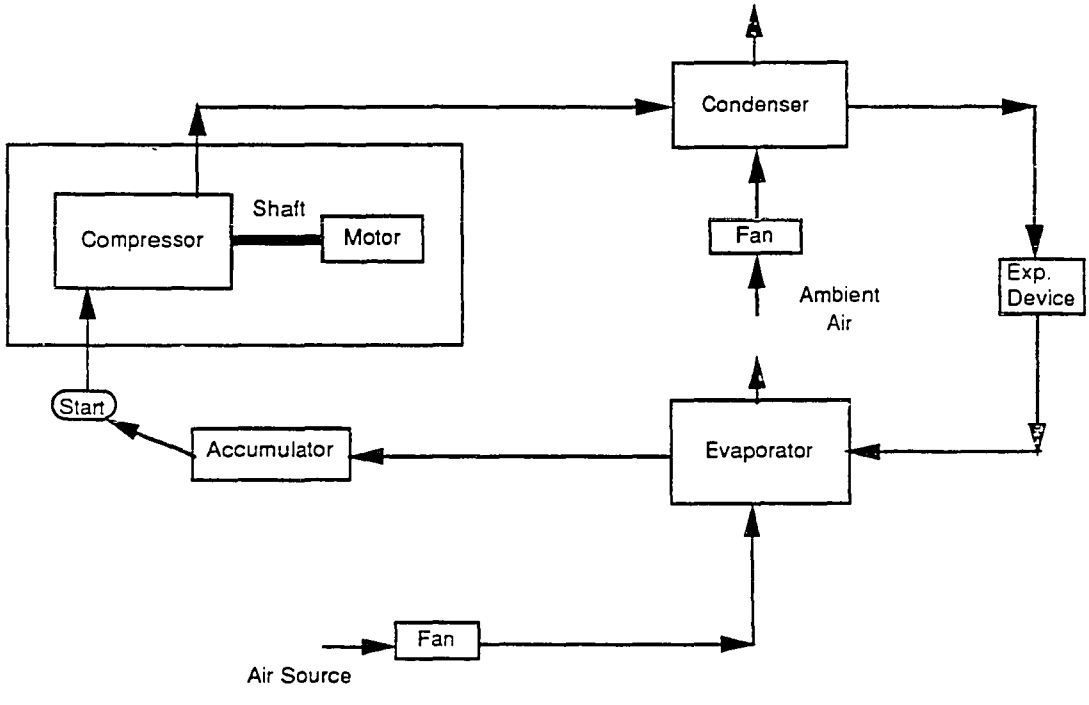

Figure 4.2 - Schematic of Computational Sequence.

- System Operating Conditions
  1. the desired indoor and outdoor air temperatures and relative humidities.
- Compressor Motor Characteristics (torque vs speed, efficiency vs speed etc.)
- Refrigerant Flow Control Devices
  1. a capillary tube,
  2. a short-tube orifice, and
  3. a thermostatic expansion valve (TXV).
- Fin-and-Tube Heat Exchanger Parameters
  1. tube size, spacing, number of rows and number of parallel circuits,
  2. fin pitch, thickness, thermal conductivity, and type (smooth, wavy, or louvered), and
  3. air flow rates at steady-state.
- Fan
  1. Input power for indoor and outdoor fans,
  2. time constant τ in sec, and
  3. steady-state flow rate.
- Initial Conditions at Start-Up

The units of the various quantities are based on the British system of measurements. The major outputs from the model include:

1. capacity and EER/COP,
2. compressor and fan power consumption,
3. sensible to total heat transfer ratio,
4. outlet dry- and wet-bulb temperatures, and
5. various pressure drops in the system.

The program contains modules to simulate: (i) electric motor/shaft (ii) hermetic vapor compression refrigerant compressor, (iii) fan, (iv) condenser, (iv) expansion device (TXV, and orifice) and (vi) evaporator. In addition to the major modules the program contains several subprograms:

a. For calculating refrigerant properties and air/water psychrometry.

b. For calculating single- and two-phase fluid, heat, mass and momentum

transfer, including evaporation and condensation inside the tubes.

A number of inputs are required to simulate a heat pump performance. Some of the important inputs are described in this section, and the rest of them are listed in Appendices A and B. Appendix A lists all the constants and Appendix B lists the variables that need initialization at the start of the simulation.

The compressor model used in TRPUMP can simulate overall performance of hermetic vapor compression refrigerant compressor. Inputs to the compressor model in addition to the constants and initial conditions are refrigerant mass flow rate at the inlet, and pressure at the outlet port and motor speed. Outputs from the module are: refrigerant pressure at inlet, flow rate and specific enthalpy at outlet.

The inputs required for the condenser and evaporator models, besides the heat exchanger parameters, are: inlet air flow rate, temperature and humidity ratio, inlet refrigerant flow rate and specific enthalpy, and refrigerant pressure at outlet. The output from the models include: state variables, air temperature and humidity ratio at outlet, the refrigerant pressure at the inlet, the refrigerant flow rate and specific enthalpy at outlet. The block diagram outlining the heat exchanger algorithm, refrigerant side heat transfer calculation and the dehumidification algorithm are shown in Figures 4.3 – 4.4, respectively.

Each component in the system is considered as a discrete control-volume and the properties in each of the control-volumes are lumped. The governing differential equations for continuity, and energy, along with the equations of state, are solved for each control-volume. The updated values of the heat pump variables (u_i, v_i, h, T,$\dot{m}$, etc.) are obtained by numerical integration

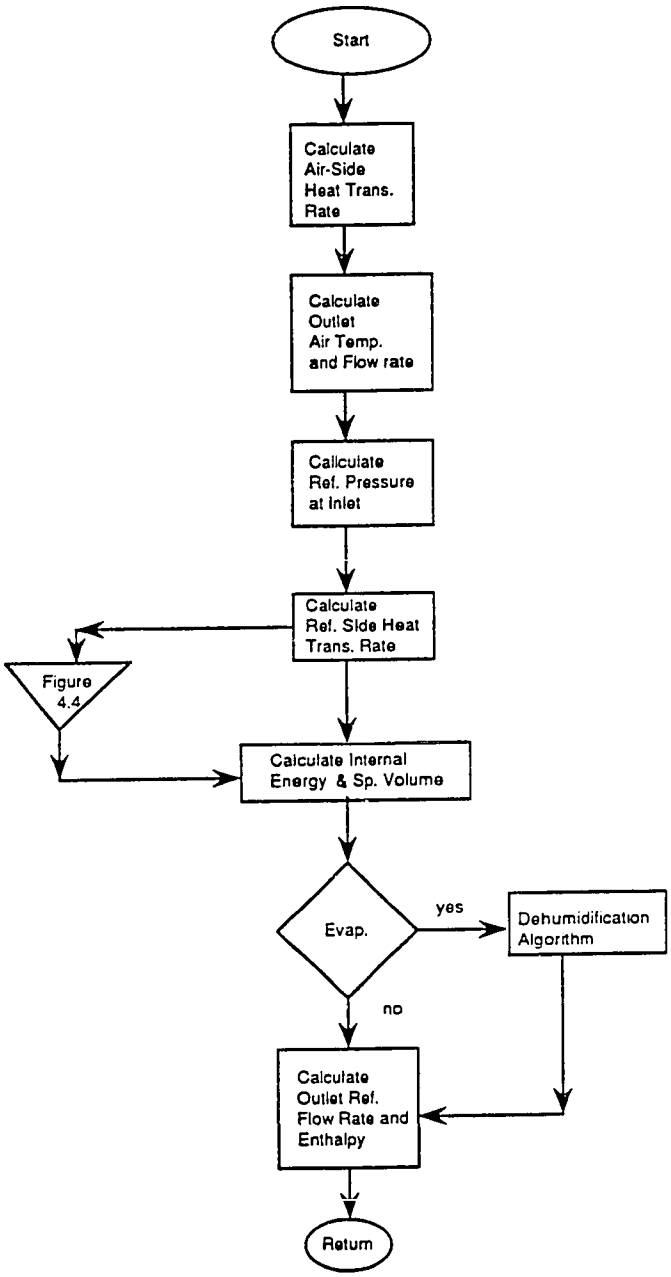

Figure 4.3 – Flow Chart of the Heat Exchanger Module.

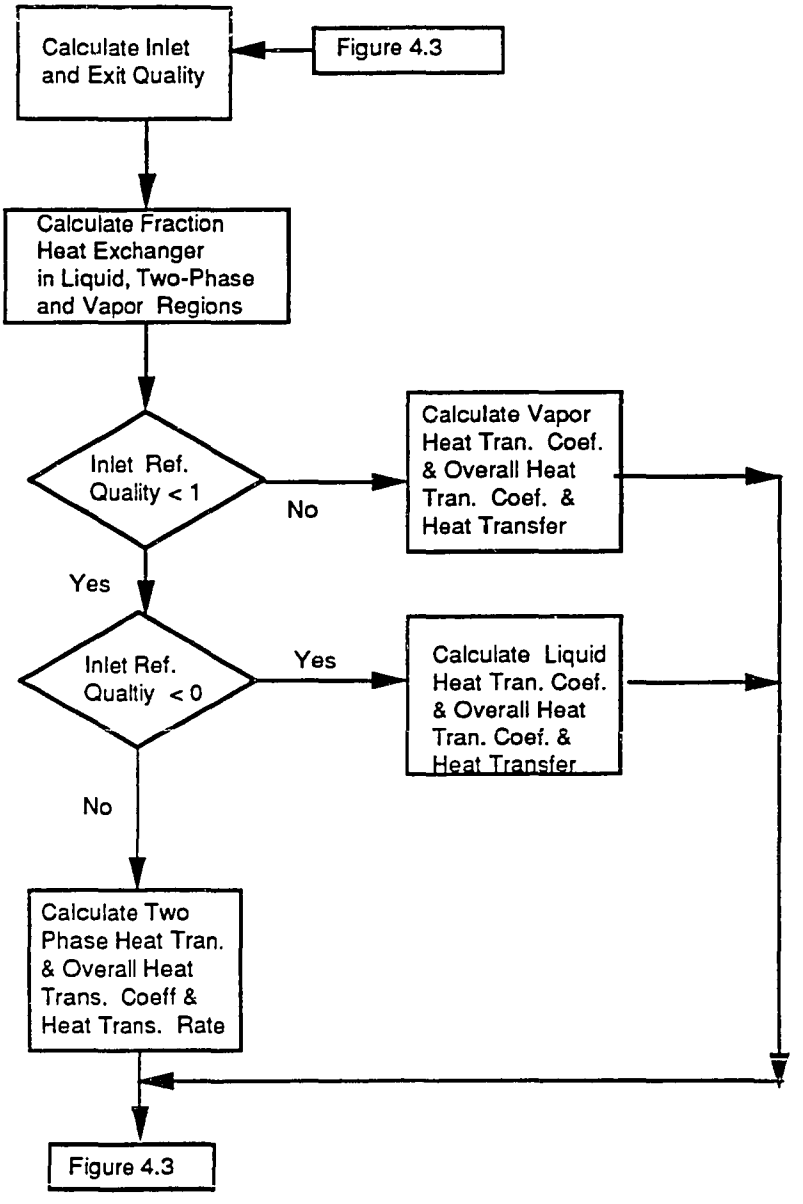

Figure 4.4 - Flow Chart of the Refrigerant-Side Heat Transfer.

with time.

The simulation starts with the initialization of the independent variables and reading of input data. There is one single subroutine which handles all the inputs and assigns them to the common blocks for each of the component modules. The simulation of the transient cycle starts with the hermetic positive displacement compressor. Low pressure refrigerant vapor enters the compressor/shaft/motor container and exits as high pressure vapor, which then goes to an air cooled condenser. The condensed refrigerant expands across a thermostatic expansion valve which controls the mass flow to maintain a constant superheat at the evaporator exit. The liquid refrigerant enters the evaporator and is vaporized by the air flowing across the coil. The low pressure refrigerant vapor from the evaporator enters the compressor through the accumulator. This process is repeated for each time step until the end of the simulation is reached. Both the condenser and the evaporator are cross-flow type of heat exchangers.

There are several numerical methods available for solving the governing differential equations: the Euler method, the fourth-order Runge-Kutta (RK) method, and the Adams-Bashforths predictor method. The TRPUMP model utilized the Euler method which employs a Taylor series expansion truncated after the first derivative. Although the Euler method is simple, its accuracy is limited and small time steps must be used to maintain stability. Other methods were investigated and the fourth-order RK method was selected for the numerical integration of the differential equations. The RK method was selected because it requires only knowledge of y_i to determine y_{i+1}. However, repeated determination of $f(x,y)$ results in less efficiency with respect to

computing time than other methods of comparable accuracy (Euler Predictor-Corrector, Adams, Milne, etc.).

SUMMARY OF MODIFICATIONS TO TRPUMP MODEL

A number of modifications were made to the TRPUMP model including:

a. The entire program has been reorganized into a more modular format so that it will be readily adapted to specific needs of a researcher. Therefore, it is easy to modify an individual module to make improvements, or replace a component with another, or added modules to increase system analysis capability. As a part of modularization of the program, all the inputs and outputs are handled by two routines. Parameters which are derivatives of more fundamental parameters (for example, cross-sectional area of a pipe can be calculated given the diameter of the pipe) are calculated within the input module.

b. Three new modules have been added to simulate the condenser, the evaporator and an expansion device. The evaporator module can now estimate sensible and latent capacities with better accuracy. The model can either use a TXV or an orifice as the expansion device.

c. The routines that were adopted from the TRPUMP and ORNL models were structured by replacing the unconditional transfer statements (such as GOTO) with conditional statements (such as IF ··· THEN ··· ELSE), to improve computational efficiency.

d. The accuracy was also improved by incorporating double precision.

e. Finally, a more accurate RK method for numerical integration was used in place of the existing Euler's method.

CHAPTER V

EXPERIMENTAL METHODOLOGY

There are a number of variables which affect the transient dehumidification performance of a heat pump: (i) the indoor dry- and wet-bulb temperatures, (ii) the outdoor dry-bulb temperature, (iii) cycling and percent ON-time, and (iv) the distribution of the refrigerant charge in the system. In this study, items (i), (ii), and (iii) are investigated.

A procedure for measuring variables was established to ensure the repeatability and reliability of the test data. The procedure followed for experimental tests and the tests performed are described below.

TESTING PROCEDURE

The first step of the testing procedure was to set the system refrigerant charge according to criteria specified by the manufacturer of the heat pump. The charge was set while the heat pump was operating in the cooling mode with an indoor dry-bulb temperature and humidity of 80 F and 50%, respectively, and an outdoor dry-bulb temperature of 95 F. The refrigerant charge was adjusted to obtain a 12 F sub-cooling of refrigerant leaving the outdoor coil.

The steady-state and cyclic tests recommended by the Department of Energy (DOE) were then run. The DOE test procedure calls for four tests: A, B, C and D. A and B are steady state wet coil tests, and are used to determine the influence of outdoor temperature on energy consumption and cooling capacity. C is a steady state dry coil test and D is a cyclic dry coil test which is used to determine the effect of cyclic performance. Test A

is used to determine the rated capacity and tests B, C, and D are used to determine the SEER of the unit.

For all tests, the psychrometric rooms were operated for more than one hour to allow the rooms and the equipment inside them stabilize to the pre-set conditions before initiating a test run. Rooms were always maintained within the tolerance prescribed by the ASHRAE Standard [1983]. For steady-state tests, the heat pump was operated for more than 30 minutes until equilibrium conditions were attained in the rooms. Data was then recorded at ten-minute intervals until four consecutive sets of readings were within the tolerance prescribed by the ASHRAE Standard [1983]. For cyclic tests, three complete cycles were run to allow for consecutively repeatable cycles. As prescribed in the test procedure, all cyclic tests except for the last cycle of a test were run with continuous indoor fan operation (i.e., during both the ON and OFF-cycles).

The cooling capacity was measured by two methods: indoor air enthalpy and the refrigerant enthalpy. All measurements and calculations were in compliance with the ASHRAE Standard [1983]. The air-side capacity is the sum of the latent and sensible capacities based on the indoor side test data and is estimated from the following equations:

$$\dot{q}_s = \frac{60 * Q_a c_{p,a} \left(T_{i,a} - T_{o,a}\right)}{\left[v_n'(1 + w_n)\right]} \tag{5.1}$$

$$\dot{q}_l = \frac{63600 * Q_a \left(w_{i,a} - w_{o,a}\right)}{\left[v_n'(1 + w_n)\right]} \tag{5.2}$$

$$\dot{q}_t = \dot{q}_l + \dot{q}_s = \frac{60 * Q_a \left(h_{i,a} - h_{o,a}\right)}{\left[v'_n(1 + w_n)\right]} \tag{5.3}$$

where,

$c_{p,a} = 0.24 + 0.44 w_n$,

Q_a = air flow rate through the coil, ft^3/min

v'_n = specific volume of the air at the nozzle conditions

The refrigerant side heat transfer is calculated from the following equation:

$$\dot{q}_r = \dot{m}_r (h_{i,r} - h_{o,r}) \tag{5.4}$$

where,

$\dot{m}_r$ = ref. flow rate, lbm/hr

$h_{i,r}$ = enthalpy of refrigerant entering the evaporator coil, Btu/hr

$h_{o,r}$ = enthalpy of refrigerant leaving the evaporator coil, Btu/hr

The steady-state energy efficiency ratio of the test unit is determined by the following equation:

$$EER_{ss} = \frac{\dot{q}_t}{E_t} \tag{5.5}$$

Appendix C provides details of the algorithms used to calculate refrigerant and air properties from pressure and temperature data. The total cyclic capacity, $q_{t,cyc}$, is the sum of the cyclic sensible and latent capacities:

$$q_{t,cyc} = q_{s,cyc} + q_{l,cyc} = \overbrace{\frac{60Q_a c_{pa}\Gamma}{[v'_n(1+w_n)]}}^{\text{Cyclic Sensible}} + \overbrace{\frac{63600Q_a\Theta}{[v'_n(1+w_n)]}}^{\text{Cyclic Latent}} \qquad (5.6)$$

where Γ and Θ are:

$$\Gamma = \int_{t_{on}}^{t_{off}} [T_{i,a}(t) - T_{o,a}(t)]\, dt$$

$$\Theta = \int_{t_{on}}^{t_{off}} [w_{i,a}(t) - w_{o,a}(t)]\, dt$$

The EER_{cyc} is the ratio of the cyclic capacity and the cyclic energy consumption and SHR_{cyc} is the ratio of the cyclic sensible capacity to the total cyclic capacity.

EXPERIMENTAL TESTS

A series of tests was run to investigate the influence of the percent ON-time and cycling rate on the transient performance of the heat pump. For these tests, the indoor and outdoor dry-bulb temperatures were set at 80 F and and 95 F, respectively, and indoor relative humidity at 50%. The test runs included three different percent ON-times and seven different cycling rates (Table 5.1).

The next set of tests investigated the influence of relative humidity (20 – 67%) on the transient cooling performance of the heat pump. For these tests, the indoor and outdoor dry-bulb temperatures were set at 78 F and 93 F, respectively. The test runs included three different percent ON-times 20, 50 and 80%, and two different cycling rates, 1.8 and 3 cycles per hour (Table 5.2).

A series of tests was run to investigate the influence of indoor dry-bulb temperature on the transient performance of the heat pump. The tests in-

Table 5.1 – Tests with Varying Percent ON-Times and Cycling Rates.

Test	ON-Time (%)	Cycling Rate (cph)	Indoor Temp. (F)	Outdoor Temp. (F)	Indoor Rh (%)
1	80	4.0	80	95	50
2	80	2.4	80	95	50
3	80	0.8	80	95	50
4	50	10.	80	95	50
5	50	6.0	80	95	50
6	50	2.0	80	95	50
7	50	1.0	80	95	50
8	20	4.0	80	95	50
9	20	2.4	80	95	50
10	20	1.2	80	95	50
11	20	0.8	80	95	50

cluded: one at constant indoor relative humidity (50%) and another at constant indoor dew-point temperature (58 F). The outdoor dry-bulb temperature was held constant at 93 F. Two different percent ON-times and two different cycling rates were used (Table 5.3 and 5.4).

To obtain results which would reflect actual operation of a heat pump in a residence, a relationship between the percent ON-time and the cycling rate of a typical residential thermostat and the percent ON-time and the outdoor dry-bulb temperature was needed. A standard relationship between percent ON-time and cycling rate used by the National Electrical Manufacturers Association (NEMA) is shown in Figure 5.1 [NEMA, 1972]. According to NEMA, a typical residential thermostat cycles three times per hour when it is ON for 50% of the time and 1.8 times per hour when it is ON for 20% or 80% of the time.

One method of estimating the percent ON-time is by calculating the ratio

Table 5.2 – Test with Varying Indoor Relative Humidity.

Test	ON-Time (%)	Cycling Rate (cph)	Indoor Temp. (F)	Outdoor Temp. (F)	Indoor RH (%)
1	80	0.8	78	93	20
2	50	3.0	78	93	20
3	20	0.8	78	93	20
4	80	0.8	78	93	30
5	50	3.0	78	93	30
6	20	0.8	78	93	30
7	80	0.8	78	93	35
8	50	3.0	78	93	35
9	20	0.8	78	93	35
10	80	0.8	78	93	40
11	50	3.0	78	93	40
12	20	0.8	78	93	40
13	80	0.8	78	93	45
14	50	3.0	78	93	45
15	20	0.8	78	93	45
16	80	0.8	78	93	50
17	50	3.0	78	93	50
18	20	0.8	78	93	50
19	80	0.8	78	93	55
20	50	3.0	78	93	55
21	20	0.8	78	93	55
22	80	0.8	78	93	62
23	50	3.0	78	93	62
24	20	0.8	78	93	62
25	80	0.8	78	93	67
26	50	3.0	78	93	67
27	20	0.8	78	93	67

of the cooling load in the conditioned space to the rated heat pump cooling capacity. The cooling load is related to the outdoor dry-bulb temperature. Therefore, the cooling load at various outdoor temperatures can be estimated using a load simulation program. The cooling load for a typical residence [Katipamula et al., 1988] with indoor dry-bulb set point temperature of 78 F and indoor relative humidity at 50% was estimated for various outdoor dry-

Table 5.3 - Tests with Varying Indoor Dry-Bulb Temperature and Constant Indoor Relative Humidity.

Test	ON-Time (%)	Cycling Rate (cph)	Indoor Temp. (F)	Outdoor Temp. (F)	Indoor RH (%)
1	80	0.8	80	93	50
2	50	3.0	80	93	50
3	80	0.8	78	93	50
4	50	3.0	78	93	50
5	80	0.8	76	93	50
6	50	3.0	76	93	50
7	80	0.8	74	93	50
8	50	3.0	74	93	50
9	80	0.8	72	93	50
10	50	3.0	72	93	50

Table 5.4 - Tests with Varying Indoor Dry-Bulb Temperature and Constant Indoor Dew-Point Temperature.

Test	ON-Time (%)	Cycling Rate (cph)	Indoor Temp. (F)	Outdoor Temp. (F)	Indoor Dew-Point (F)
1	80	0.8	80	93	58
2	50	3.0	80	93	58
3	80	0.8	78	93	58
4	50	3.0	78	93	58
5	80	0.8	76	93	58
6	50	3.0	76	93	58
7	80	0.8	74	93	58
8	50	3.0	74	93	58
9	80	0.8	72	93	58
10	50	3.0	72	93	58

bulb temperatures using commercially available software TRNSYS (TRaNsient SYstem Simulation) [Klein, et al., 1983]. The rated capacity of the test unit

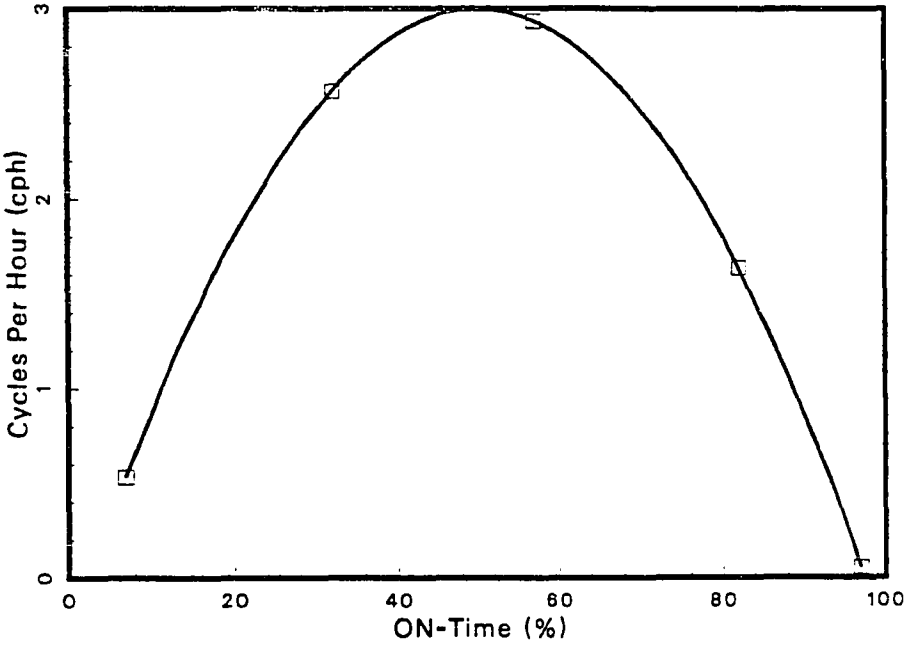

Figure 5.1 – Typical Residential Thermostat Cycling Rate (NEMA).

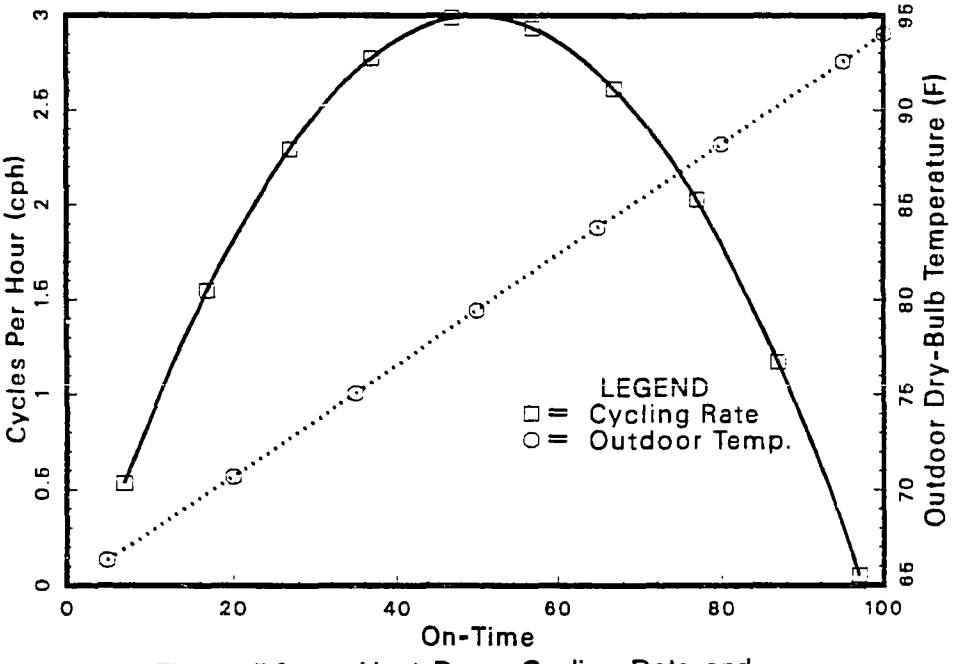

Figure 5.2 – Heat Pump Cycling Rate and Outdoor Temperature vs Percent ON-Time.

was 3 tons. The relationship between the percent ON-time and outdoor dry-bulb temperature is super imposed on Figure 5.1 and shown in Figure 5.2. Selecting an outdoor temperature fixes the percent ON-time of the unit, and thereby the the cycling rate. A series of tests at various outdoor temperatures (Table 5.5) was run. The indoor temperature and relative humidity for these test were set at 78 F and 50%, respectively.

Table 5.5 - Tests with Varying Outdoor Dry-Bulb Temperature.

Test	ON-Time (%)	Cycling Rate (cph)	Indoor Temp. (F)	Outdoor Temp. (F)	Indoor RH (%)
1	95	0.8	78	100	50
2	95	0.8	78	95	50
3	85	1.25	78	90	50
4	70	2.50	78	85	50
5	60	3.00	78	82	50

DEFINITION OF TERMINOLOGY

A number of variables are used in the literature to quantify the transient performance of a heat pump. These include: the cyclic energy efficiency ratio (EER_{cyc}), the part load factor (PLF), the cooling load factor (CLF) and the degradation coefficient (C_D). The EER_{cyc} is the ratio of the cyclic heat removal rate from the conditioned space (Btu/hr) to the cyclic energy input (Watts). A non-dimensional parameter which is widely used to compare the steady-state and cyclic efficiency is the part load factor (PLF). It is a ratio of the cyclic energy efficiency and the steady-state energy efficiency. Since it is non-dimensional, it can be used to compare the cyclic performance under

varying test conditions. This variable was used extensively in this study to compare the cyclic performance.

In 1979, the Department of Energy (DOE) amended its test procedures for rating central air-conditioners to include a rating methodology for heat pumps, and to modify the existing testing procedures. The major modification of the amendment was inclusion of cyclic testing. The new procedure called for seasonal ratings which would account for the cyclic losses during the part load operation of the conditioning units. To estimate the seasonal energy efficiency ratio (SEER) the test procedure prescribed two options: (i) use the cyclic dry coil test (Test C,D) directly, or (ii) assume a degradation coefficient and calculate the PLF. In doing so, the test procedure assumed that (1 - PLF) varied linearly with (1 - CLF) and the slope of this relationship was assumed to be independent of the other variables (ON-time, ambient conditions, etc.,). This slope was called the coefficient of degradation (C_D):

$$C_D = \frac{\left[1 - \frac{EER_{cyc}}{EER_{ss}}\right]}{1 - CLF} \tag{5.7}$$

The test procedure assigned a value of 0.25 for C_D if the manufacturers preferred to avoid cyclic testing. Given C_D the PLF and SEER can be estimated for a given CLF. In Eq. 5.7 CLF (cooling load factor) is a ratio of total cyclic cooling during the specified ON-time to the steady-state cooling over the entire cycle (ON + OFF) at constant ambient conditions:

$$CLF = \frac{q_{t,cyc}}{\dot{q}_{ss}\left(t_{on} + t_{off}\right)} \tag{5.8}$$

It captures the effects due to part load operation and percent ON-time on the cooling capacity.

CHAPTER VI

BASE-CASE STEADY-STATE AND CYCLIC TESTS

To compare the steady-state results with those from the manufacturer a base case steady-state test was run. In addition, the transient characteristics of a typical cyclic test were analyzed.

STEADY-STATE TEST RESULTS

The DOE Test A was run to compare the experimental results with those from the manufacturer. The indoor and outdoor rooms were maintained at 80 and 95 F, respectively. The indoor relative humidity was maintained at 50% and the air flow rate was 1200 cfm. The indoor and outdoor dry-bulb and the indoor relative humidity profiles for Test A are shown in Figure 6.1. The changes in the temperatures at steady-state condition are within the tolerance prescribed by the ASHRAE Standard [1983] (within 2 F for dry-bulb temperature and 1 F for the dew-point temperature).

The total instantaneous cooling capacity obtained from the air-enthalpy and refrigerant enthalpy calculation varied less than five percent during cooling operation (Figure 6.2). This agreement was within the ASHRAE test standard requirements [1983] and was observed in all test data that were retained during the current experimentation. Only air-side measurements were used to characterize the capacity of the various tests. The average performance characteristics for the base case steady-state Test A are shown in Table 6.1. The steady-state results compared well with the manufacturer's data (within 4%).

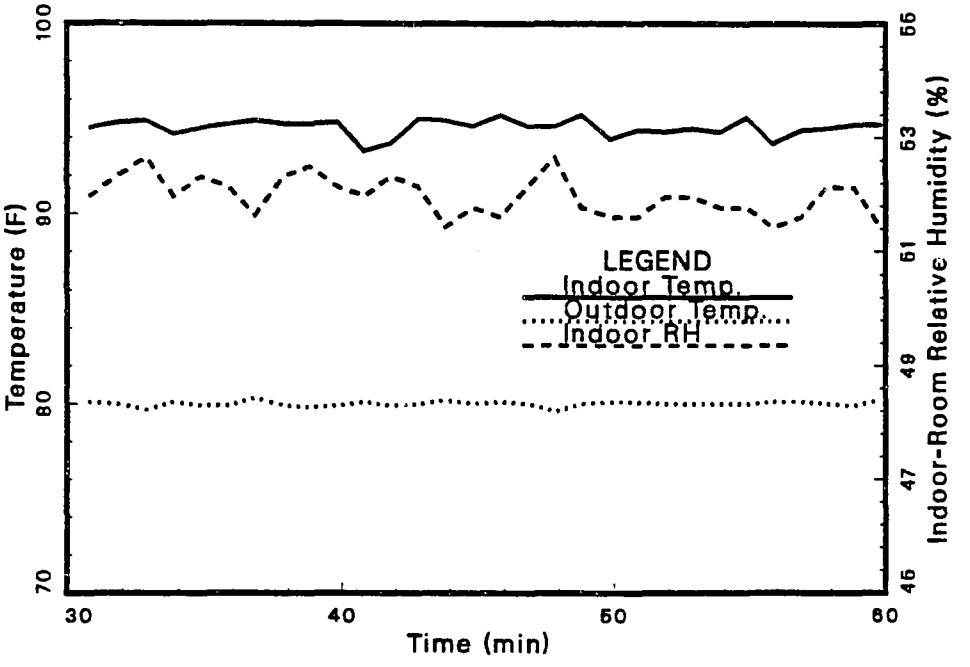

Figure 6.1 – Psychrometric Room Characteristics for a Steady-State Test.

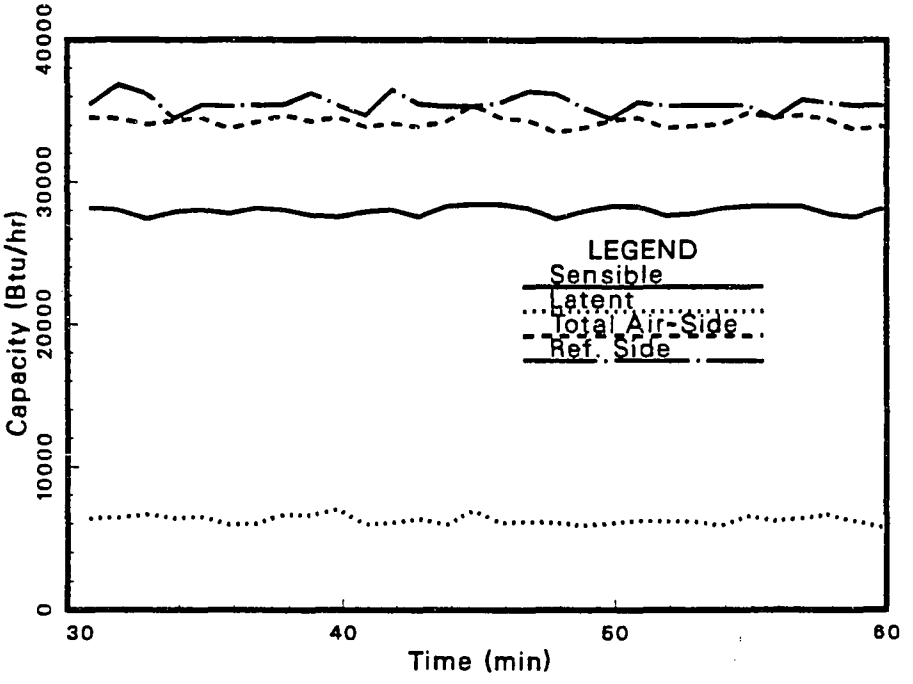

Figure 6.2 – Comparison of Air-Side and Refrigerant-Side Capacities.

Table 6.1 – Average Performance Characteristics for Base-Case Steady-State Test A.

Mass Flow Rate (lbm/min)	AIR-SIDE			REF. - SIDE	Power† Consumption (kW)	EER
	Latent Capacity (Btu/hr)	Sensible Capacity (Btu/hr)	Total Capacity (Btu/hr)	Total Capacity (Btu/hr)		
8.25	6,699	28,899	35,598	34,793	3.18	11.2

†(Compressor + Outdoor Fan)

CHARACTERISTICS OF TRANSIENT RESPONSE

The overall performance of the heat pump operating in cycles can be characterized by measuring total cyclic capacity, total cyclic energy consumption, time required to reach steady-state, cyclic energy efficiency ratio (EER_{cyc}). In addition to overall system performance, the details of the transient refrigerant and the air-side dynamics must be analyzed carefully to completely understand the transient behavior of the heat pump. The air-side dynamics can be studied by measuring the temperature drop and moisture removal rate across the evaporator coil.

The results for a typical cyclic test (T9M10) are described below. The integrated average room conditions for the cyclic test are shown in Table 6.2 and the room conditions are shown in Figure 6.3. The deviation of the room conditions from the set-point were within the tolerance prescribed by the ASHRAE Standard [1983]. After completion of two ON/OFF cycles, data were collected for the third cycle.

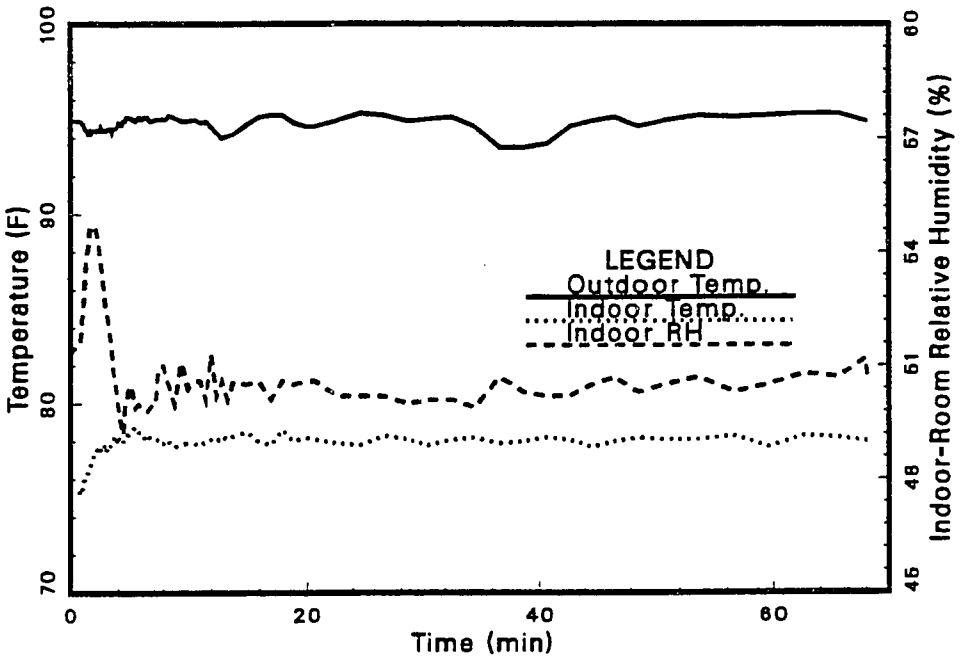

Figure 6.3 – Psychrometric Room Characterisitics for a Cyclic Test.

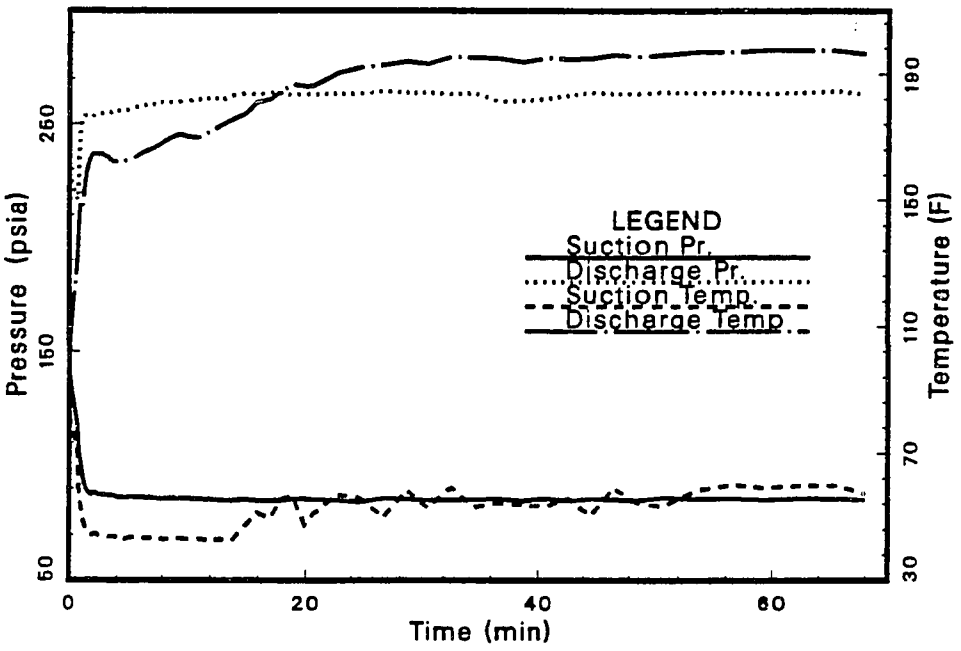

Figure 6.4 – Compressor Suction and Discharge Pressure and Temperature.

Table 6.2 - Integrated Average Room Conditions for the Typical Cyclic Test.

Indoor Dry-Bulb (F)	Indoor Relative Humidity (%)	Outdoor Dry-Bulb (F)
78.03 (78)†	50.53 (50)†	94.82 (95) †

† Set-Point

At startup, the compressor reached steady-state speed almost instantaneously. Therefore, the suction and discharge pressures approached the steady-state values quickly (Figure 6.4). The refrigerant in the evaporator at startup was saturated. The sudden drop in the suction pressure caused two phenomena. First, the refrigerant began to flash within the evaporator. This vaporization rapidly cooled the evaporator. This phenomenon was characterized by the rapid increase in sensible capacity during the first 75 to 90 seconds after start-up (Figure 6.5). The figure also showed the rate of moisture removal across the evaporator coil. Since two cycles were run before data were collected, the evaporator coil collected moisture at the end of the second cycle and was also at a lower temperature than the indoor room at the time of startup. Therefore, the moisture removal is negative at startup due to moisture being blown from the wet evaporator coil into the air stream.

The second phenomenon was the buildup of liquid refrigerant in the accumulator during startup. This can be seen by studying the surface temperatures of the accumulator and the compressor (Figure 6.6). A sharp

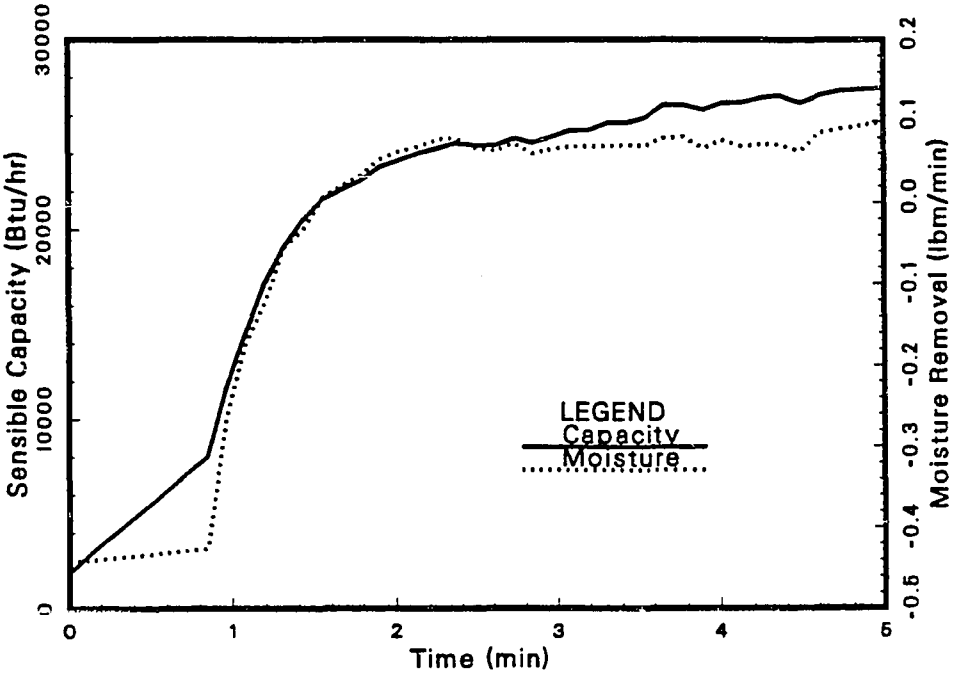

Figure 6.5 – Sensible Capacity and Moisture Removal Across the Evaporator Coil.

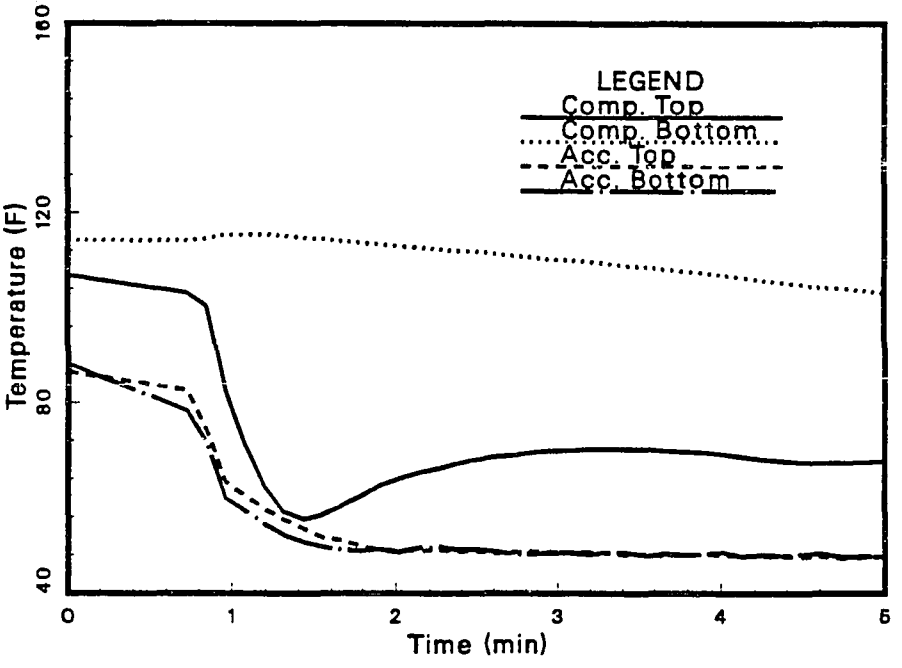

Figure 6.6 – Accumulator and Compressor Surface Temperatures.

drop in the compressor shell temperature indicated that a portion of the liquid refrigerant from the accumulator probably reached the compressor and boiled inside the shell. Any liquid that reached the accumulator and/or the compressor was lost temporarily for cooling purposes, and contributed to the cycling losses.

After an initial spike, the power drops to about 3 kW and quickly rose again (Figure 6.7). The rise in the power consumption corresponded to the liquid reaching the compressor shell. The second peak in power occurred a few seconds after the last of the liquid in the shell boiled. The compressor shell temperature steadily dropped during this time. The surface temperature lagged behind the power because of the capacitance effect of the compressor. The power increased because of the increase in mass flow. Once the liquid in the shell boiled, the compressor began to pull down the low side pressure. As the low-side pressure dropped, so did the suction vapor density and, hence, compressor power decreased. The refrigerant mass flow rate increased rapidly because the thermal expansion valve (TXV) was completely open for the first 60 seconds and then gradually levelled off.

After a linear increase for the first 45 seconds, the sensible capacity rose rapidly because of flashing of the refrigerant in the evaporator (Figure 6.8). The latent capacity was negative after startup because of moisture evaporation from the wet evaporator coil into the supply air stream. It took almost 90 seconds before dehumidification began to occur (Figure 6.8). It took almost 15 minutes for the total capacity to approach the steady-state (Figure 6.9).

At startup, much of the liquid refrigerant is transferred into the accumula-

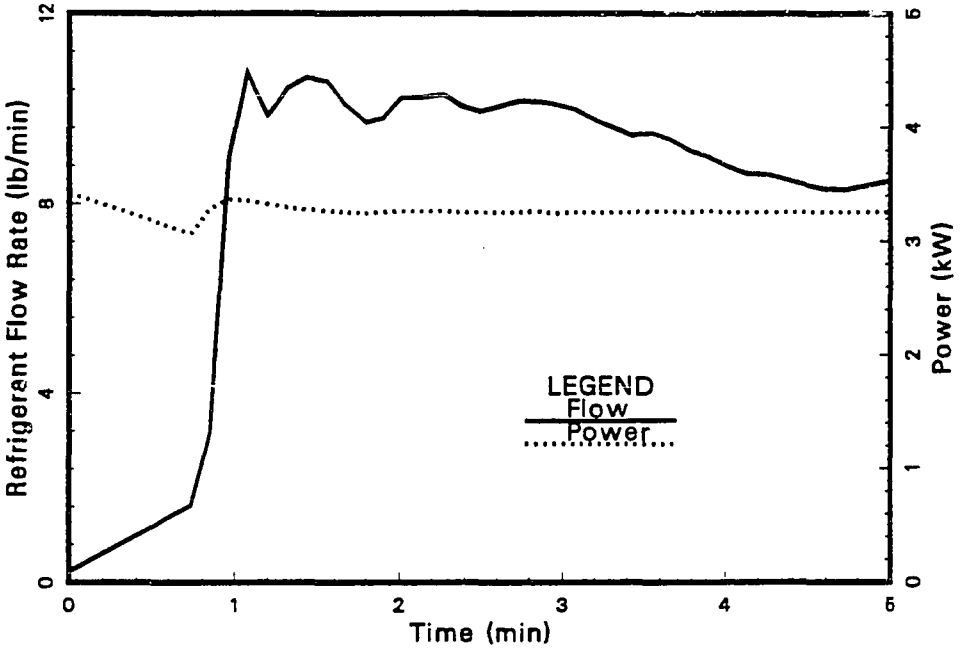

Figure 6.7 – Refrigerant Mass Flow Rate and Power Consumption.

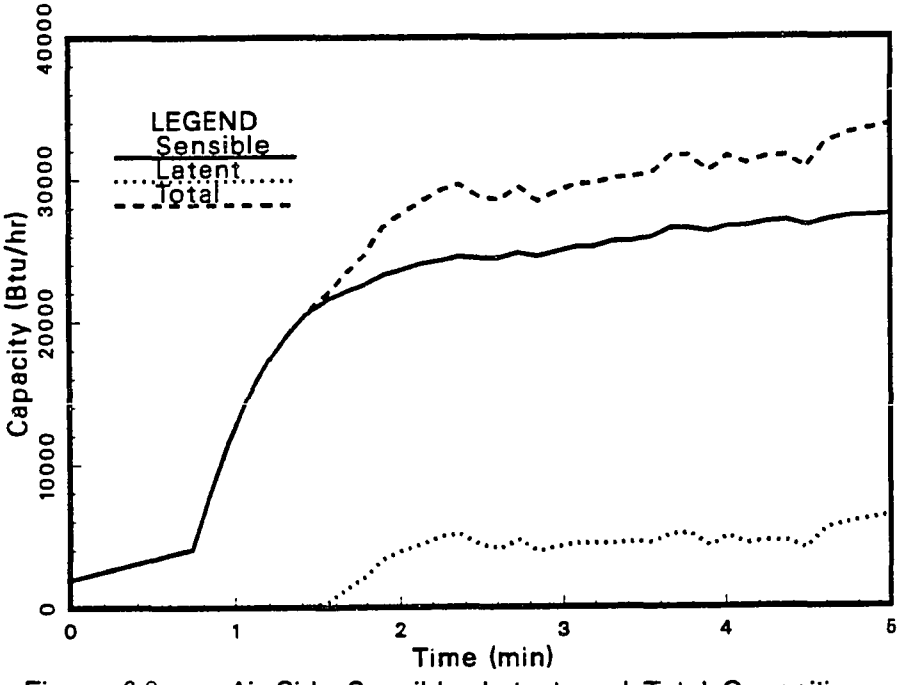

Figure 6.8 – Air-Side Sensible, Latent, and Total Capacities.

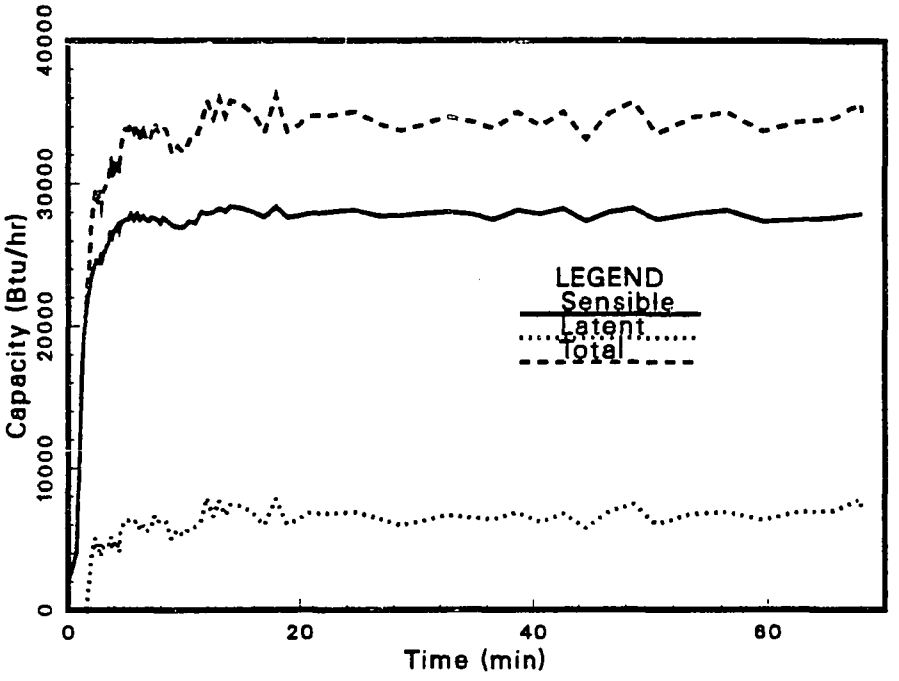

Figure 6.9 – Air-Side Sensible, Latent and Total Capacities 0–70 Minutes.

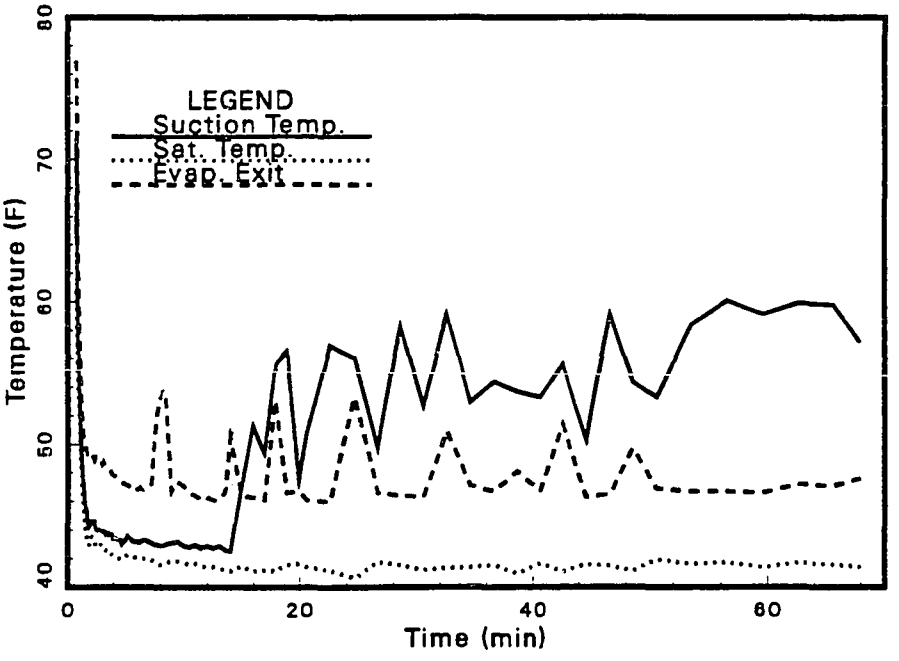

Figure 6.10 – Evaporator Exit, Compressor Suction and Saturation Temperatures.

tor. The accumulator had two sight glasses for monitoring refrigerant levels in the accumulator. Immediately after start-up (30 to 45 seconds), the accumulator was filled with liquid refrigerant (viewed through the watch glasses). It took about 15 minutes after start-up for all the liquid refrigerant in the accumulator to boil off. Since it took 15 minutes for all the refrigerant to vaporize, the cooling capacity did not reach steady-state until that time. This characteristic can be noted, as seen in Figure 6.10, by observing the suction temperature which is measured immediately downstream of the accumulator (location 20) and the saturation temperature corresponding to the suction pressure at the same location (47). For the first two minutes, the suction temperature was almost the same as the saturation temperature, and it closely followed the saturation temperature for about 14 minutes. The third curve in the Figure 6.10 was the refrigerant temperature at the exit of the evaporator coil which was upstream of the accumulator (location 24). The fluctuation of the evaporator exit temperature was not evident at the suction port until 14 minutes after start-up. Because the accumulator had saturated refrigerant, in it, the vapor coming out of the evaporator for the first 14 minutes, was cooled and probably partially condensed. The fluctuations in the evaporator exit temperature was probably due to "hunting" (successive under or over correction) of the TXV.

The sub-cooling at the entrance of the expansion device, the superheat at the exit of the evaporator and the refrigerant mass flow rate are shown in Figure 6.11. It took almost 15 minutes to achieve the steady-state sub-cooling level (11 F). The superheat at the exit fluctuated between 1.5 F and 8 F, with an average superheat of 4 F. The fluctuation was because of hunting of the TXV. Hunting was also responsible for fluctuation in the refrigerant mass

flow rate. However, the peaks of the flow rate laged behind the peaks of the superheat. The pressure drop across the expansion device increased for the first 15 minutes and then remained almost constant (Figure 6.12). At steady-state, the pressure drops in the condenser and evaporator were 3 and 16 psi, respectively (Figure 6.12).

The integrated cyclic cooling capacity and the energy consumption were obtained by a numerical integration of the instantaneous values over the time of the cycle. The integrated power and capacity were then used to estimate the EER_{cyc} (Table 6.3).

The deviation of the cyclic performance data from the steady-state performance is shown in Table 6.4. The values in the table are normalized with the expected steady-state values.

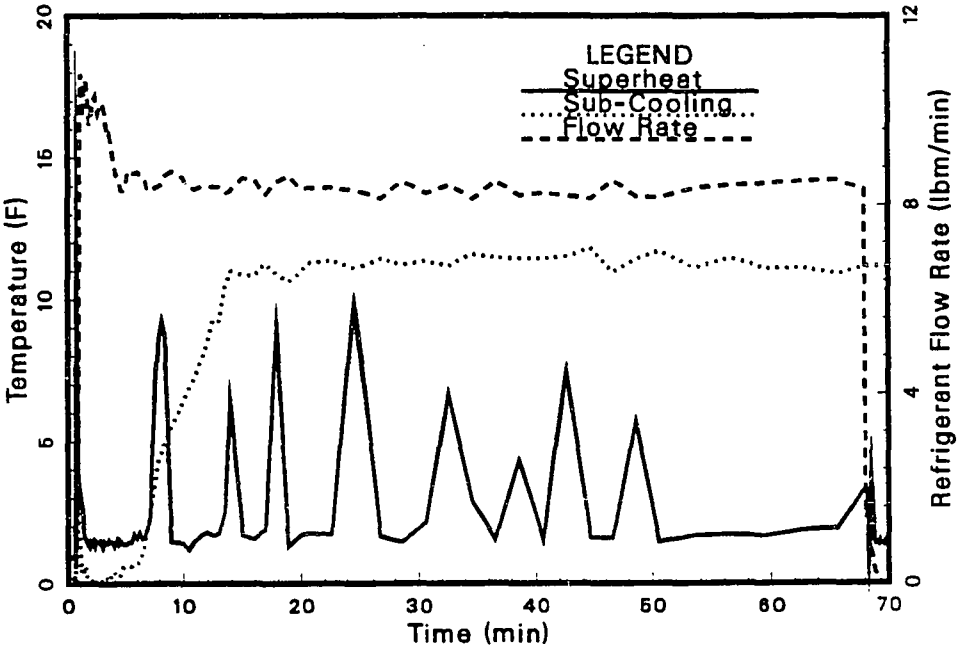

Figure 6.11 – Superheating and Sub-Cooling Characteristics.

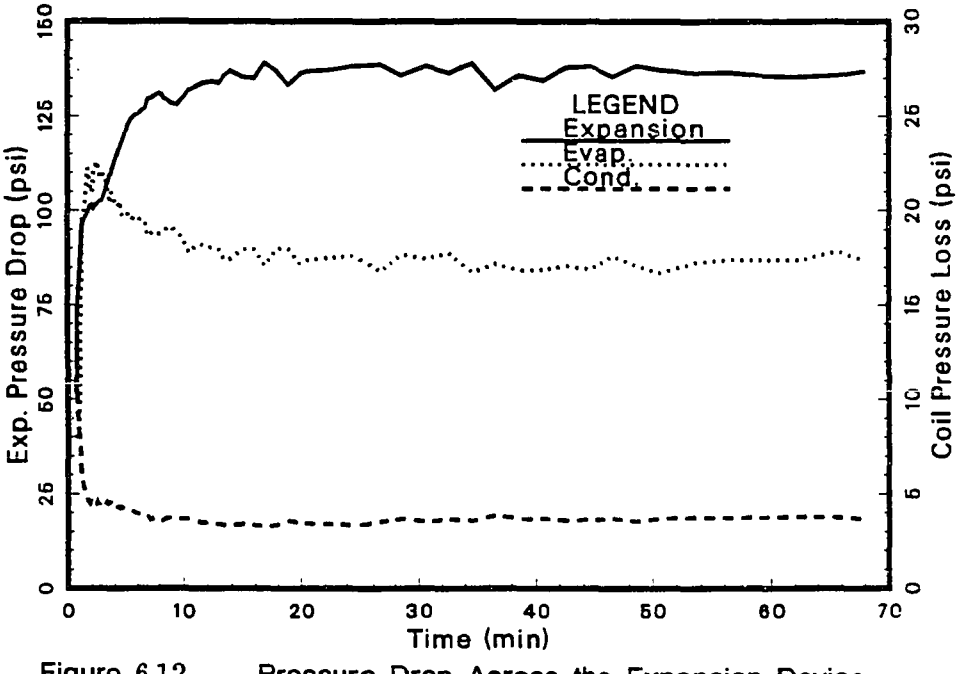

Figure 6.12 – Pressure Drop Across the Expansion Device and Pressure Loss in Evaporator and Condenser Coils.

Table 6.3 - Cyclic Performance Characteristics for T9M10.

Mass Flow Rate (lbm/min)	AIR-SIDE			Energy† Consumption (kW-hr)	Cycle Time (min)	EER
	Latent Capacity (Btu)	Sensible Capacity (Btu)	Total Capacity (Btu)			
8.41	7,178	30,903	38,081	3.72	67.5	10.24

Table 6.4 - Deviation of Cyclic Performance From the Steady-State.

Mass Flow Rate	AIR-SIDE			Energy† Consumption	C_D	EER
	Latent Capacity	Sensible Capacity	Total Capacity			
1.01	0.943	0.989	0.980	1.01	0.245	0.971

† (Compressor + Outdoor Fan)

CHAPTER VII

EXPERIMENTAL RESULTS

There are a number of variables which affect the transient performance of a heat pump. In this study, five variables were indentified as the most important for understanding the transient behavior: the indoor and outdoor dry-bulb temperatures, indoor relative humidity, percent ON-time and thermostat cycling rate. The influence of these five variables on the transient performance was investigated. To isolate the effect of those variables on the cyclic cooling performance of the heat pump, a parametric study was conducted by varying one parameter and keeping the others constant. The base values of the variables for the parametric study were: (i) indoor dry-bulb temperature of 78 F, (ii) indoor relative humidity of 50%, (iii) outdoor dry-bulb temperature of 93 F and (iv) indoor flow rate of 1200 cfm. The percent ON-times and cycling rates were based on a standard relationship developed by NEMA [1972].

First, the effects of cycling (0.8 to 10 cph) and percent ON-time (20, 50 and 80%) on the cyclic losses are presented. All the other variables were fixed for these tests. Next, the effects of indoor relative humidity (20 to 67%) on cyclic losses were studied. Two sets of tests were run to investigate the effects of indoor dry-bulb temperature (72 to 80 F) on cyclic losses. One set was run at constant indoor relative humidity (50%) and other at constant indoor dew-point temperature (58 F). At constant relative humidity, the moisture content in the air-stream increased with the indoor dry-bulb temperature and at constant dew-point temperature the moisture content in the air-stream remained constant. Therefore, the effect of the indoor temperature on the cyclic losses would be better understood. The effects of the outdoor dry-bulb temperature

(82 to 100 F) on the cyclic losses were also investigated.

Based on the functional relationship of PLF and C_D with the five independent varibles (indoor dry-bulb temperature and relative humidity, outdoor dry-bulb temperature, percent ON-time, and cycling rate), a multiple linear regression analysis was performed on the experimental data. The analysis yielded two general equations to predict the PLF and C_D. Finally, the dehumidification performance and the total system performance were summarized.

The overall performance of the heat pump operating in cycles was characterized by measuring total cyclic capacity, total cyclic energy consumption, time required for the system to reach steady-state, and cyclic energy efficiency ratio (EER_{cyc}). In addition to overall system performance, a number of non-dimensional parameters were used to quantify the sensible, latent and the total cyclic performance of the heat pump. The transient sensible capacity response was quantified by measuring the temperature drop across the evaporator coil. The normalized sensible capacity, which is the ratio of the cyclic to the steady-state sensible capacity, was used to compare the sensible response to different tests. The latent capacity response was quantified by measuring the moisture removal rate across the evaporator coil. The normalized latent capacity was used to compare the latent response to different tests. The total cyclic system response was quantified by calculating the part load factor (PLF) and coefficient of degradation (C_D). Because these two parameters are non-dimensional, they were used to compare the system response to different tests.

EFFECTS OF CYCLING RATE AND PERCENT ON-TIME ON CYCLIC LOSSES

A series of tests was conducted for cycling rates from 0.8 to 10 cycles per hour (cph), and percent ON-times of 20, 50 and 80%. The indoor and outdoor dry-bulb temperatures were 80 and 95 F, respectively, and the indoor relative humidity was 50%. The set of ambient conditions was the same as recommended by ASHRAE for Test A. The comparison of the cyclic to steady-state performance results is shown in Figure 7.1. The ordinate of the graph is the ratio of the cyclic to steady-state energy efficiency ratio, and was defined as the part load factor (PLF). This ratio has been plotted against the cooling load factor (CLF), as defined in Chapter VI. The three separate lines drawn through the data represent the loci of data with percent ON-times of 20, 50 and 80%, respectively. Each test point is labeled with the actual cycling rate.

The PLF and CLF both decreased as the cycling rate increased and percent ON-times decreased. Because the EER_{cyc} is a product of the EER_{ss} and PLF, the EER_{cyc} also decreases with either an increase in cycling rate or decrease in percent ON-time (Figure 7.1). Since most of the cycling losses occur during the first few minutes after start-up, the heat pump experiences maximum loss at high cycling rates and low percent ON-times. The load curve in Figure 7.1 was obtained by interpolating between the data at constant percent ON-times to reflect the expected cycling rate based on the curve shown in Figure 5.1. Thus this curve represents a typical residential load and cycling rate for the given percent ON-time. For this curve, the PLF decreased from 0.95 at 80% ON-time and 1.8 cph to about 0.75 at 20% ON-time and 1.8 cph.

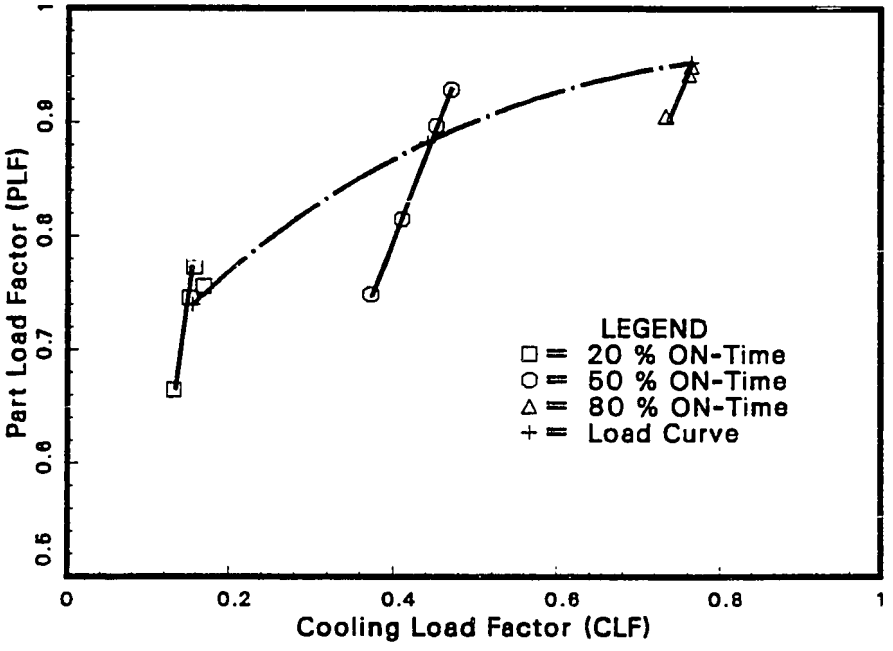

Figure 7.1 - Change in Part Load Factor with Cooling Load Factor for Various Cycling Rates and Percent ON-Times.

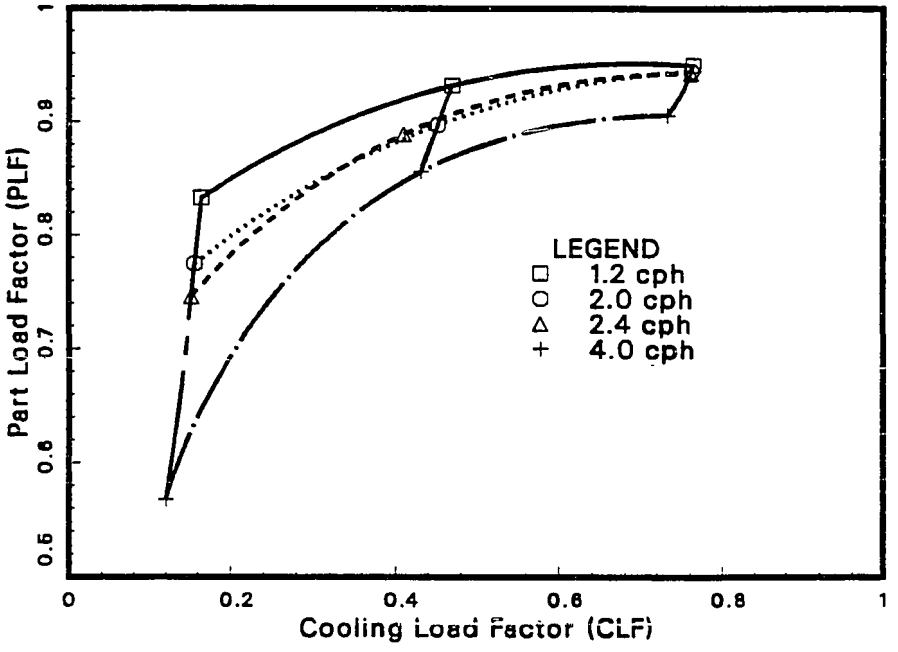

Figure 7.2 - Change in Part Load Factor with Cooling Load Factor for Constant Cycling Rate.

Figure 7.2 shows the change in PLF with CLF for four different cycling rates. The curves were obtained by interpolating the data shown in Figure 7.1 at constant percent ON-times. The PLF increased with cycling rate and CLF. The plots showed that at low CLF's and high cycling rates the increase in PLF was very rapid. As the CLF increased (beyond 0.5), the corresponding increase in the PLF became smaller. As the cycling rate increased at low percent ON-times (20%), the OFF-time also increased, which gave more time for the refrigerant to migrate into the evaporator coil. Therefore, the change in the PLF with cycling rate at low percent ON-times was greater than at high percent ON-times. For decreasing cycling rates, the curves tended to flatten out even for low CLFs. As the cycling rate decreased, the run time of the unit increased (at constant percent ON-time). Because the unit experienced maximum losses during the first few minutes after start-up, the PLF increased with increase in ON-time. Therefore, the curves tended to flatten out at low cycling rates even at low CLFs.

Both the normalized latent and sensible capacities increased with percent ON-time and decreased with cycling rate (Figure 7.3). The effect of cycling rate and percent ON-time was more severe on the latent capacity. As the cycling rate increased, the deviation of the latent capacity from the expected steady-state capacity increased. However, the deviation decreased as the percent ON-time increased. Although the effect of cycling rate and percent ON-time on the sensible capacity was not as severe as latent capacity, the trends were similar.

The loss in cooling capacity increased with the cycling rate and decreased with the percent ON-time (Figure 7.4). The combination of high cy-

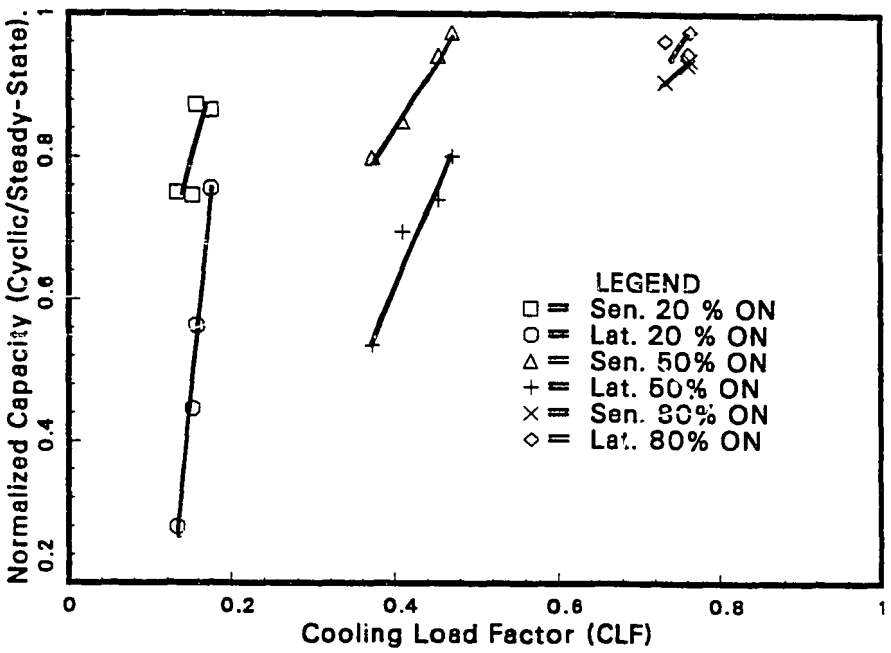

Figure 7.3 - Change of Normalized Sensible and Latent Capacities at Various Cycling Rates and Percent ON-Times.

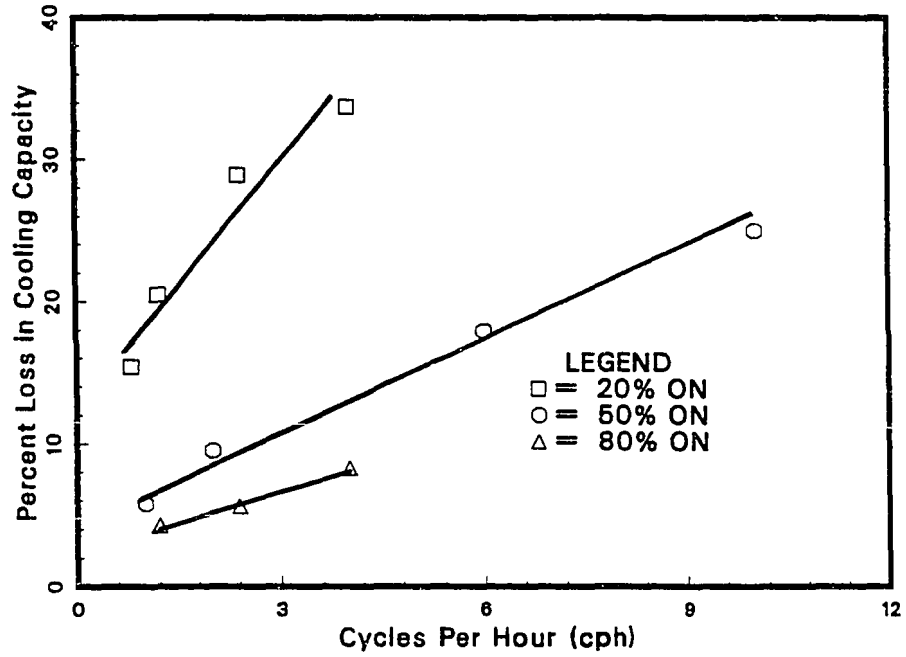

Figure 7.4 - Loss in Cooling Capacity at Various Cycling Rates.

cling rate and low percent ON-time produced a maximum loss in the cooling capacity. The maximum change in the normalized energy consumption was less than 9% (Figure 7.5). The change at 50% and 80% ON-times was less than 2% even at high cycling rates.

The C_D was plotted against the CLF for three different percent ON-times (Figure 7.6). The curve drawn across the three lines was based on the typical residential load curve. The degradation in performance increased linearly with an increase in cycling rate. The C_D at 50% ON-time was less than the C_D at 80% and 20% ON-time for a given cycling rate. This characteristic can be clearly understood by studying the relationship between (1-PLF) and (1-CLF) with percent ON-time for a given cycling rate (Figure 7.7). Although both the factors decreased with the percent ON-time, the decrease in the factor (1-PLF) was clearly non-linear. Therefore, C_D, which is the ratio of (1-PLF) to (1-CLF) had a non-linear relationship with percent ON-time.

The constant C_D curves for various cycling rates and CLFs are shown in Figure 7.8. The locus of the markers on the curves represented 20%, 50% and 80% ON-time values respectively, and shifting from left to right on a constant C_D curve represented moving from 20 to 80 percent ON-time. The curves flattened with a decrease in the cycling rate, indicating that at low cycling rates (less than 1 cph), C_D was less dependent on CLF. The locus of the markers are linear and the shape of the curves are symmetric about the apex of the curves. This was another indication that the change in C_D with CLFs was linear and merely shifted either left or right of the apex for a given percent ON-time.

The constant C_D curves for various cycling rates and PLFs are shown

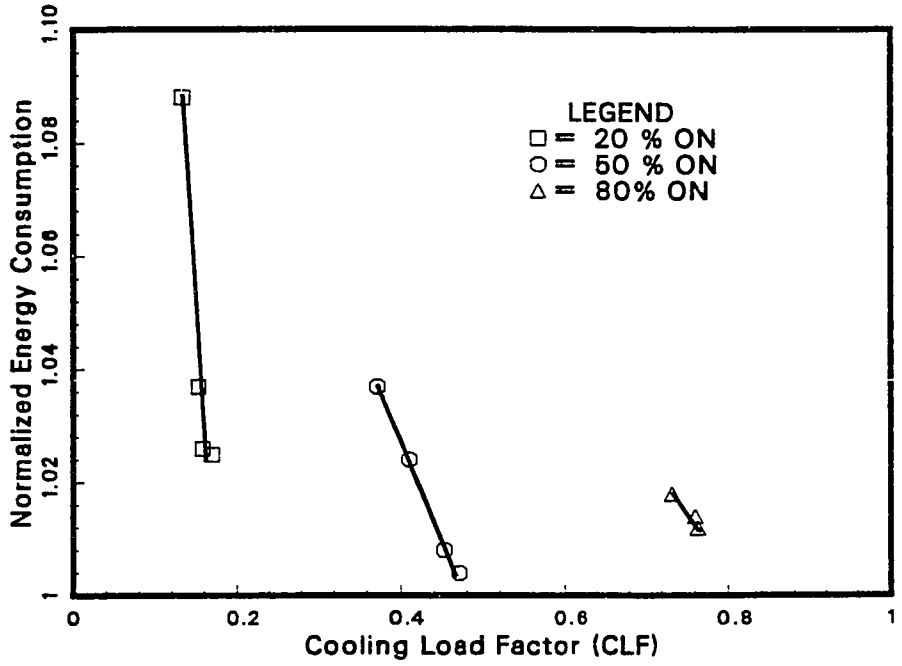

Figure 7.5 – Change in Normalized Energy Consumption with CLF at Various Cycling Rates and Percent ON-Times.

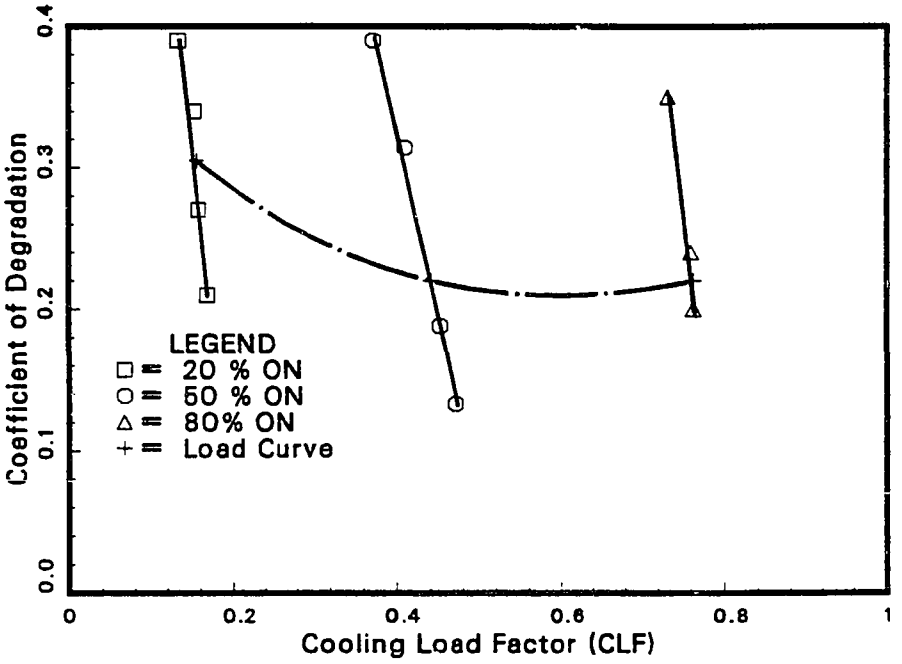

Figure 7.6 – Change in Coefficient of Degradation at Various Cycling Rates and Percent ON-Times.

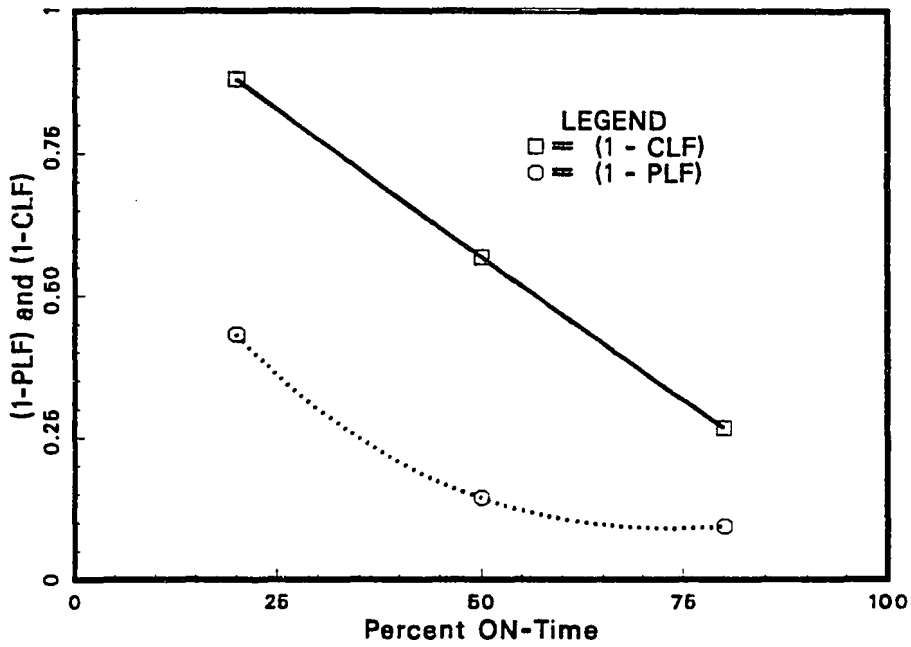

Figure 7.7 - Relationship Between (1 - PLF) and (1 - CLF) with Percent ON-Time.

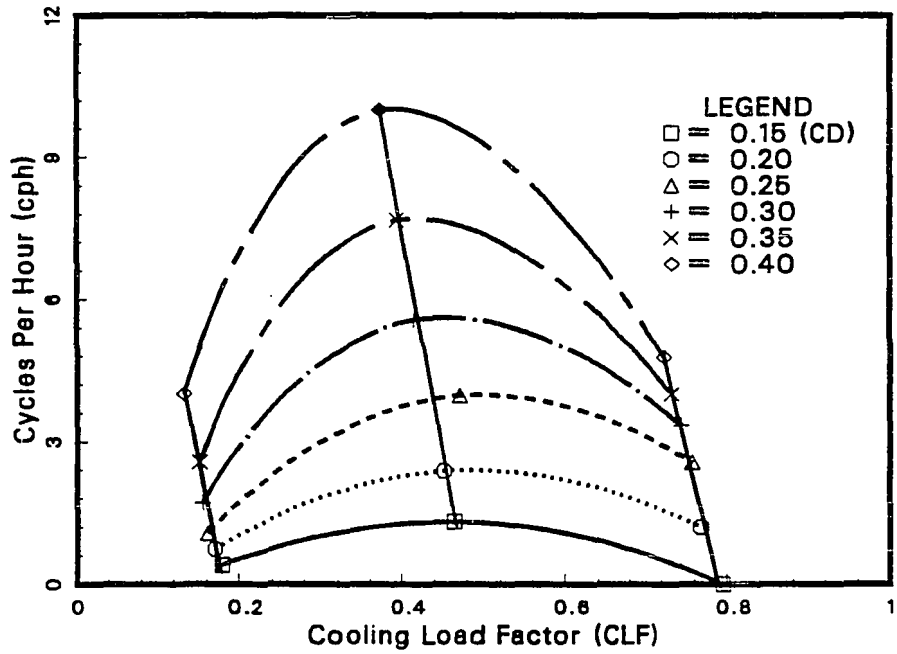

Figure 7.8 - Constant Coefficient of Degradation Curves at Various Cycling Rates and CLFs.

in Figure 7.9. The locus of the markers on the curves represented 20%, 50% and 80% percent ON-times respectively. Shifting from left to right on a constant C_D curve represented moving from 20 to 80 percent ON-time. The constant C_D curves showed a non-linear trend even at low cycling rates. The C_D increased with cycling rate. The locus of the markers clearly showed an exponential increase in cycling rate with decrease in PLF. The rate of increase decreased as the percent ON-time increased. Also as the percent ON-time increased, the shift (to the right) of the locus representing the constant percent ON-time decreased.

The trends in the Figures 7.8 and 7.9 have shown that C_D is linearly dependent on CLF and exponentially dependent on PLF for a given percent ON-time. Figure 7.10 shows the change in EER_{cyc} with run time for three different percent ON-times. For a run time of less than 12 minutes, the EER_{cyc} increased sharply and then gradually levelled off. The rapid increase of EER_{cyc} for small ON-times was due to two reasons: (i) the response to the change in capacity (Figure 6.5) was exponential and reached steady-state after 15 minutes. (ii) The energy consumed at start-up was greater than the steady-state energy consumption and it took about 5 minutes to reach steady-state. Therefore, EER_{cyc} increased sharply initially, and then began to level off.

For a given ON-time, EER_{cyc} increased with percent ON-time (Figure 7.10). For example, at 3 minutes, the EER_{cyc} was greater at 50% ON-time than at 20% ON-time. One of the reasons for cyclic losses was due to refrigerant migration into the evaporator during the OFF cycle [Mulroy and Didion, 1985]. For a given cycling rate if the percent ON-time increases, the

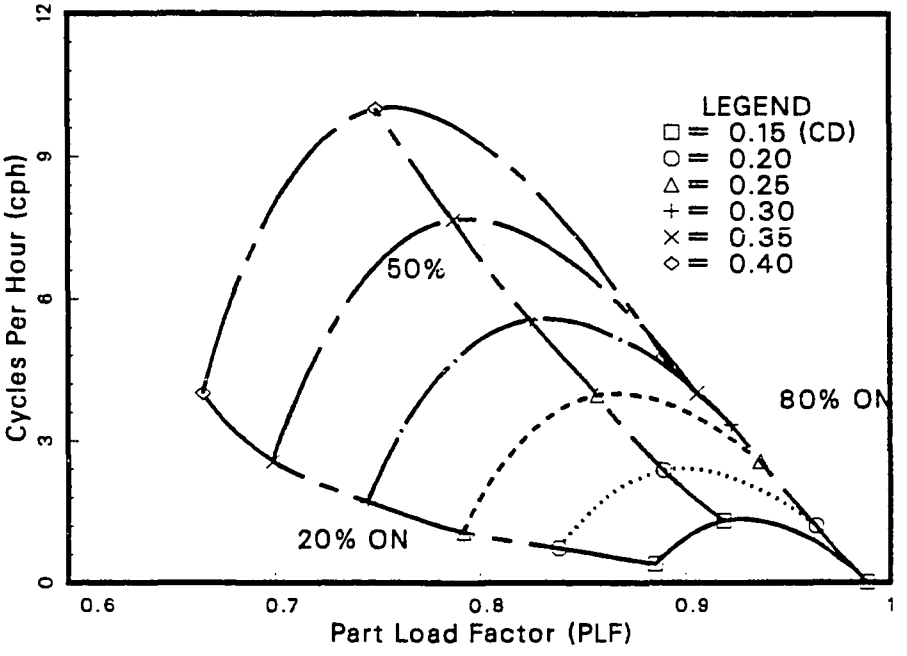

Figure 7.9 – Constant Coefficient of Degradation Curves at Various Cycling Rates and PLFs.

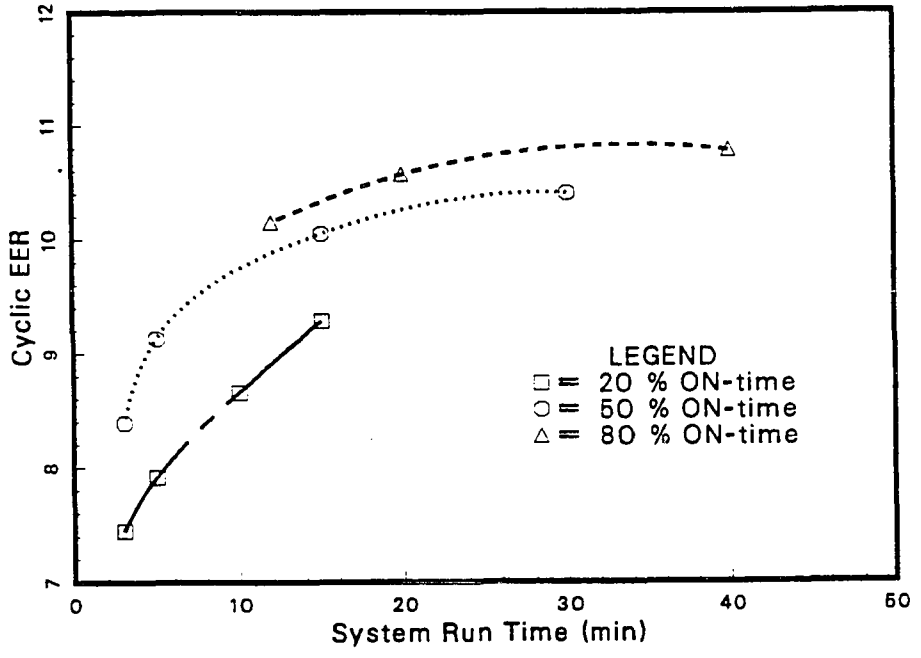

Figure 7.10 – Change in Cyclic EER with Unit Run Time for Three Different Percent ON-Times.

OFF-time decreases. Therefore, the refrigerant had less time to migrate into the evaporator which increases the EER_{cyc}.

EFFECTS OF INDOOR HUMIDITY ON CYCLIC LOSSES

A series of tests for indoor relative humidities ranging from 20% to 67% was run. The indoor and outdoor dry-bulb temperatures were held constant for all the test runs at 78 F and 93 F, respectively. The indoor air flow rate was also constant at 1200 cfm. The data were collected for three different percent ON-times (20, 50, 80) at every indoor relative humidity. The cycling rate based on the NEMA curve (Figure 5.1) at 20 and 80 percent ON-time was 1.8 cph and 3 cph at 50 percent ON-time.

The steady-state sensible capacity decreased with an increase in relative humidity (Figure 7.11). The time required for the system to reach steady-state increased with decrease in relative humidity. It took approximately 6 minutes, after start-up, for the sensible capacity to reach steady-state for an indoor humidity of 67 %. At 20 % Rh, it took almost 12 minutes for the capacity to reach steady-state. As the indoor relative humidity decreased, there was more capacity available for sensible cooling. However, to realize the sensible cooling, the average temperature of the evaporator coil must decrease with a decrease in relative humidity. Because the evaporator coil temperature had to be lower to dehumidify at lower humidities, it took longer for the system to reach steady-state.

The response of the moisture removal rate across the evaporator coil is shown in Figure 7.12 for three different indoor relative humidities. Initially, at start-up, the moisture removal rate was negative, because moisture evaporated

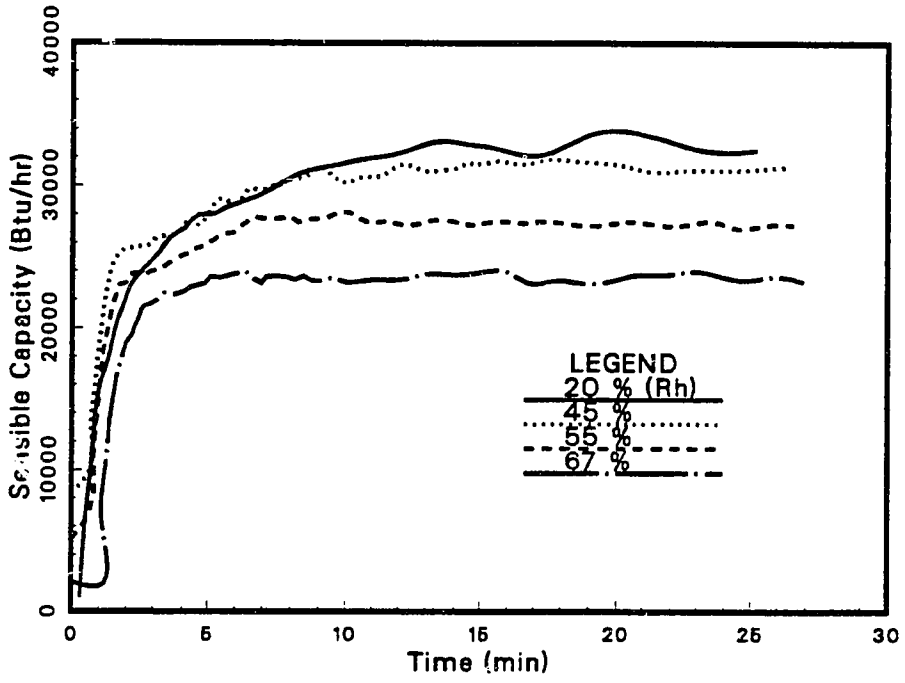

Figure 7.11 - Response of Cyclic Sensible Capacity at Various Indoor Relative Humidities (80% ON-Time).

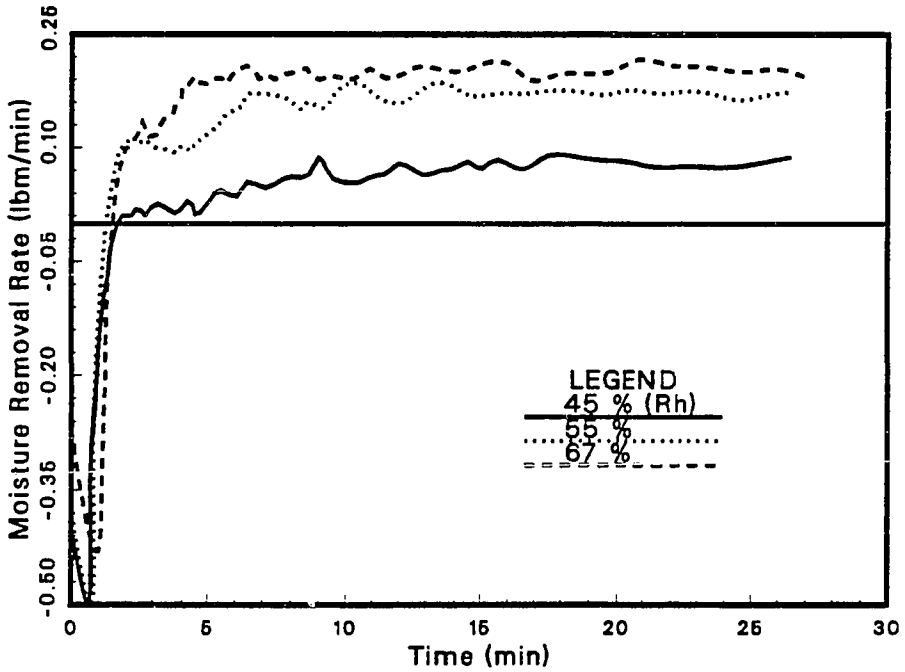

Figure 7.12 - Response of Moisture Removal Across the Evaporator Coil at Various Indoor Relative Humidities (80% ON-Time).

from the wet evaporator coil into the air-stream. Dehumidification began between 75 and 90 seconds after start-up. The steady-state moisture removal rate increased with increasing indoor relative humidity. The moisture removal rate reached steady-state faster with increasing indoor relative humidity. It took 6 minutes, after start-up, for the moisture removal rate to reach steady-state for an indoor relative humidity of 67 %, whereas it took almost 12 minutes at 45 % Rh. There was no dehumidification below 45% Rh.

The change in the sensible capacity response at 20 percent ON-time is shown in Figure 7.13. The trends are similar to the 80 percent ON-time case. However, the difference in capacity at 67 % Rh and 20 % Rh was smaller. Since the run time was only 7 minutes the system never reached steady-state. The response of the moisture removal rate across the evaporator coil at 20 percent ON-time is shown Figure 7.14. The trends are similar to 80 percent ON-time case.

The change in the normalized sensible capacity with relative humidity for three different percent ON-times is shown in Figure 7.15. The normalized capacity increased with an increase in indoor relative humidity. The slope of the curves increased with a decrease in percent ON-time. The normalized latent capacity increased linearly with an increase in the indoor relative humidity (Figure 7.16). The slope increased with decrease in percent ON-time.

As with the normalized sensible capacity, the PLF increased with increase in indoor relative humidity (Figure 7.17). The slope of the curves increased with decrease in percent ON-time. The change in C_D with relative humidity for three different percent ON-times is shown in Figure 7.18. C_D decreased with

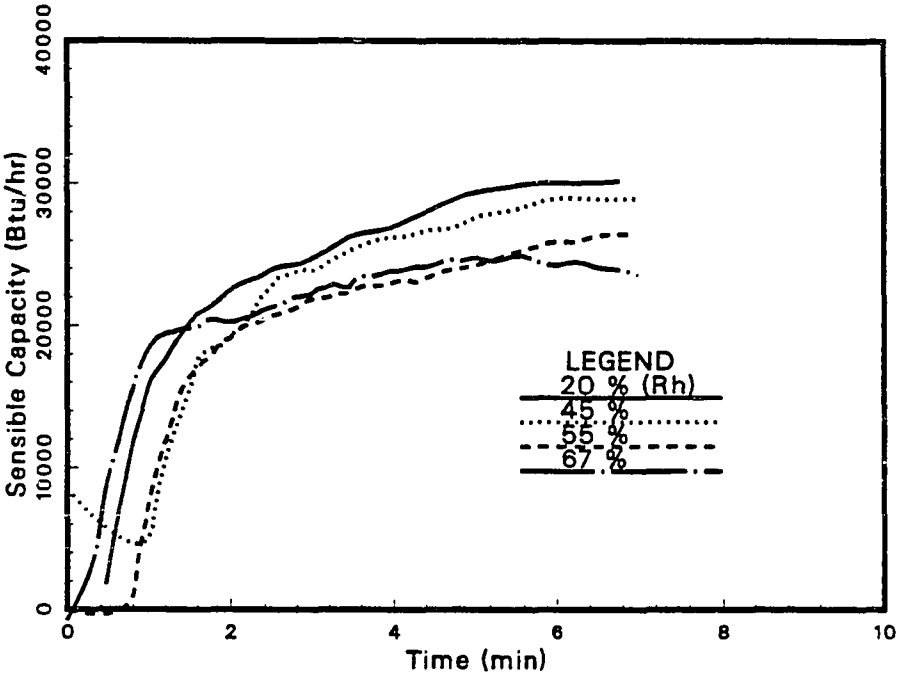

Figure 7.13 – Response of Cyclic Sensible Capacity at Various Indoor Relative Humidities (20% ON-Time).

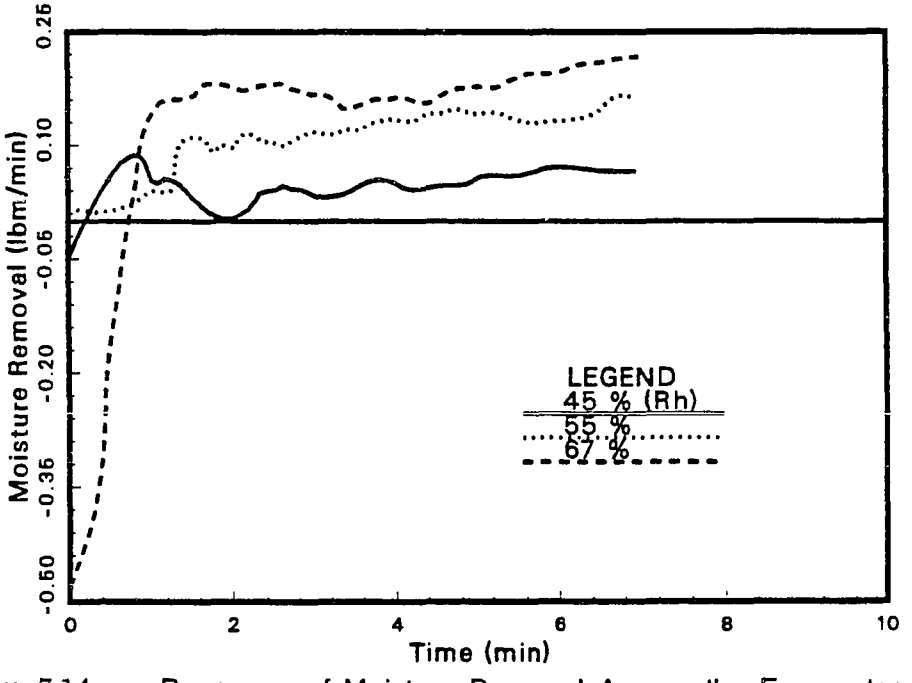

Figure 7.14 – Response of Moisture Removal Across the Evaporator Coil at Various Indoor Relative Humidities (20% ON-Time).

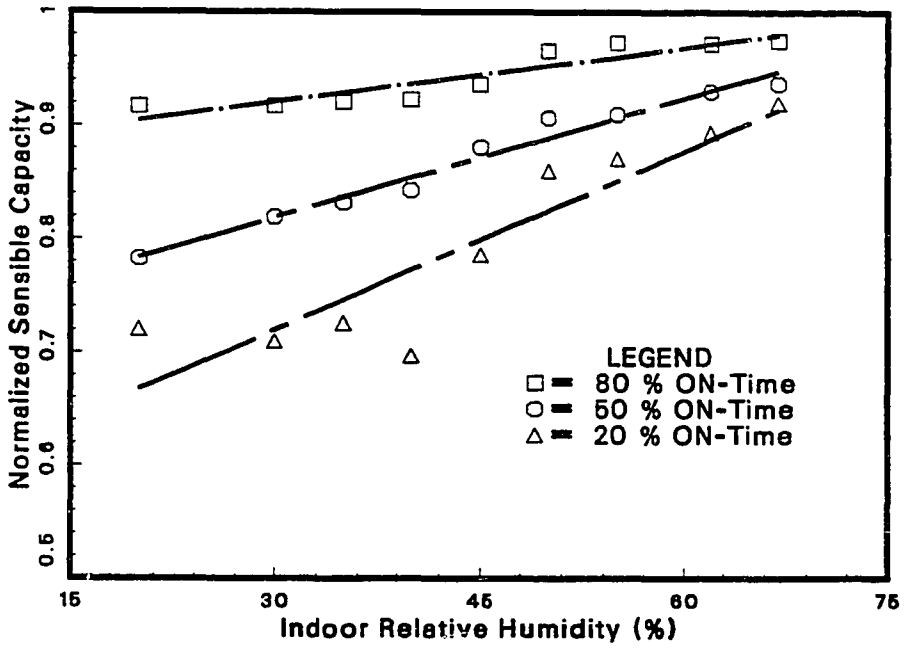

Figure 7.15 – Change in Cyclic Sensible Capacity with Indoor Relative Humidity.

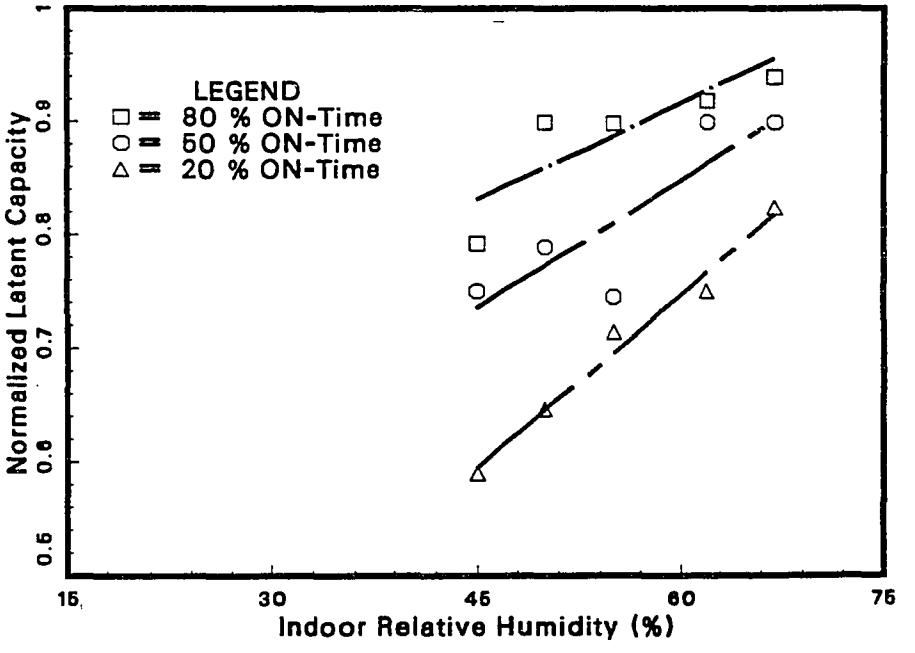

Figure 7.16 – Change in Cyclic Latent Capacity with Indoor Relative Humidity.

an increase in relative humidity for all three percent ON-times. in general, the C_D at 50 percent ON-time was less than at 80 and 20 percent ON-times. The top line on the graph corresponded to 80 percent ON-time followed by 20 and 50 percent ON-times, respectively.

The PLF increased with both CLF and relative humidity linearly, for a given percent ON-time (Figure 7.19). The change in PLF with relative humidity decreased as the percent ON-time increased. At 20 percent ON-time, the PLF increased from 0.65 (20% Rh) to 0.87 (67% Rh); the corresponding increase at 80 percent ON-time was 0.9 to 0.95.

As with the PLF, the normalized sensible capacity increased linearly with an increase in CLF and relative humidity, for a given percent ON-time (Figure 7.20). Also the change in normalized sensible capacity with relative humidity decreased as the percent ON-time increased. The change in normalized latent capacity with CLF also showed similar trends (Figure 7.21) except at 80 percent ON-time and 45% Rh. The average relative humidity at those test condition was slightly lower than the corresponding values at 50 and 20 percent ON-time. The change in normalized latent capacity at 20 percent ON-time was 0.6 to 0.82 and 0.9 to 0.95 at 80 percent ON-time (with the exception of the 45% Rh case).

The C_D decreased linearly with an increase in CLF and relative humidity, for a given percent ON-time (Figure 7.22). In general, the C_D at 50 percent ON-time was slightly lower than at 80 percent ON-time. The change in C_D at 20 percent ON-time was 0.16 to 0.40, at 50 percent ON-time it was 0.15 to 0.37, and at 80 percent ON-time it was 0.2 to 0.38.

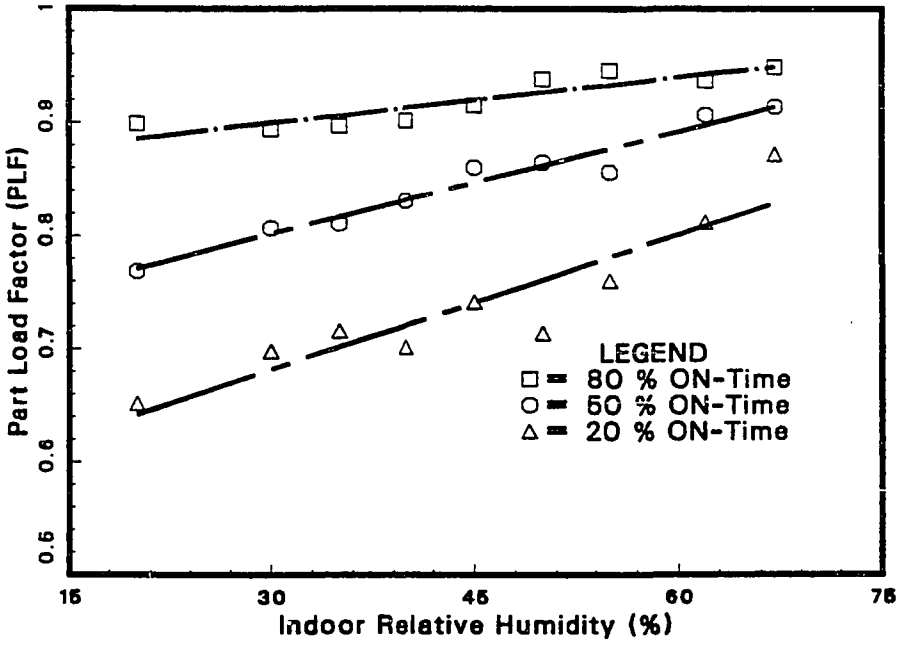

Figure 7.17 – Change in Part Load Factor with Indoor Relative Humidity.

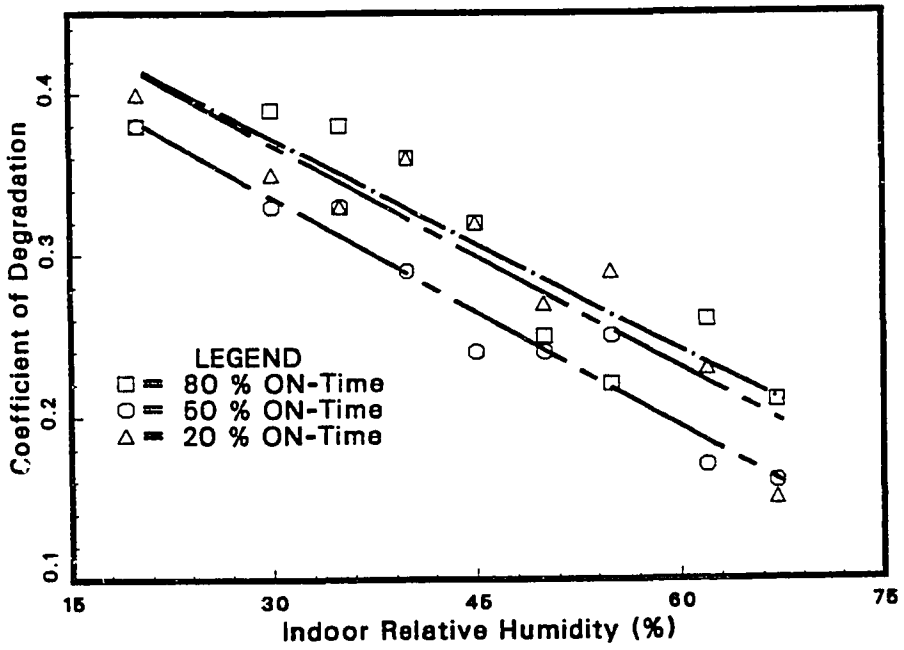

Figure 7.18 – Change of Coefficient of Degradation with Indoor Relative Humidity.

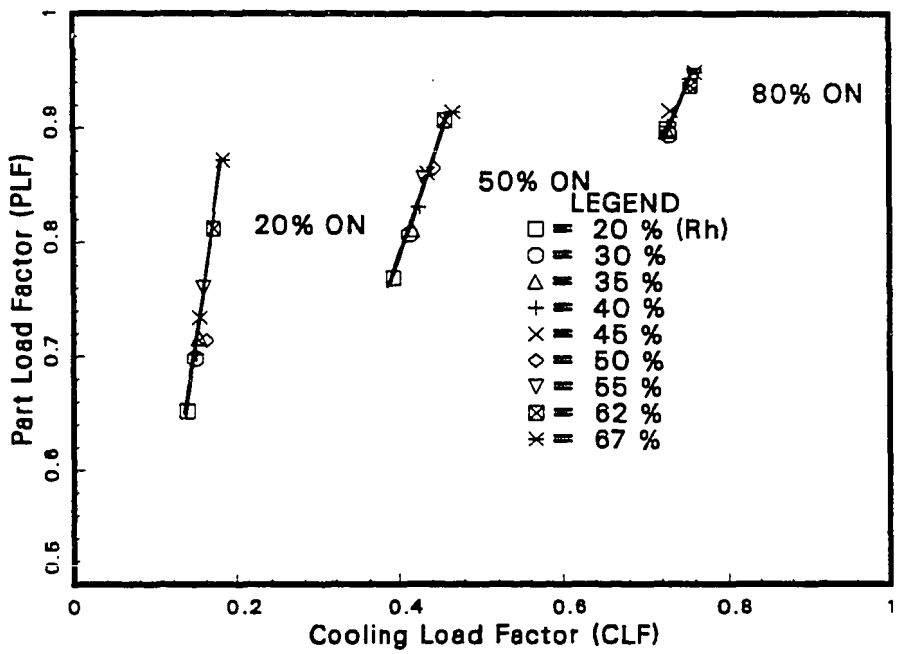

Figure 7.19 - Change in PLF with CLF for Various Indoor Relative Humidities and Percent ON-Times.

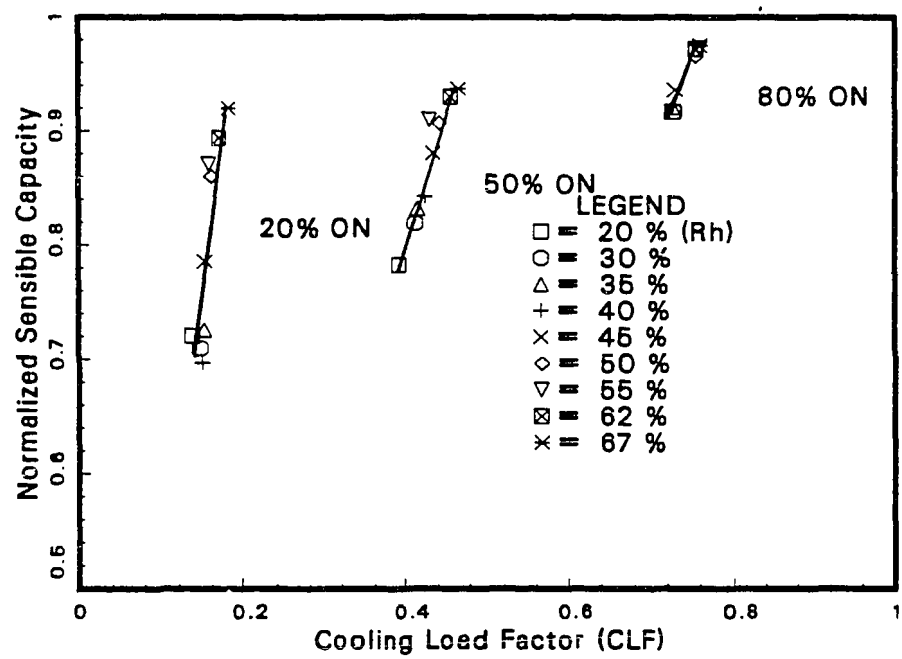

Figure 7.20 - Change in Cyclic Sensible Capacity with CLF at Various Indoor Relative Humidities.

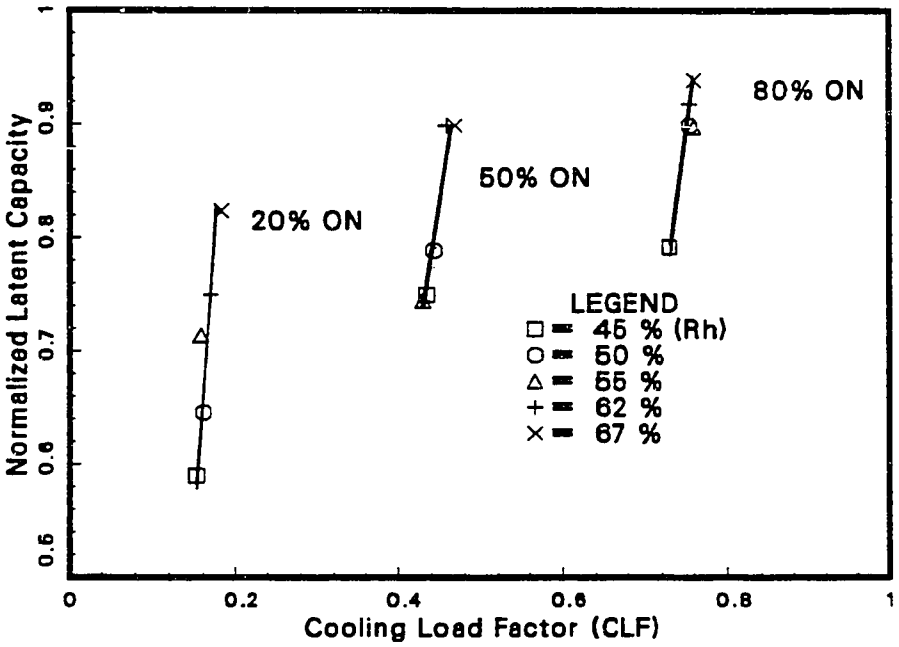

Figure 7.21 – Change in Normalized Latent Capacity with CLF at Various Indoor Relative Humidities.

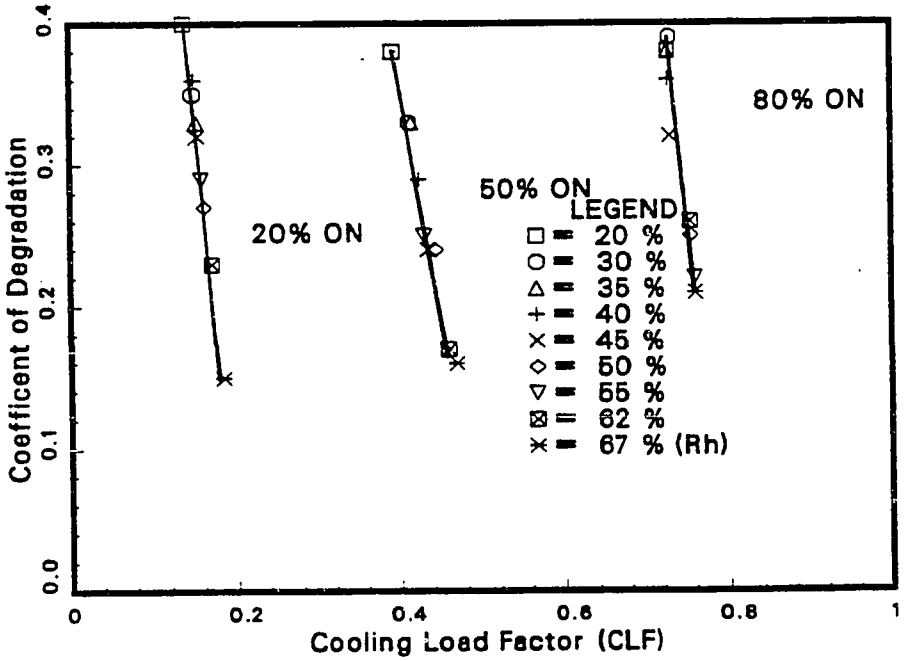

Figure 7.22 – Change in Coefficient of Degradation with CLF at Various Indoor Relative Humidities.

EFFECTS OF INDOOR ROOM DRY-BULB TEMPERATURE ON CYCLIC LOSSES

A series of tests for indoor dry-bulb temperatures ranging from 72 to 80 F were run. The outdoor dry-bulb temperature and indoor air flow-rate were held constant for all the test runs at 93 F and 1200 cfm, respectively. Two sets of tests were run: one at constant indoor relative humidity (50%) and the other at constant indoor dew-point temperature (58 F). The data were collected for two different percent ON-times (50, 80) at every indoor dry-bulb temperature. The cycling rate based on the NEMA curve (Figure 5.1) was 1.8 cph at 80 percent ON-time and 3 cph at 50 percent ON-time.

Constant Relative Humidity

The responses of the cyclic sensible capacity and moisture removal at 50 percent ON-time for constant indoor relative humidity are shown in Figures 7.23 and 7.24. The sensible capacity at the end of cycle for 80 F indoor temperature was higher than 76 F and 72 F. Moisture removal increased with an increase in the indoor dry-bulb temperature. Because moisture in the air-stream increases with an increase in indoor temperature at constant relative humidity, the moisture removal capacity also increases. The moisture removal was negative for the first 75 to 90 seconds after start-up due to evaporation of moisture left on the coil from the previous cycle.

The response of cyclic sensible capacity at 80 percent ON-time was similar to the trends at 50 percent ON-time. At the end of the cycle, the sensible capacity at 72 F was higher than that with 76 F but lower than with 80 F. Steady-state capacity was approached at approximately the same time for all three temperatures. As with 50 percent ON-time, the moisture removal

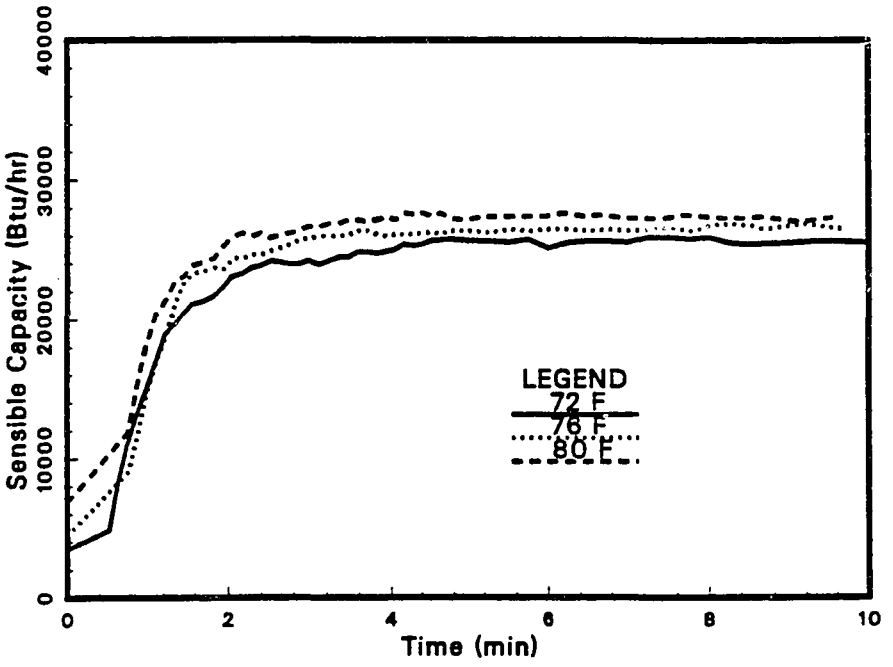

Figure 7.23 – Response of Cyclic Sensible Capacity at Various Indoor Temperatures and Constant Relative Humidity (50% ON-Time).

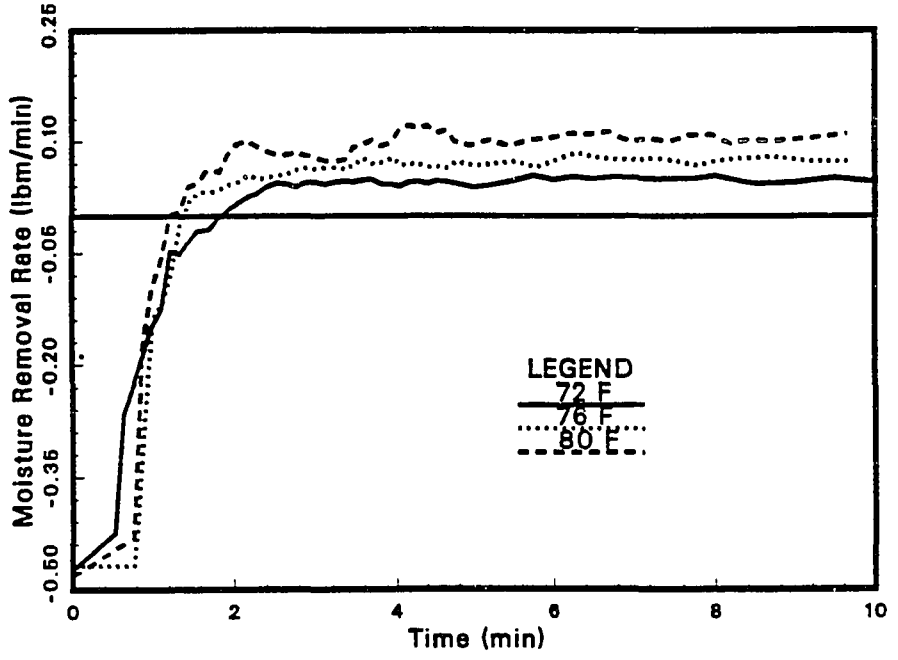

Figure 7.24 – Response of Moisture Removal Rate at Various Indoor Temperatures and Constant Relative Humidity (50% ON-Time).

increased with an increase in indoor temperature.

The normalized sensible capacity remained almost constant with an increase in indoor temperature for a given percent ON-time (Figure 7.25). In contrast, the normalized cyclic latent capacity decreased with decreasing indoor temperature (Figure 7.26). The results for the 50 percent ON-time showed a larger slope and variation than the 80% ON-time. The drop in latent capacity was primarily due to the smaller moisture content in the air at lower temperatures. As the indoor temperature dropped, the unit was not able to extract as much moisture from the air, which decreased the latent capacity. Therefore, at start-up very little dehumidification occurred. At 72 F indoor temperature, the moisture removal remained negative for the first 2 minutes after start-up (Figure 7.24).

The PLF for 80 percent ON-time was greater than at 50 percent ON-time (Figure 7.27). The PLF at 80 percent ON-time showed little dependence with indoor temperature. However, the results at 50 percent ON-time showed a larger slope. The increase in slope at 50 percent ON-time was due to an increase in slope of the normalized latent capacity with indoor temperature. At 50 percent ON-time, the PLF at 72 F indoor temperature was 0.82 which was lower than the PLF at any other indoor temperature. The C_D decreased with an increase in indoor temperature for both percent ON-times (Figure 7.28). The C_D at 72 F indoor temperature and 50% ON-time was high (0.31) because the normalized latent capacity was low. The C_D at 50 percent ON-time was lower than at 80 percent ON-time.

To better quantify the transient response of the total capacity at various indoor temperatures, a first order exponential curve was fitted through the

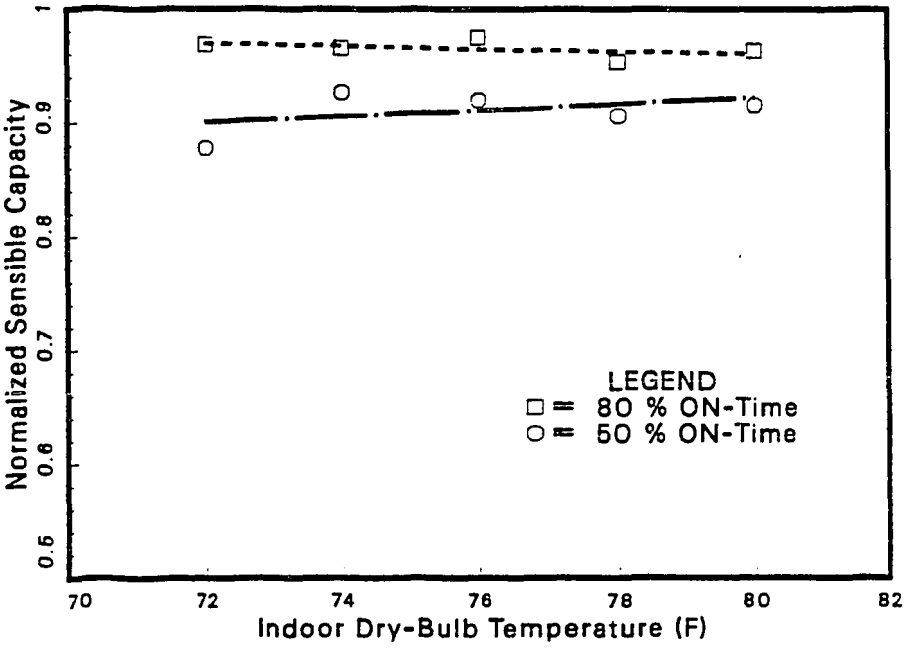

Figure 7.25 – Change in Normalized Sensible Capacity with Indoor Dry-Bulb Temperature and Constant Indoor Relative Humidity.

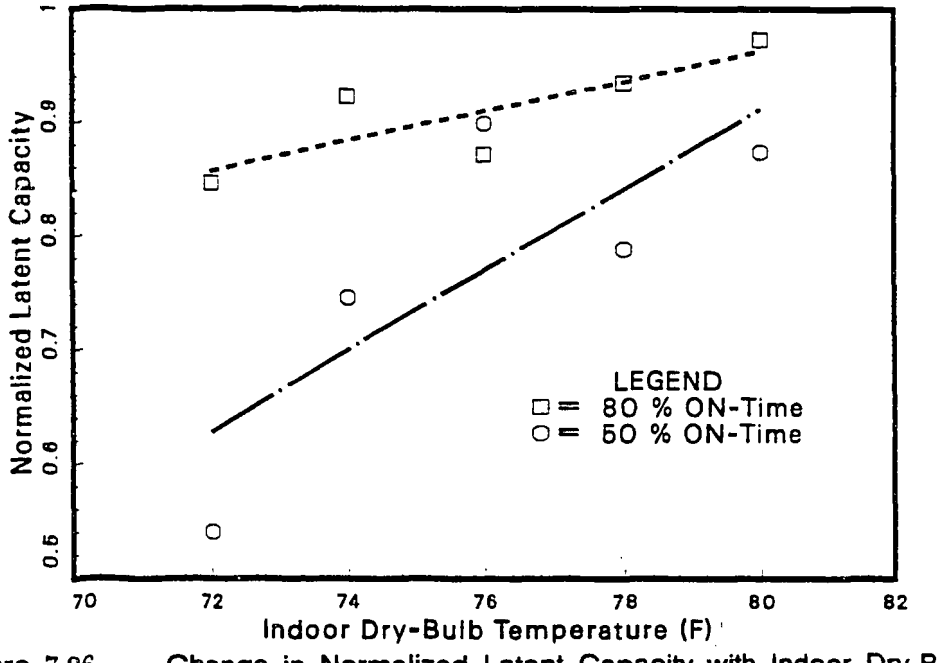

Figure 7.26 – Change in Normalized Latent Capacity with Indoor Dry-Bulb Temperature and Constant Indoor Relative Humidity.

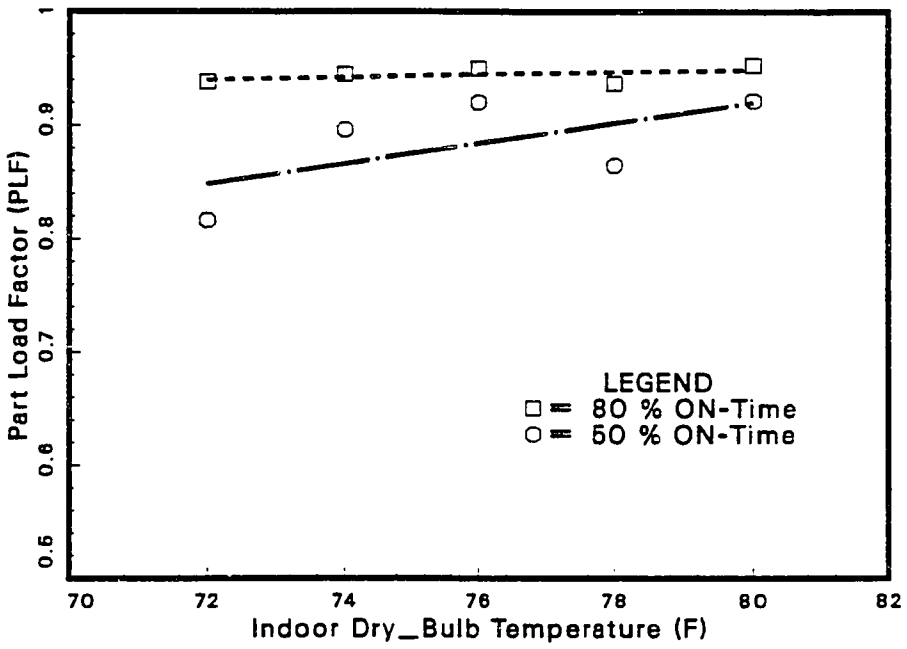

Figure 7.27 - Change in Part Load Factor with Indoor Dry-Bulb Temperature and Constant Indoor Relative Humidity.

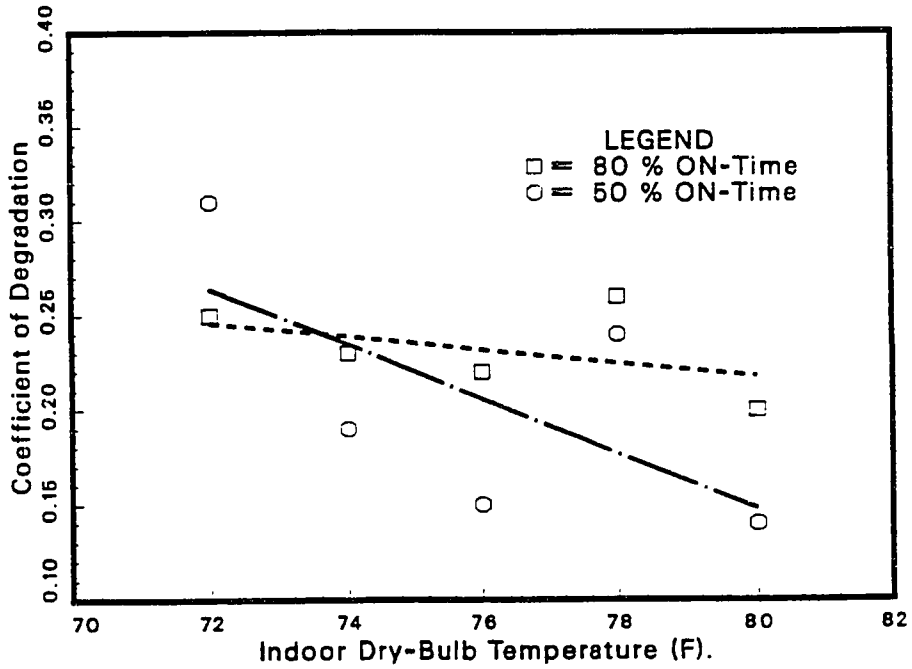

Figure 7.28 - Change in Coefficient of Degradation with Indoor Dry-Bulb Temperature and Constant Indoor Relative Humidity.

experimental data:

$$\frac{Q_{cyc}(t)}{\dot{Q}_{ss}t_{ON}} = (1 - e^{-t/\tau}) \qquad (7.1)$$

where,

t = time in minutes

τ = time constant

The higher the value of τ, the longer it takes for the total capacity to reach steady-state. The values of τ are tabulated in Table 7.1. The change in the value of τ was small. However, it decreased with indoor temperature except at 78 F. With an increase in indoor dry-bulb temperature, the average coil temperature also increased. Therefore, the coil reached steady-state quicker.

Constant Dew-Point

At constant dew-point conditions, the moisture content in the air-stream is also constant. Therefore, to study the transient response of the heat pump under such condtions, a series of tests was run with constant dew-point temperature. The cyclic sensible capacity at the end of the cycle for both 80 and 50 percent ON-times increased with an increase in indoor temperature. Moisture removal at the end of the cycle for both 80 and 50 percent ON-times decreased with an increase in the indoor temperature. The increase in the indoor dry-bulb temperature could be expected to increase the driving potential for the sensible cooling. Therefore, the sensible capacity increased and the latent capacity decreased at the end of the cycle. The time at which dehumidification started increased with an increase in indoor temperature. At

Table 7.1 – Time Constants at Various Indoor Temperatures.

Indoor Temperature (F)	Time Constant τ (min)
72	1.812
74	1.685
76	1.484
78	1.806
80	1.223

72 F indoor temperature, it started after 60 seconds, whereas at 80 F, it started after 120 seconds.

The normalized sensible capacity decreased slightly at 80 percent ON-time. It increased slightly with indoor temperature at 50 percent ON-time (Figure 7.29). There was a slight increase in normalized latent capacity with indoor temperature for both 80 and 50 percent ON-times (Figure 7.30). There was no change of PLF with indoor temperature for both 50 and 80 percent ON-times (Figure 7.31). With the exception of the 72 F indoor temperature, there was no change in C_D at 80 percent ON-time (Figure 7.32).

EFFECTS OF OUTDOOR DRY-BULB TEMPERATURE ON CYCLIC LOSSES

A series of tests for outdoor dry-bulb temperatures ranging from 82 to

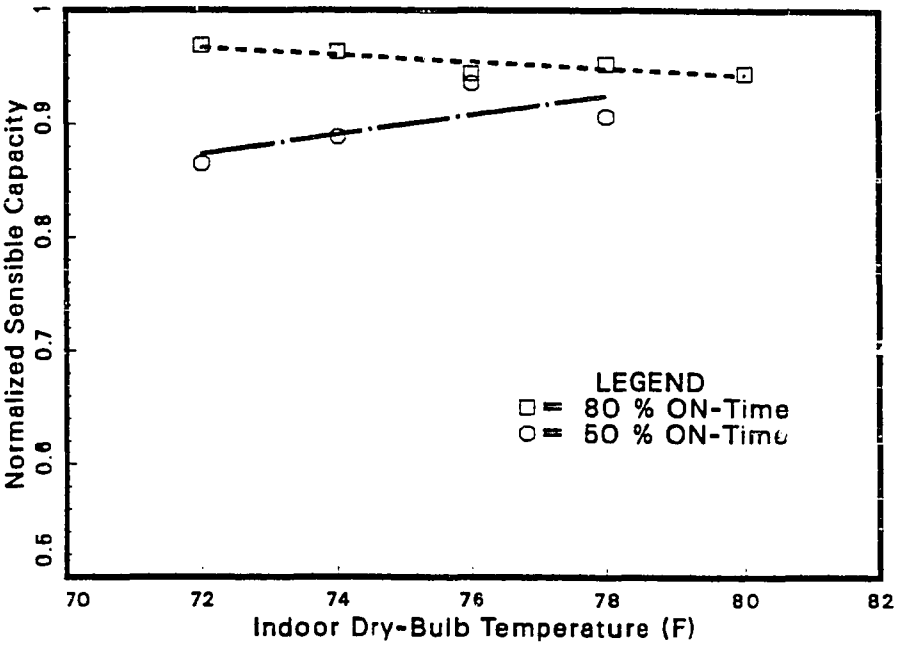

Figure 7.29 - Change in Normalized Sensible Capacity with Indoor Dry-Bulb Temperature and Constant Indoor Dew-Point Temperature.

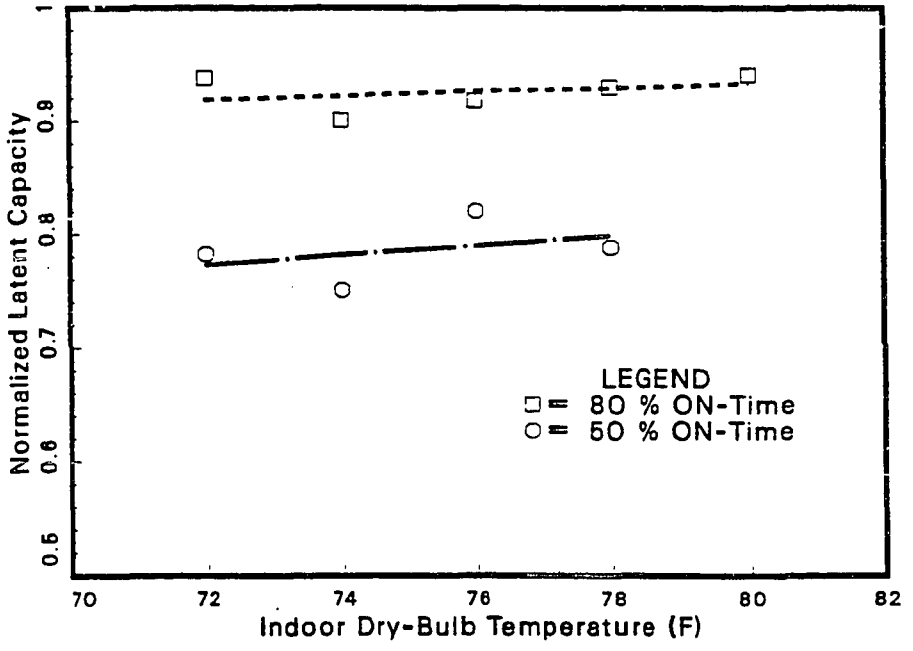

Figure 7.30 - Change in Normalized Latent Capacity with Indoor Dry-Bulb Temperature and Constant Indoor Dew-Point Temperature.

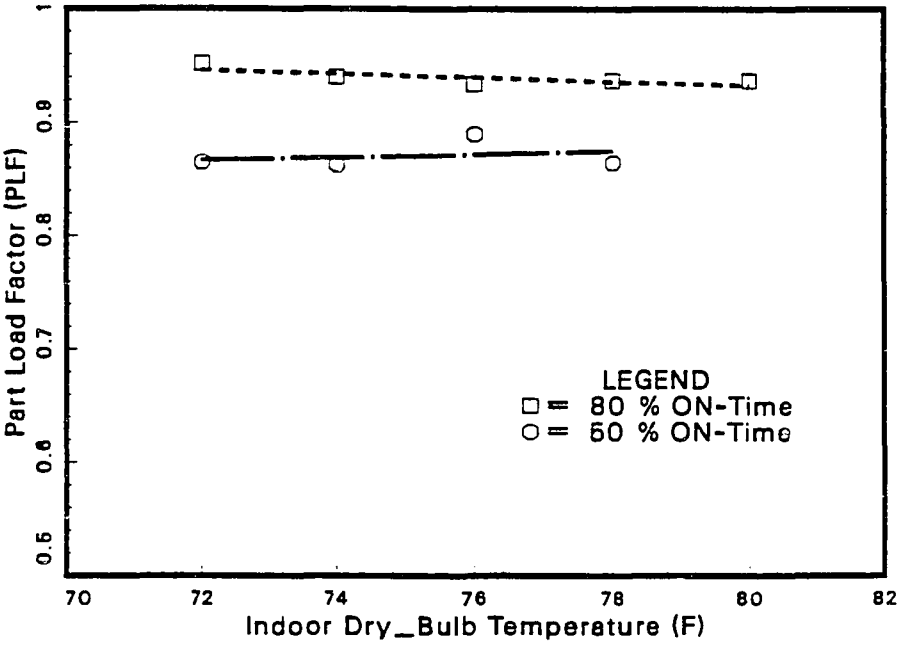

Figure 7.31 – Change in Part Load Factor with Indoor Dry-Bulb Temperature at Constant Dew-Point Temperature.

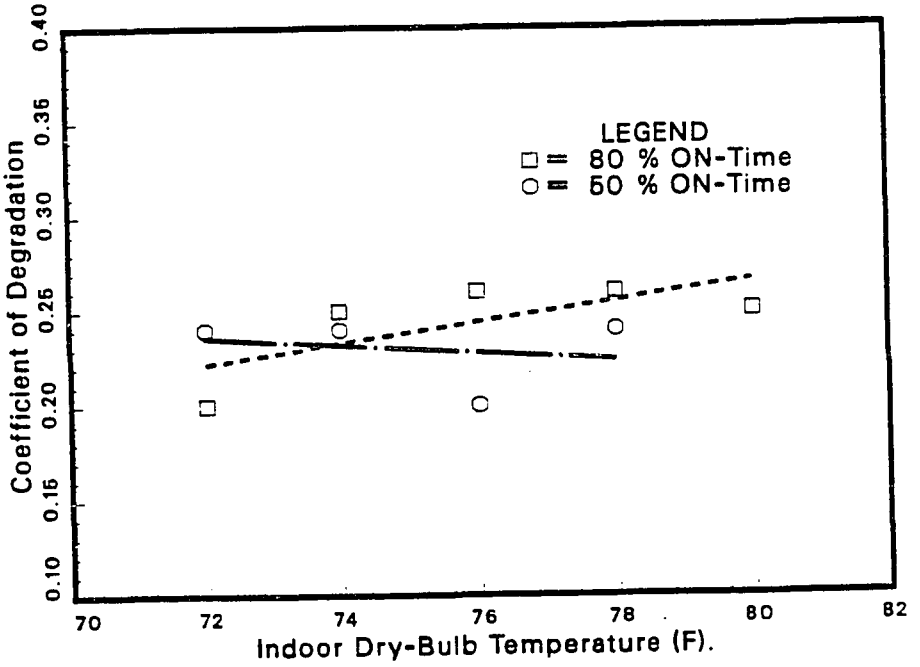

Figure 7.32 – Change in Coefficient of Degradation with Indoor Dry-Bulb Temperature at Constant Dew-Point Temperature.

100 F was run. The indoor dry-bulb temperature, relative humidity and air flow rate were fixed for all test runs at 78 F, 50% and 1200 cfm, respectively. The relationship from Chapter V between the percent ON-time, the cycling rate and the outdoor dry-bulb temperature was used to obtain results which would reflect actual operation of a heat pump in a residence. The percent ON-times and the corresponding cycling rates at a given outdoor dry-bulb temperature are shown in Table 7.2.

Table 7.2 – Percent ON-Times and Cycling Rates at a Given Outdoor Dry-Bulb Temperature.

Outdoor Dry-Bulb Temperature (F)	Percent ON-Time (%)	Cycling Rate (cph)	ON/OFF Time (min)
82	60	3.00	12.0/3.0
85	70	2.50	16.8/7.2
90	85	1.25	40.8/7.2
95	90	0.80	67.5/7.5
100	90	0.80	67.5/7.5

The change in sensible response with outdoor dry-bulb temperatures is shown in Figure 7.33. Although the steady-state sensible capacity decreased slightly with outdoor temperature, all the curves approached steady-state

approximately 6 minutes after start-up. The response of moisture removal rate is also similar (Figure 7.34). The system approached steady-state approximately 6 minutes after start-up for all the temperatures. There was a slight increase (3%) in normalized sensible capacity with outdoor temperature (Figure 7.35). The normalized latent capacity increased from 0.82 at 82 F to 0.94 at 95 F (Figure 7.36). The PLF increased from 0.93 at 82 F to 0.97 at 95 F (Figure 7.37). The increase in normalized sensible and normalized latent capacities and PLF with outdoor temperature was due to an increase in percent ON-time.

The C_D also increased with outdoor temperature (Figure 7.38). The C_D increased because an increase in percent ON-time produced a small change in PLF. At the same time, the CLF increased linearly with percent ON-time. This characteristic can be seen in Figure 7.39, where the change in (1-PLF) and (1-CLF) with outdoor temperature are shown. The factor (1-CLF) decreased from 0.441 at 82 F to 0.125 at 100 F, whereas the factor (1-PLF) decreased from 0.068 at 82 F to 0.039 at 100 F.

DEVELOPMENT OF A GENERAL EQUATION TO ESTIMATE PLF AND C_D

The Department of Energy (DOE) proposed a new testing methodology for heat pumps in 1979. In addition to the conventional steady-state tests, it included cyclic testing as well. A new factor, C_D, was defined to estimate the seasonal energy efficiency ratio (SEER). The test procedure called for the calculation of C_D for one set of ambient conditions or to use a default value of 0.25. However, the experimental results have shown that there can be a wide variation in both the PLF and C_D with the five variables (indoor and outdoor dry-bulb temperature, indoor relative humidity, percent ON-time and

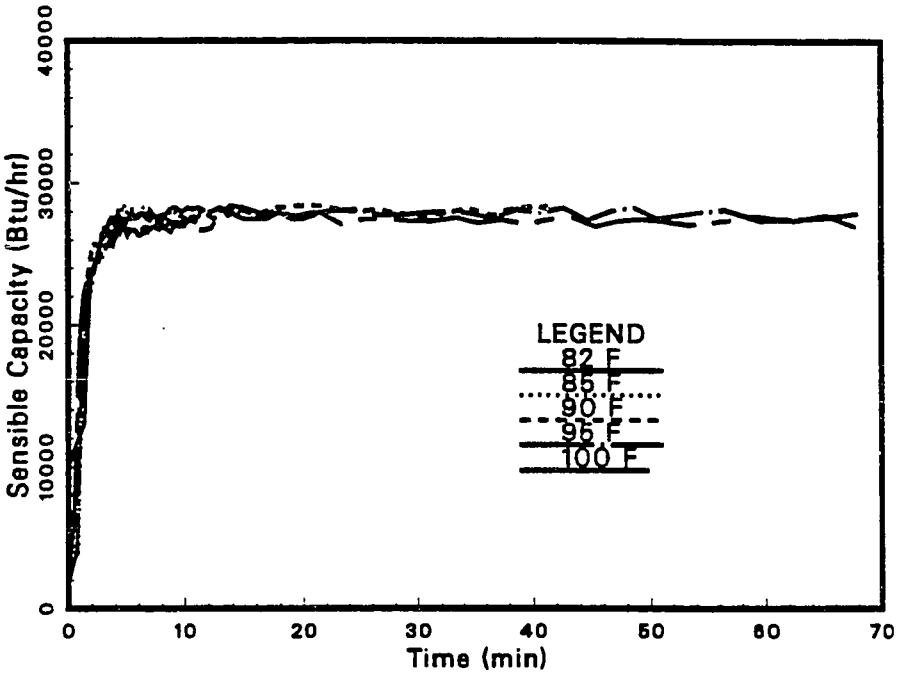

Figure 7.33 – Response of Cyclic Sensible Capacity at Various Outdoor Dry-Bulb Temperatures.

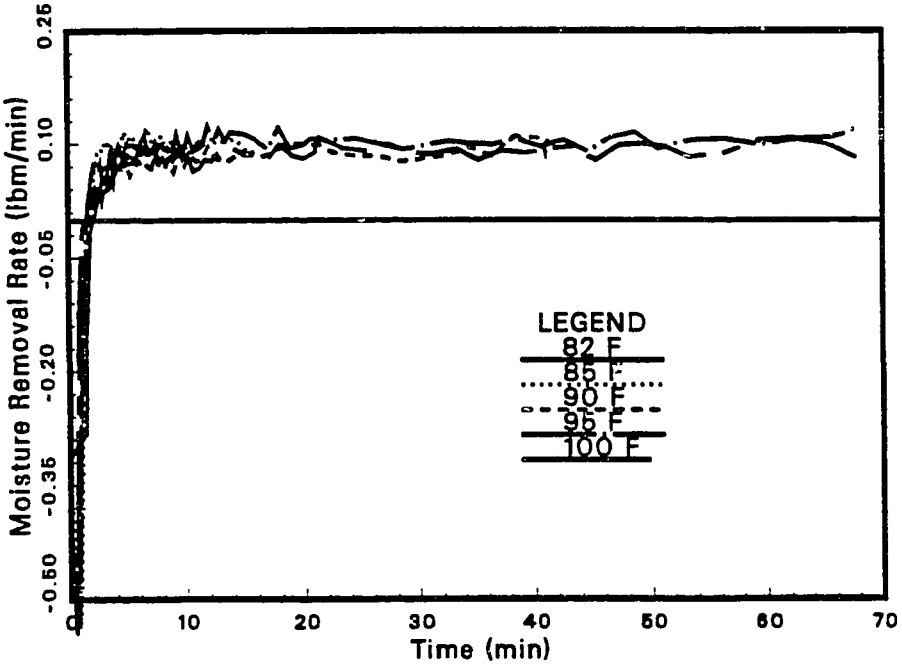

Figure 7.34 – Response of Moisture Removal Across the Evaporator Coil at Various Outdoor Dry-Bulb Temperatures.

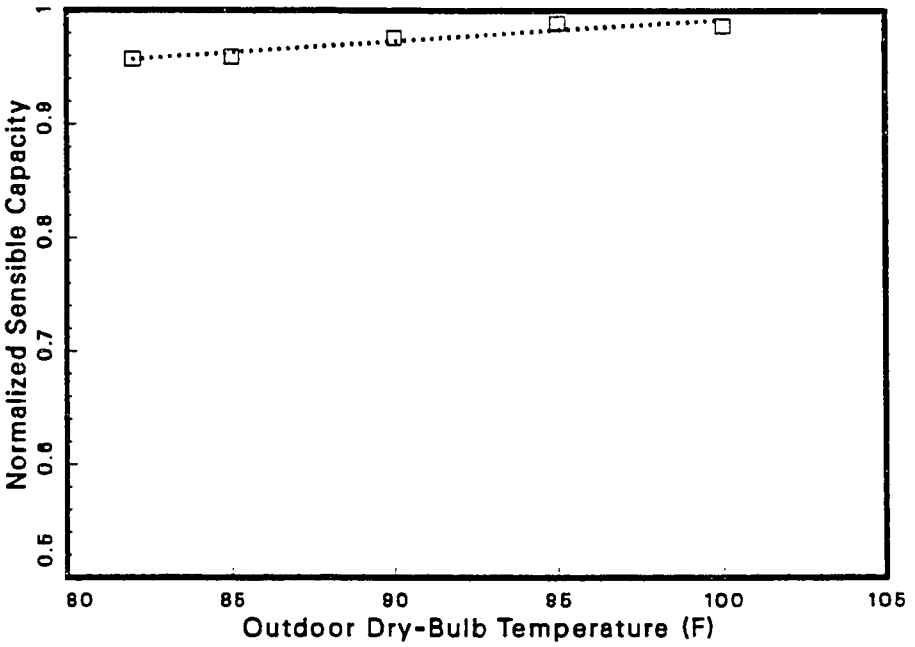

Figure 7.35 – Change in Normalized Sensible Capacity with Outdoor Dry-Bulb Temperature.

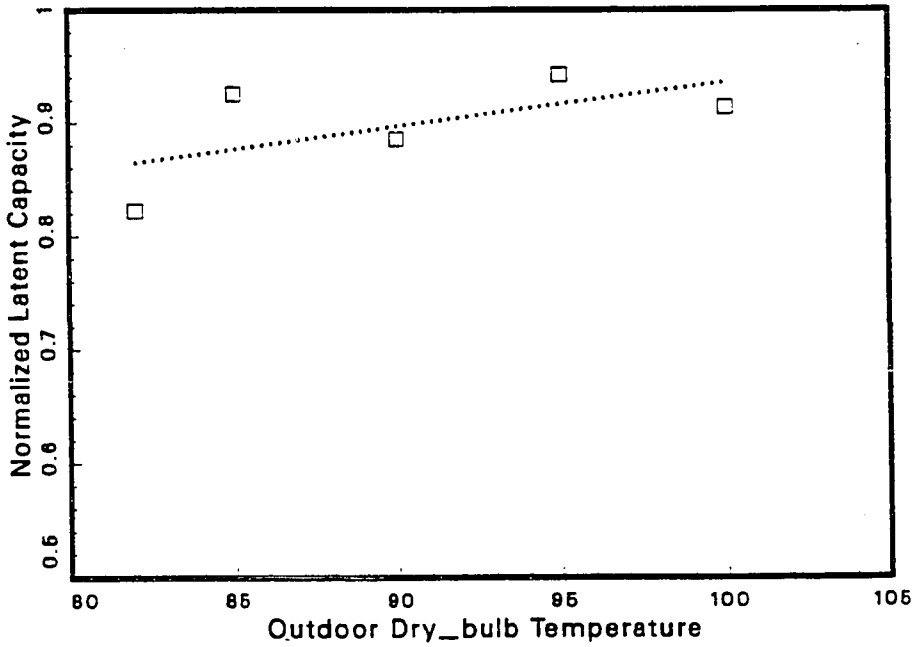

Figure 7.36 – Change in Normalized Latent Capacity with Outdoor Dry-Bulb Temperature.

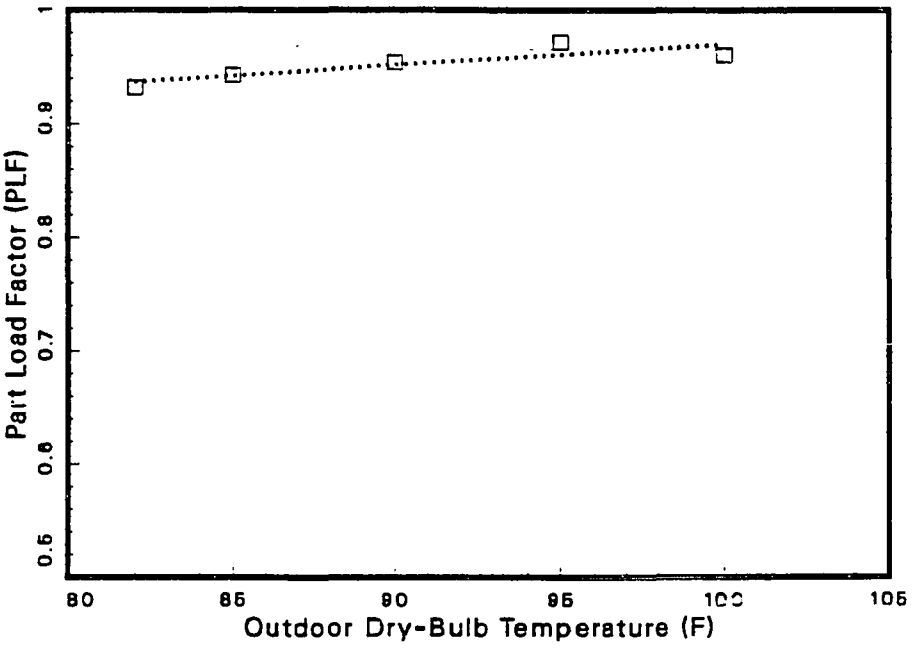

Figure 7.37 – Change in Part Load Factor with Outdoor Dry-Bulb Temperature.

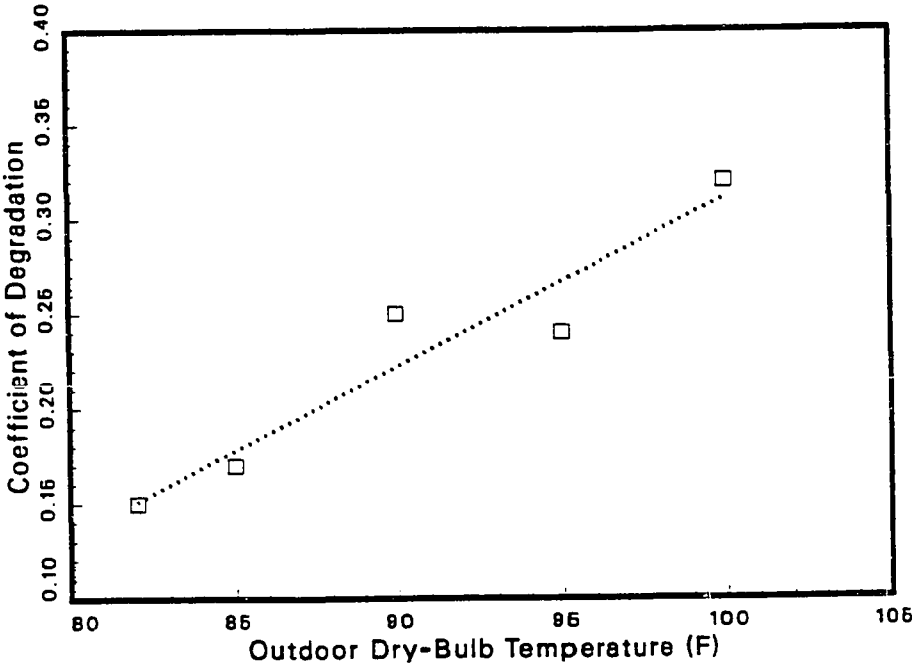

Figure 7.38 – Change in Coefficient of Degradation with Outdoor Dry-Bulb Temperature.

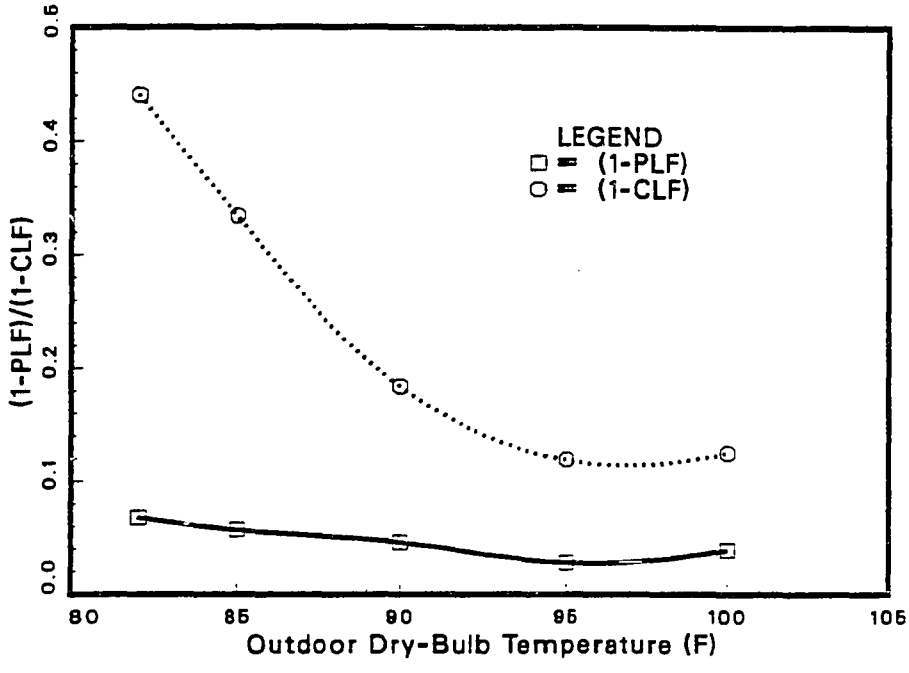

Figure 7.39 - Change in (1-PLF) and (1-CLF) with Outdoor Dry-Bulb Temperature.

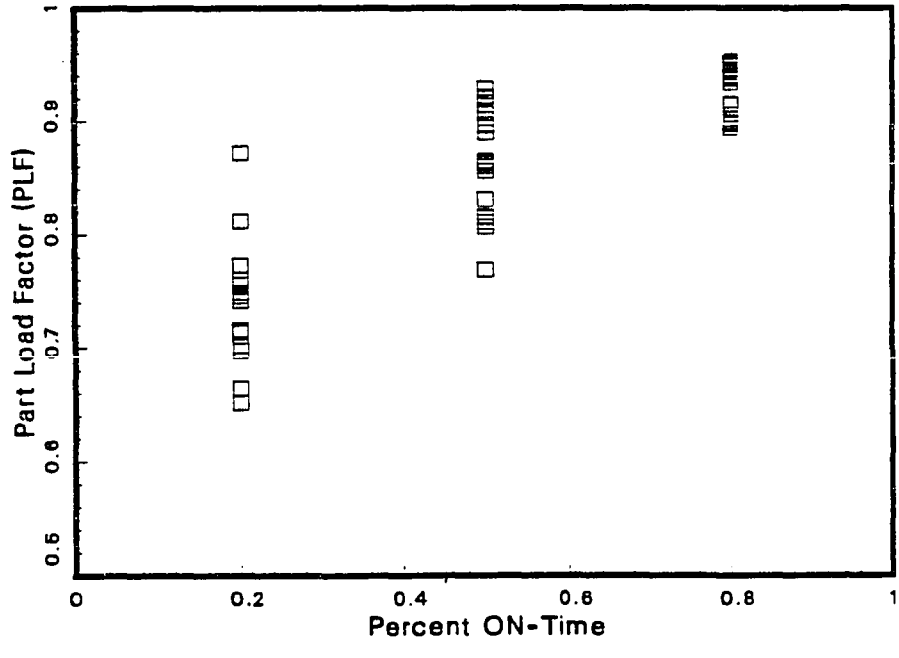

Figure 7.40 - Relationship of PLF with Percent ON-Time.

cycling rate) investigated in the present study.

Therefore, statistical analysis was performed on the experimental data to isolate the variables which affect the cyclic losses. In addition, two general equations were developed to estimate the PLF and C_D based on their functional relationship with the five dependent variables. The range for which the equations are valid are: (i) percent ON-time 20 to 95%, (ii) cycling rate 0.8 to 10, (iii) indoor relative humidity 20 to 67%, (iv) indoor dry-bulb temperature 72 to 80 F and (v) outdoor dry-bulb temperature 82 to 100 F. The total number of experiments was 64.

Because the PLF is an accepted indicator of cyclic loss and because C_D is a function of PLF, the relationship of PLF with the other variables was studied first. As the percent ON-time increased, the scatter in PLF decreased (Figure 7.40). The increase in PLF with percent ON-time was non-linear. This can be seen in Figure 7.41 where the change in PLF with percent ON-time at various cycling rates and constant indoor conditions (80 F and 50% Rh) and outdoor conditions (95 F) is shown. At 20 percent ON-time, the system run time varied from 3 to 10 minutes and the system OFF-time varied from 12 to 40 minutes. At 80 percent ON-time, the system ran from 12 to 40 minutes and the system was OFF from 3 to 10 minutes. Because the cyclic losses were maximum for the first few minutes after start-up, the PLF increased with an increase in run time. However, as the system OFF-time increased, the amount of refrigerant that migrated into the evaporator increased. Therefore, there was a decrease in PLF with an increase in system OFF-time even if the system run time remained constant.

The functional relationship between PLF and percent ON-time was similar

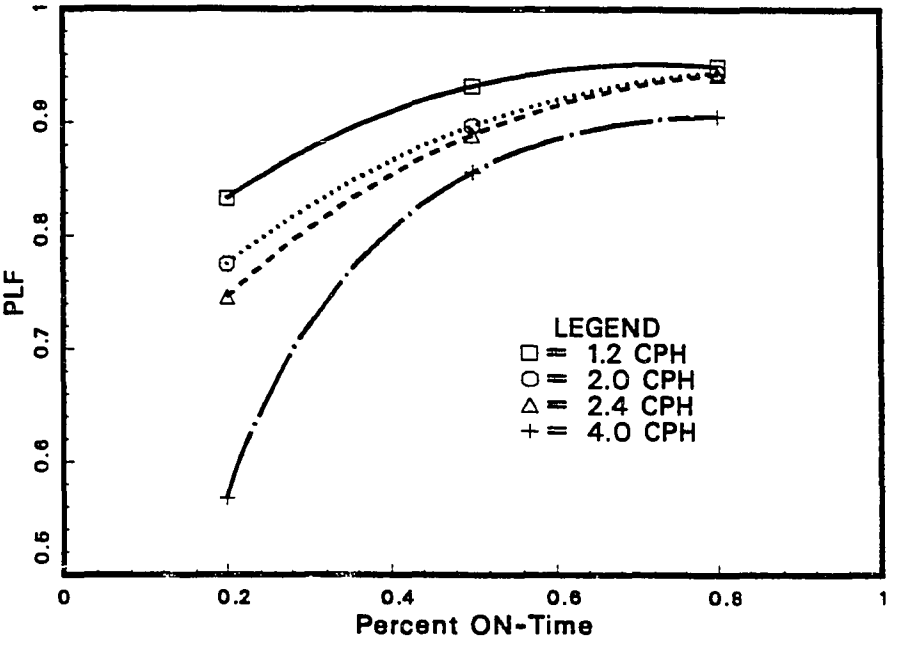

Figure 7.41 - PLF vs Percent ON-Time at Various Cycling Rate and Constant Indoor and Outdoor Conditions.

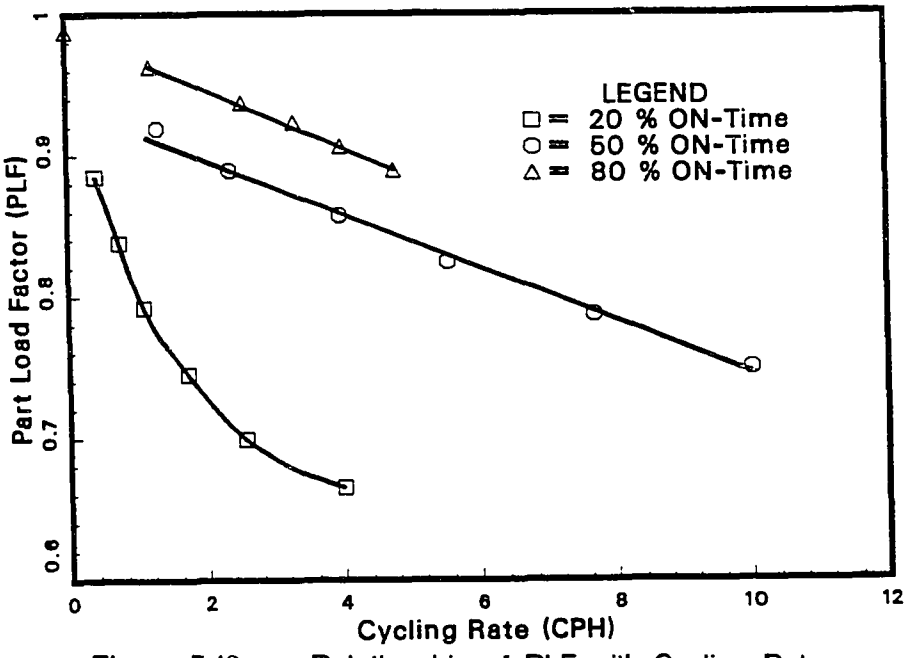

Figure 7.42 - Relationship of PLF with Cycling Rate at Constant Indoor and Outdoor Conditions.

to that of the total capacity response with ON-time. It increased sharply for low percent ON-times and flattened at high percent ON-times. The equation which gave a best fit for the experimental data was of the form:

$$PLF(ON,OFF) = \left[1 - e^{-\alpha * PON - \beta * (1-PON)}\right] \qquad (7.2)$$

where PON is percent ON-time and α and β are constants which were obtained from a non-linear least squares regression analysis of the experimental data. The values of α and β which resulted in a best fit are 3.59 and 1.37, respectively.

The change in PLF with cycling rate is shown in Figure 7.42. The relationship between PLF and CPH was approximated as a linear one. The change in PLF with relative humidity is shown in Figure 7.17. The relationship was assumed linear for a given percent ON-time. The variations of PLF with indoor and outdoor dry-bulb temperatures are shown in Figures 7.27, 7.31 and 7.37. The changes were small and linear.

Based on the functional relationship of PLF with the five independent variables, a multiple linear regression analysis was performed on the experimental data. The regression model relating the PLF to the five independent variables is of the form:

$$PLF = \beta_0 + \beta_1 PLF(ON,OFF) + \beta_2 Rh + \beta_3 CPH + \beta_4 T_i + \beta_5 T_o \qquad (7.3)$$

The summary of the statistical analysis is shown in Table 7.3. The second column shows the estimate of the parameter and the third column tells whether

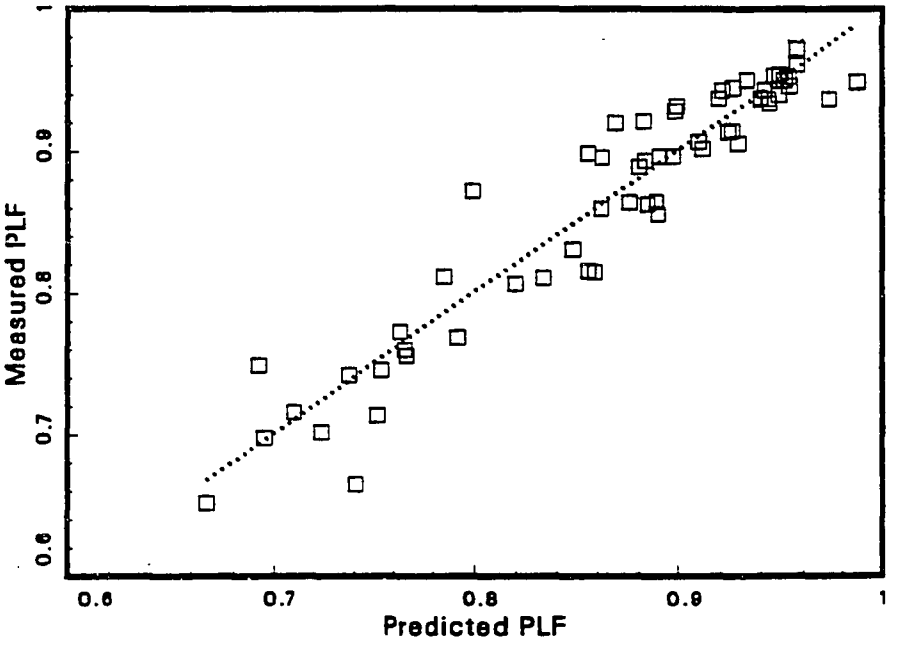

Figure 7.43 – Measured vs Predicted Part Load Factor.

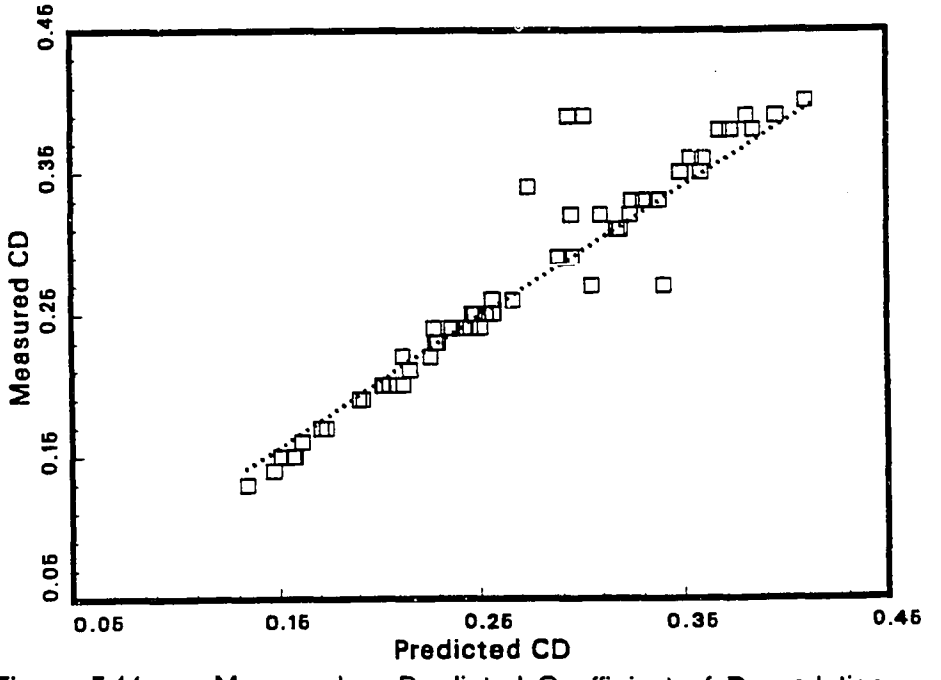

Figure 7.44 – Measured vs Predicted Coefficient of Degradation.

the parameter is statistically significant to be included in the model. Based on the number of degrees of freedom (60) and the confidence interval of 95%, a variable is not statistically significant if the absolute value in the third column is less than 1.67. The value for the outdoor temperature was found to be less than 1.67. Therefore, it was not included in the final relation. The higher the value in the third column, the greater is the contribution of that variable to the relation.

Table 7.3 - Summary of Statistical Analysis.

Parameter	Estimate	Test for H0: Parameter = 0 ?
β_0	-0.9264	-5.554
$\beta_1(PLF)$	1.5650	20.077
$\beta_2(Rh)$	0.2800	8.239
$\beta_3(CPH)$	-0.0068	-2.536
$\beta_4(T_i)$	0.0030	1.773

A plot of the measured PLF and the predicted is shown in Figure 7.43. The R-squared value was 0.91, which shows a excellent agreement.

The C_D is defined as the ratio of (1 - PLF) to (1 - CLF), where

$$PLF = \frac{EER_{cyc}}{EER_{ss}} \tag{7.4}$$

and

$$CLF = \frac{Q_{cyc}}{\dot{Q}_{ss}(t_{on} + t_{off})} \tag{7.5}$$

$$PLF \approx \frac{Q_{cyc}}{\dot{Q}_{ss} t_{on}} \tag{7.6}$$

since $E_{cyc}/E_{ss} \approx 1$, substituting Eq. 7.6 in Eq. 7.5:

$$CLF = \frac{PLF\ t_{on}}{(t_{on} + t_{off})} \tag{7.7}$$

where $t_{on}/(t_{on} + t_{off}) =$ PON, therefore, C_D :

$$C_D \approx \frac{(1 - PLF)}{(1 - PLF * PON)} \tag{7.8}$$

Using the above relationship a linear least square analysis was performed on the experimental data which yielded a R-squared of 0.91. The slope for the fit was 1.0426 and the intercept was -0.00435 which was statistically insignificant. The plot of the measured and predicted values is shown in Figure 7.44. Substituting Eq. 7.3 in Eq. 7.8 the C_D can now be estimated in terms of the four independent variables: indoor dry-bulb temperature and relative humidity, percent ON-time and cycling rate.

$$C_D = \frac{1 + .9264 - .2800Rh - 1.5650PLF(ON,OFF) + .0068CPH - .0030T_i}{1 - [-.9264 + .2800Rh + 1.5650PLF(ON,OFF) - .0068CPH + .0030T_i]\,PON} \tag{7.9}$$

The PLF can be estimated for a wide range of operating conditions with the help of Eq. 7.3. Therefore, SEER can be estimated more realistically. According to the ASHRAE Standard [1983] the SEER is defined as:

$$SEER = \frac{\sum_{j=1,n} LF(T_j)\dot{q}_{ss}(T_j)n_j}{\sum_{j=1,n} \frac{LF(T_j)E_{ss}(T_j)n_j}{PLF}} \tag{7.10}$$

where

$$LF(T_j) = \frac{BL(T_j)}{\dot{q}_{ss}(T_j)} \tag{7.11}$$

where the buliding load, $BL(T_j)$, can be estimated from:

$$BL(T_j) = \frac{(5j-3)}{(T_{od}-65)} \frac{\dot{q}_{ss}(T_{od})}{\text{size factor}} \tag{7.12}$$

where T_{od} is the outdoor design temperature and the size factor is the amount of over or undersizing desired. For all the equations:

$j = 1,2,3\ldots,n$ correspond to the j^{th} temperature bin

$n =$ total number of non-zero temperature bins in the climatic region

Substituting Eq. 7.11 into Eq. 7.10

$$SEER = \frac{\sum_{j=1,n} BL(T_j) n_j}{\sum_{j=1,n} \frac{BL(T_j) E_{ss} n_j}{\dot{q}_{ss}(T_j) PLF}} \tag{7.13}$$

$$EER_{ss}(T_j) = \frac{\dot{q}_{ss}}{E_{ss}}$$

$$SEER = \frac{\sum_{j=1,n} BL(T_j) n_j}{\sum_{j=1,n} \frac{BL(T_j) n_j}{EER_{ss}(T_j) PLF}} \tag{7.14}$$

The PLF is independent of the outdoor temperature; however, it is dependent on percent ON-time and cycling rate, which in turn are functions of the outdoor dry-bulb temperature. The standard requires PLF to be estimated at only one ambient condition. Therefore, the Eq. 7.14 along with Eq. 7.3 may provide a more realistic estimate of SEER.

SUMMARY OF TRANSIENT BEHAVIOR

Although a number of tests were run for a wide range of operating conditions, a general characterization of the transient behavior of heat pumps was not possible. However, this study illuminated certain trends required to characterize both the transient sensible and dehumidification performance of heat pumps. In the following section these characteristics are summarized.

Summary of Dehumidification Performance

For almost all tests, moisture removal was negative at start-up because the moisture which had collected on the evaporator coil during the OFF cycle evaporated into the air-stream at start-up. In comparison, sensible capacity began almost instantly. Dehumidification began 60 to 150 seconds after

start-up depending on the indoor ambient conditions, percent ON-time and cycling rate. The outdoor dry-bulb temperature had no effect on the transient dehumidification process.

The dehumidification response increased with an increase in percent ON-time and decrease in cycling rate. The effect of percent ON-time and cycling rate was more severe on the latent capacity than on the sensible capacity. For example, the normalized latent capacity at 20 percent ON-time and cycling rate of 4 cph was 0.28. At the same conditions, the normalized sensible capacity was 0.78. At high percent ON-times, the normalized latent capacity was comparable with normalized sensible capacity (7%).

The transient dehumidification response increased with indoor relative humidity. However, the dehumidification process did not begin until 60 seconds after start-up even at high relative humidity (67%). It took 6 minutes after start-up, for the latent capacity to reach steady-state at 67% indoor relative humidity and about 12 minutes at 45% indoor relative humidity. The normalized latent capacity increased with an increase in indoor relative humidity.

The response of the transient dehumidification increased with an increase in indoor dry-bulb temperature at constant indoor relative humidity. However, at constant indoor dew-point temperature the response decreased. There was an increase in the normalized latent capacity with indoor temperature for both constant indoor relative humidity and constant dew-point temperature.

The outdoor dry-bulb temperature had little effect on the transient dehumidification. The normalized latent capacity increased slightly with outdoor dry-bulb temperature because of an increase in the percent ON-time.

Summary of Overall Performance

The effect of five variables (indoor and outdoor dry-bulb, indoor relative humidity, percent ON-time and cycling rate) on the transient performance was studied in detail. The results indicated that PLF, which is a ratio of cyclic EER to steady-state EER, can be as low as 0.65. At low percent ON-times and high cycling rates, the cyclic losses were maximum. At high percent ON-times, low cycling rates and high relative humidities, the cyclic losses were minimum. Even at the most favorable conditions, it took almost 6 minutes for the system to reach steady-state. At 80 F indoor temperature, indoor relative humidity of 50 % Rh and 95 F outdoor temperature (Test A), it took 12 minutes for the system to reach steady-state. There was a wide variation of C_D with the five variables (0.1 to 0.4). In general, the C_D at 50 percent ON-time was less than at 80 and 20 percent ON-times.

Because most of the cycling losses occurred during the first few minutes after start-up, the PLF increased with percent ON-time. However, at low cycling rates the PLF did not vary significantly with percent ON-time (0.75 at 20% ON-time and 0.85 at 80% ON-time). The combination of high cycling rates and low percent ON-times caused maximum cyclic losses. The percent ON-time was found to be the single most important parameter in determining the cyclic losses of a heat pump. The C_D increased linearly with an increase in cycling rate for a given percent ON-time.

The transient system response increased with an increase in indoor relative humidity. It took approximately 6 minutes, after start-up, for the system to reach steady-state for an indoor relative humidity of 67%, whereas it took almost 12 minutes at 20% RH. There is a 22% increase in PLF

with relative humidity change from 20 to 67% at 20 percent ON-time. The increase in transient response with relative humidity was due to: (i) A decrease in steady-state sensible capacity which also indicates that the average coil temperature increased; therefore, the coil reached steady-state faster. (ii) An increase in dew-point temperature of the air-stream; therefore, dehumidification began early. (iii) An increase in sensible heat transfer coefficient for relative humidities greater than 40% because of a thin water film on the evaporator coil. The C_D decreased with an increase in the indoor relative humidity. The difference in C_D between 20 and 80 percent ON-times was very small (less than 5%).

There was a slight increase in transient response with indoor temperature. The transient response did not change with outdoor temperature. However, there was an increase in PLF with outdoor temperature because of an increase in percent ON-time. There was a slight increase in PLF with indoor temperatures. The C_D decreased with an increase in the indoor dry-bulb temperature at constant relative humidity at both 50 and 80 percent ON-times. There was no change in the C_D with indoor temperature at constant dew-point temperature. The C_D increased with an increase in outdoor dry-bulb temperature.

CHAPTER VIII

MODEL RESULTS

A number of researchers have successfully modeled the transient performance of heat pumps. The present model, which is a modified version of TRPUMP, is a useful extension to the previous work. In this chapter, the results estimated by the model are compared with the experimental results which were discussed in the previous chapter.

Before the parametric runs were attempted, a suitable time step was chosen. For a stable solution to the differential equations the time step, Δt, could not be too large. If the value was too small, the computer processing time became excessive and the round-off errors increased. The optimum time-step was determined by internal halving. That is, the model was first run with an arbitrary time step, then the time step was halved and the model was run again. If the two results did not match, the internal halving procedure was repeated until two successive run results agreed to a pre-set desired accuracy of 0.1%. Table 8.1 shows the effect of the time step on selected variables. The optimum time step was 0.4 milli seconds.

SIMULATION OF TRANSIENT CHARACTERISTICS

The indoor and outdoor conditions for the simulation are shown in Table 6.2. Initially, the system was assumed to be at a constant pressure. The initial temperatures at various points in the system are shown in Table 8.2. The state of the refrigerant (enthalpy, entropy, internal energy, etc.,) in each of the components was estimated from the refrigerant relationships, since the pressure and temperature of each component were known.

Table 8.1 - Affect of Time-Step on Selected Variables.

Variable	Δt 0.0002	0.0004	0.0008	0.0016	0.0032
Total Air Cap. (Btu)	36,049	36,023	36,156	36,195	—
Total Ref. Cap. (Btu)	35,792	35,964	36,113	36,174	—
EER_{cyc}	9.92	9.92	9.94	9.97	UNSTABLE
SHR_{cyc}	0.817	0.817	0.815	0.814	
$\dot{m}_{ref}$ (lbm)	98.31	98.35	98.29	98.28	—
$Energy_{cyc}$ (Watts)	550	550	550	550	—

The simulated transient response of the suction and discharge pressures are compared with the experimental response in Figure 8.1. The simulated suction pressure followed the experimental response very closely. There was a rapid rise in the simulated discharge pressure and at the end of a ten minute cycle. It was 7% lower than the measured discharge pressure. The simulated transient suction and discharge temperatures are shown in Figure 8.2. Both the simulated temperatures followed the experimental curves closely for about 40 seconds. Thereafter, the simulated suction temperature was higher and the simulated discharge temperature was lower than the experimental values.

The comparison of transient response of the power consumption and mass flow rate of the refrigerant are shown in Figure 8.3. Initially, there was

Table 8.2 - Initial Temperatures for Selected Components.

Component	Temperature (F)
Compressor Wall	90
Condenser	93
Evaporator	80
Air Entering Condenser Coil	95
Air Entering Evaporator Coil	78

a rapid rise in the simulated mass flow rate, and it leveled off and closely followed the measured flow rate after 3 minutes. The simulated transient power consumption curve closely followed the experimental curve.

The comparison of sensible, latent and total capacities is shown in Figure 8.4. The simulated sensible capacity rose rapidly and, therefore, reached steady-state faster. However, the simulated latent capacity followed the measured capacity closely. The simulated results showed that the system reached steady-state after 4 minutes, whereas the measured results showed that the system took 6 minutes to reach steady-state. Because the model does not account for the refrigerant dynamics during the off cycle, and also because of the rapid rise in the refrigerant mass flow rate, the simulated capacity reached steady-state faster.

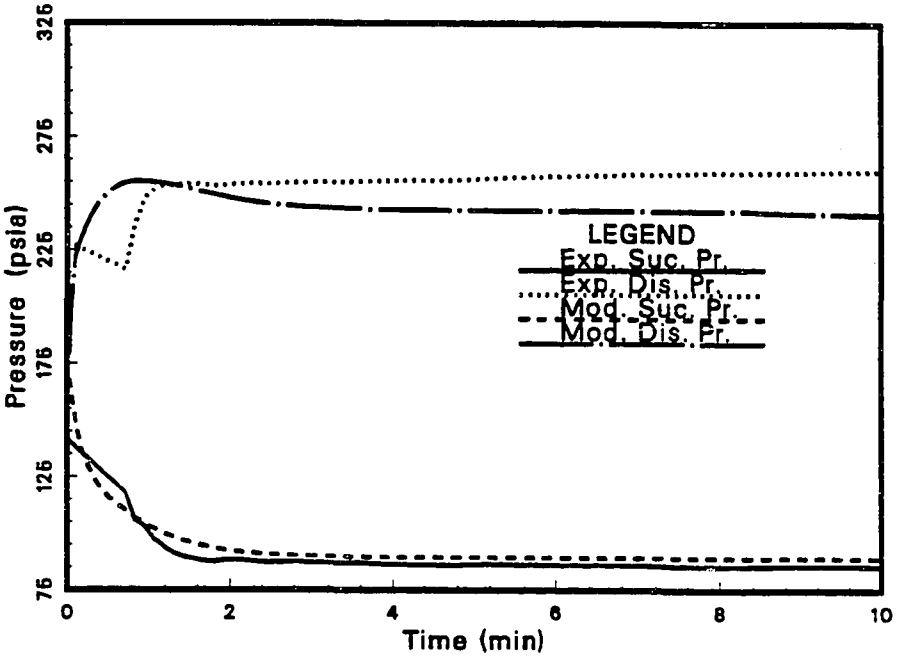

Figure 8.1 – Comparison of Compressor Suction and Discharge Pressure.

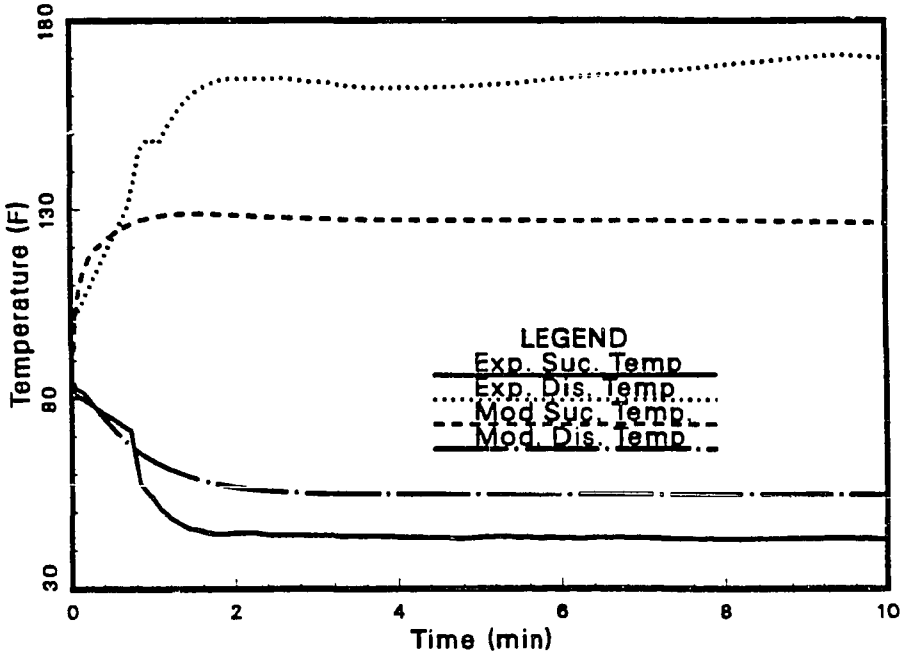

Figure 8.2 – Comparison of Compressor Suction and Discharge Temperature.

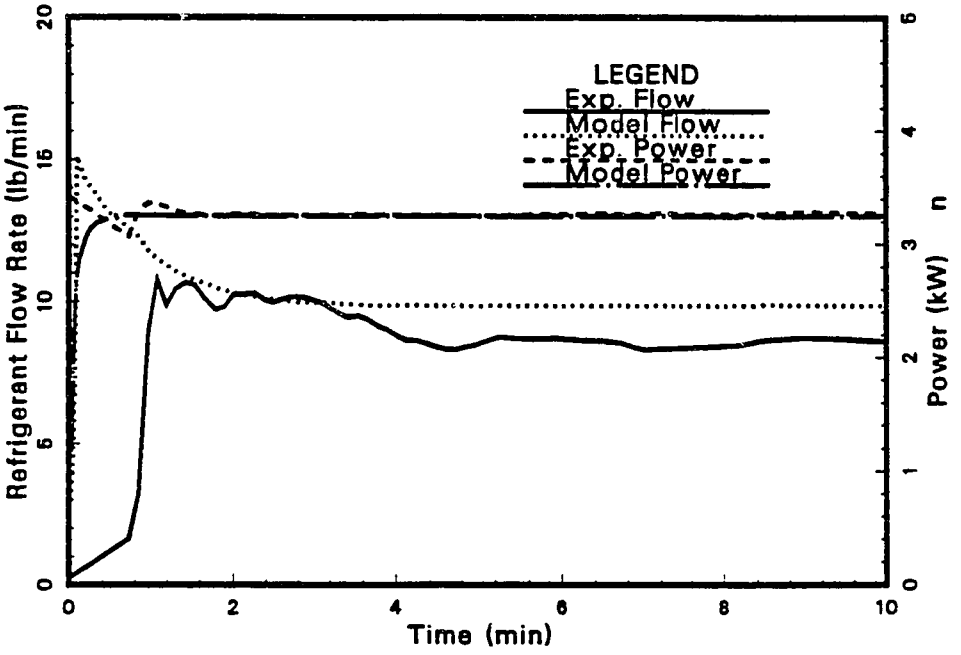

Figure 8.3 – Comparison of Refrigerant Mass Flow Rate and Power Consumption.

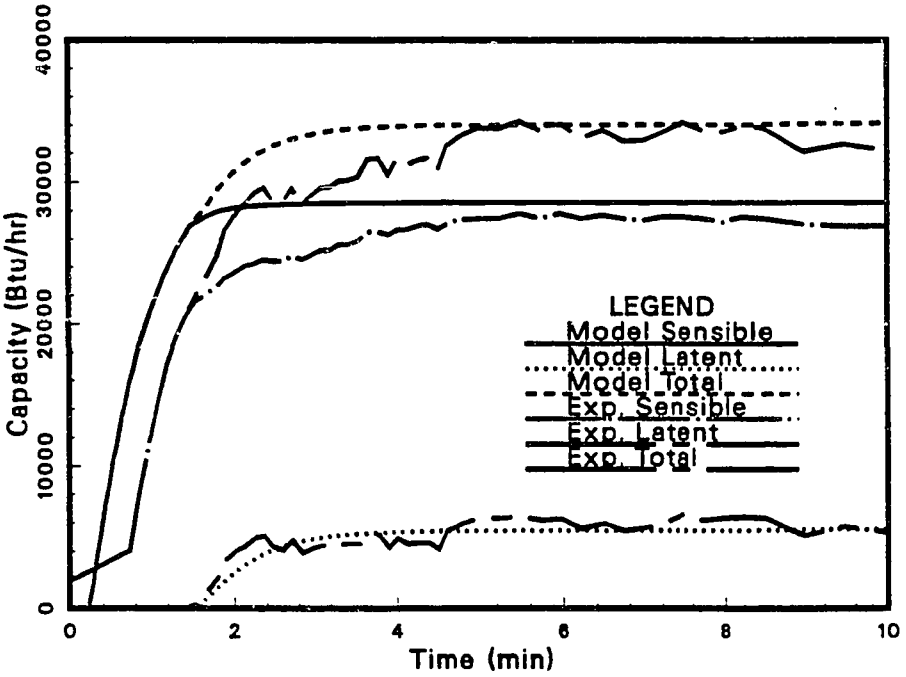

Figure 8.4 – Comparison of Air-Side Latent, Sensible, and Total Capacities.

COMPARISON OF RESULTS AT VARIOUS INDOOR RELATIVE HUMIDITIES

The model was run for various indoor relative humidities and the simulated results were compared with the measured results. The indoor and outdoor dry-bulb temperatures, the indoor air flow rate, and the percent ON-times are given in Table 5.2. The comparison of sensible and latent response at 20 % and 67 % indoor relative humidities and 20 percent ON-time is shown in Figures 8.5 and 8.6. There was a rapid rise in the simulated response at 20 % Rh, and it reached steady-state faster than the measured response. However, the simulated results at 67 % Rh closely followed the measured values. The comparison of the normalized capacities at 80 and 20 percent ON-times is shown in Figures 8.7 and 8.8, respectively. The simulated normalized capacities increased with an increase in the indoor relative humidity. However, at low relative humidities, the simulated normalized capacity was higher than measured value.

As the relative humidity increased, the simulated results matched the measured results. With an increase in the indoor relative humidity, the measured response reached steady-state faster. Therefore, the simulated results compared well at high relative humidities with the measured results. As the percent ON-time decreased, the deviation of the simulated sensible capacity from the measured value increased. The simulated normalized capacities were higher because: (i) As the percent ON-time decreased, the effect of the cycling losses became more severe. The present model was not capable of modeling shut-down. Therefore, it could not account for all the losses. (ii) The model was based on a lumped parametric approach. Thus, the losses due to off-cycle refrigerant migration into the evaporator and

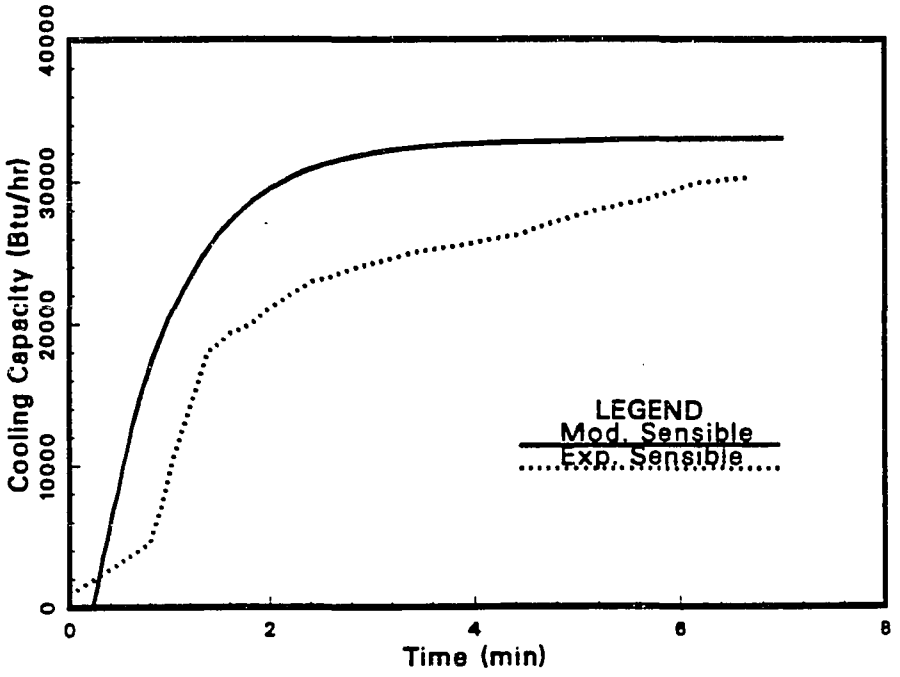

Figure 8.5 – Comparison of Cyclic Sensible and Latent Response at 20 % Indoor Relative Humidity and 20 Percent ON-Time.

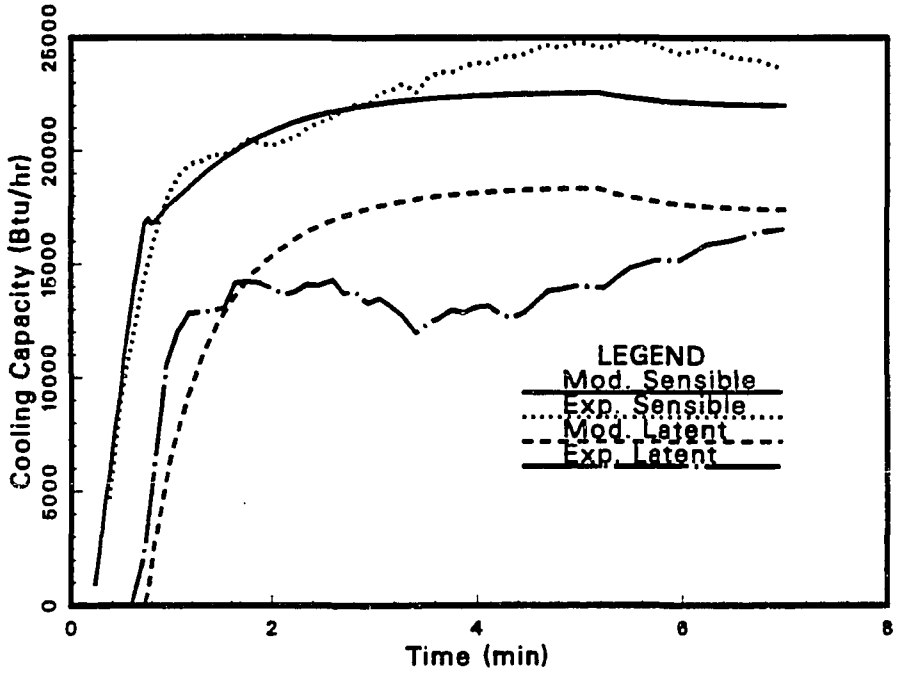

Figure 8.6 – Comparison of Cyclic Sensible and Latent Response at 67 % Indoor Relative Humidity and 20 Percent ON-Time.

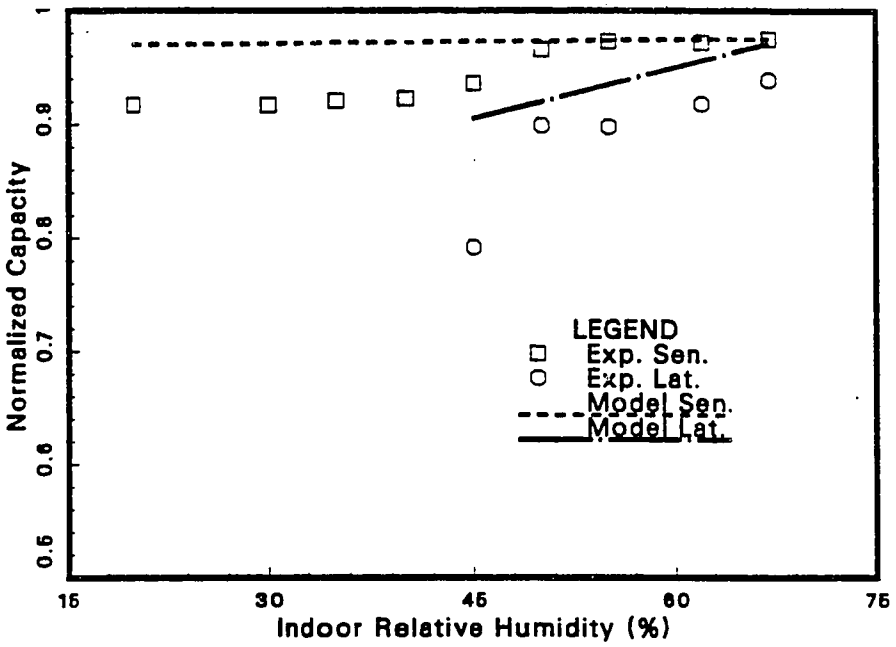

Figure 8.7 – Comparison of Normalized Sensible and Latent Capacities at Various Indoor Relative Humidities and 80 Percent ON-Time.

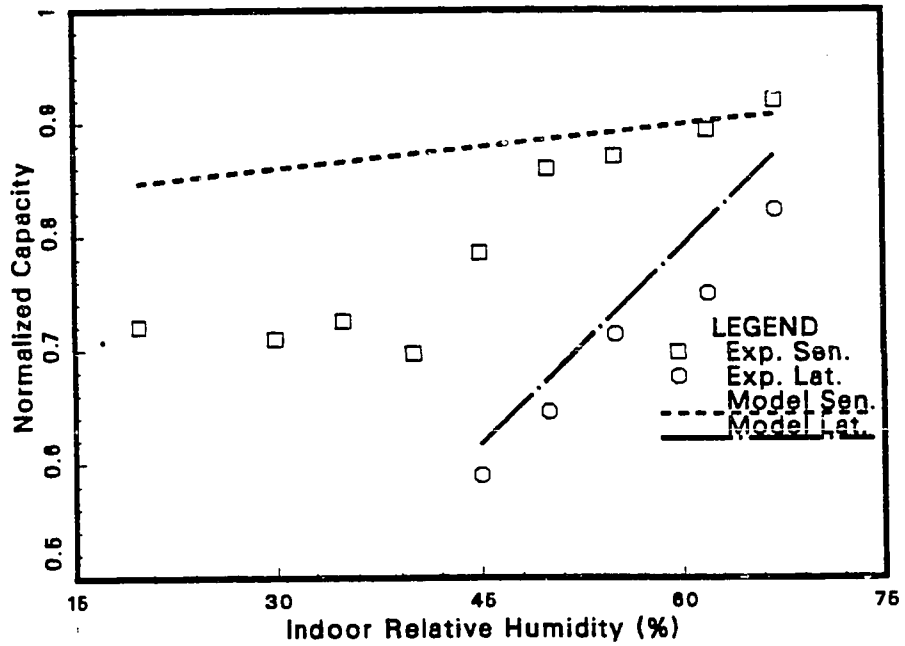

Figure 8.8 – Comparison of Normalized Sensible and Latent Capacities at Various Indoor Relative Humidities and 20 Percent ON-Time.

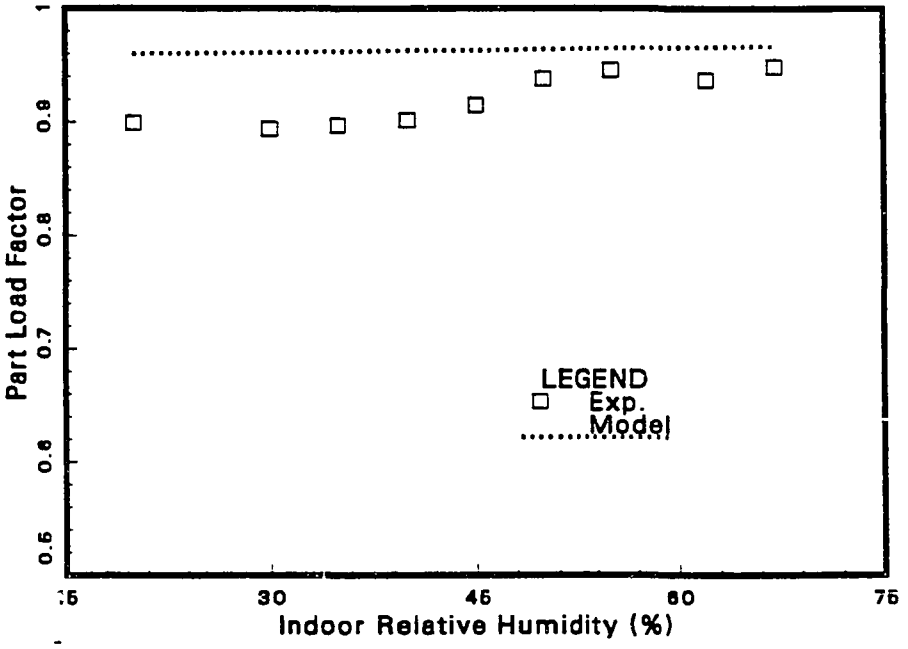

Figure 8.9 – Comparison of Part Load Factors at Various Indoor Relative Humidities and 80 Percent ON-Time.

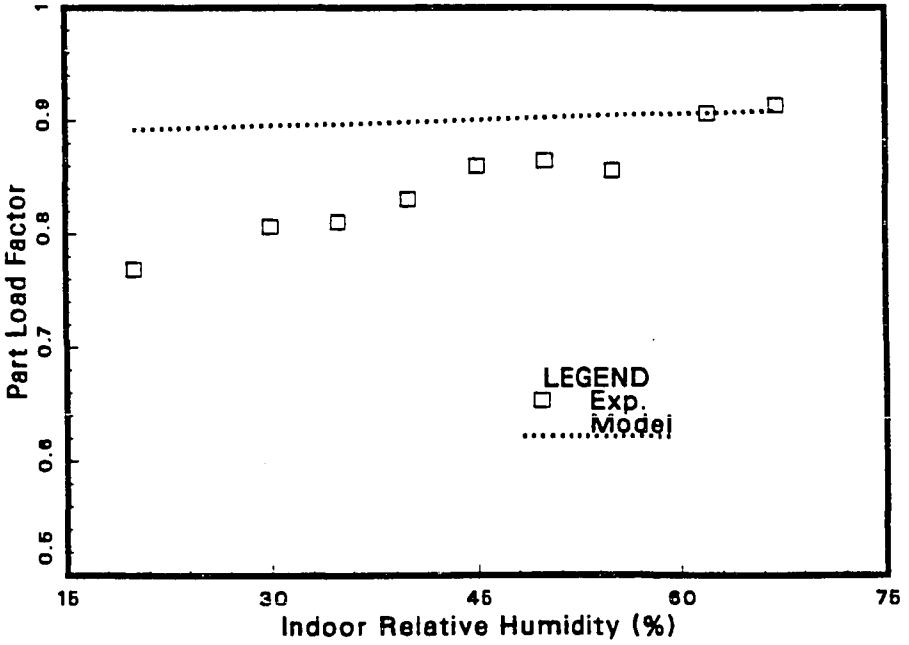

Figure 8.10 – Comparison of Part Load Factors at Various Indoor Relative Humidities and 20 Percent ON-Time.

accumulator were not modeled. The comparison of the part load factor (PLF) at various indoor relative humidities is shown in Figures 8.9 and 8.10. The trends were similar to that of the normalized capacities.

COMPARISON OF RESULTS AT VARIOUS INDOOR DRY-BULB TEMPERATURES

The comparison of the latent and sensible responses at 80 F and 76 F indoor dry-bulb temperatures, 50% indoor relative humidity and 80 percent ON-time is shown in Figures 8.11 and 8.12, respectively. For both cases the simulated sensible response reached steady-state faster than for the measured case. However, the simulated latent response closely followed the measured response. The comparison of normalized capacities at various indoor dry-bulb temperatures and constant indoor relative humidity of 50% is shown in Figures 8.13 and 8.14, respectively. The simulated results compared well with the measured results for both 80 and 50 percent ON-times. The PLFs for the simulated results also compared well with the measured values (Figures 8.15 and 8.16).

The comparison of the latent and sensible responses at 78 F and 72 F indoor dry-bulb temperatures, 58 F dew-point temperature and 80 percent ON-time is shown in Figures 8.17 and 8.18, respectively. The simulated response at 78 F reached steady-state faster than the measured response. However, the simulated results at 72 F closely followed the measured values. There was also a good agreement of the simulated normalized capacity with the measured results at various indoor dry-bulb temperatures and constant indoor dew-point temperature (Figures 8.19 and 8.20).

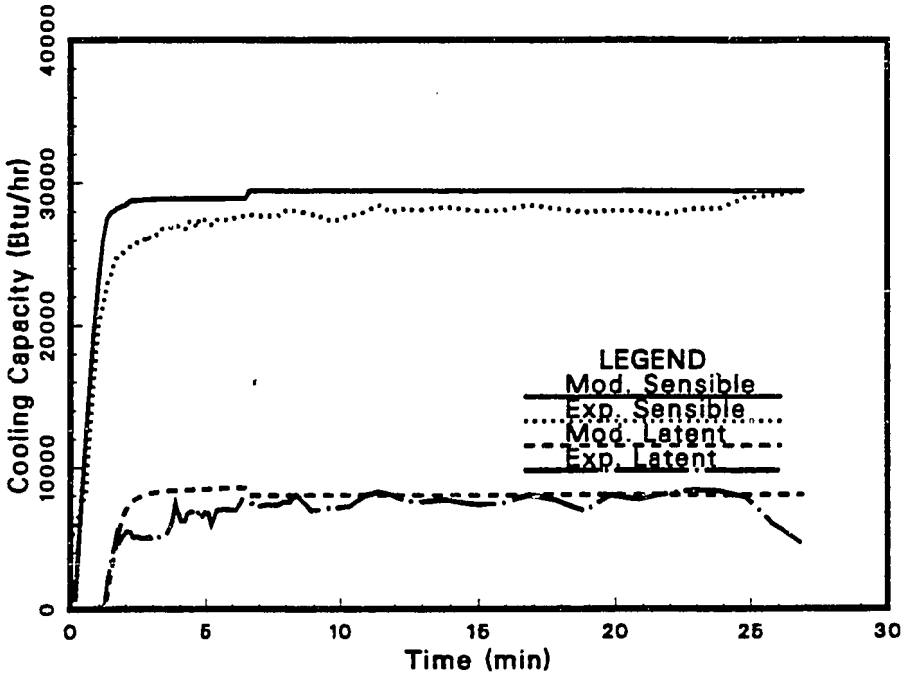

Figure 8.11 – Comparison of Cyclic Sensible and Latent Response at 80 F Indoor Dry-Bulb Temperature and 80 Percent ON-Time.

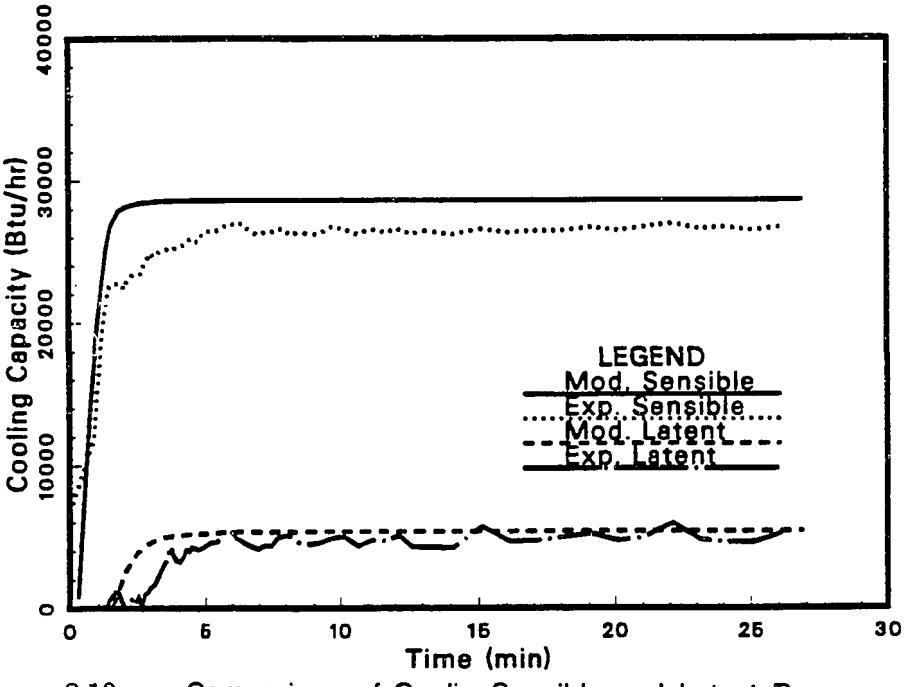

Figure 8.12 – Comparison of Cyclic Sensible and Latent Response at 76 F Indoor Dry-Bulb Temperature and 80 Percent ON-Time.

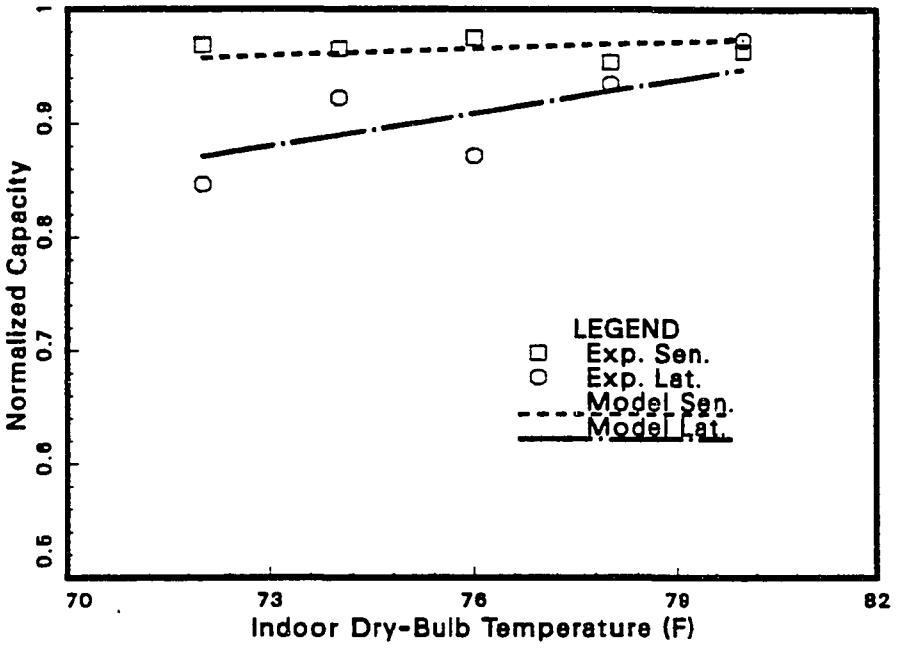

Figure 8.13 - Comparison of Normalized Sensible and Latent Capacities at Various Indoor Temperatures, 50 % Rh and 80 Percent ON-Time.

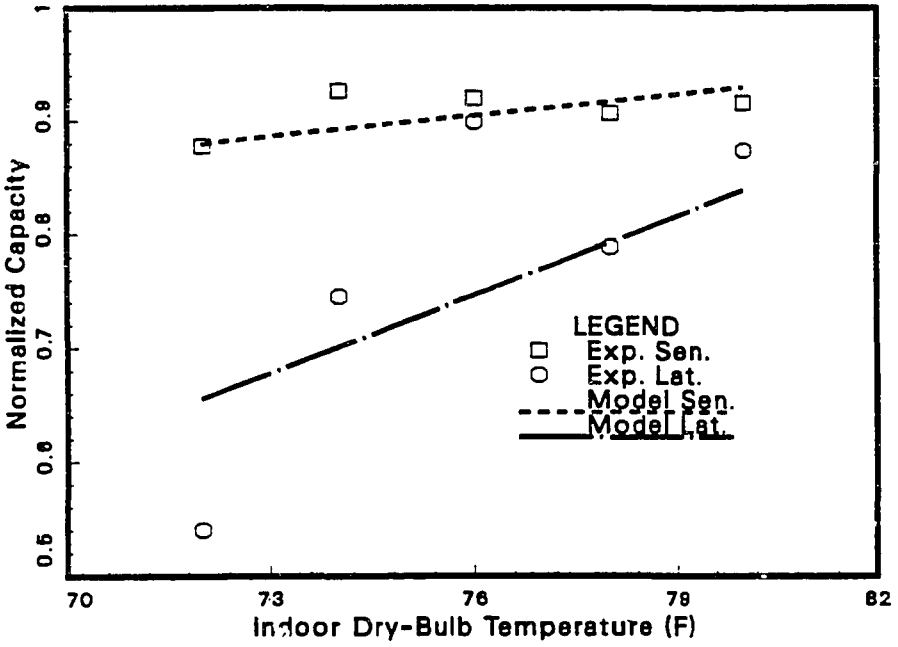

Figure 8.14 - Comparison of Normalized Sensible and Latent Capacities at Various Indoor Temperatures, 50 % Rh and 50 Percent ON-Time.

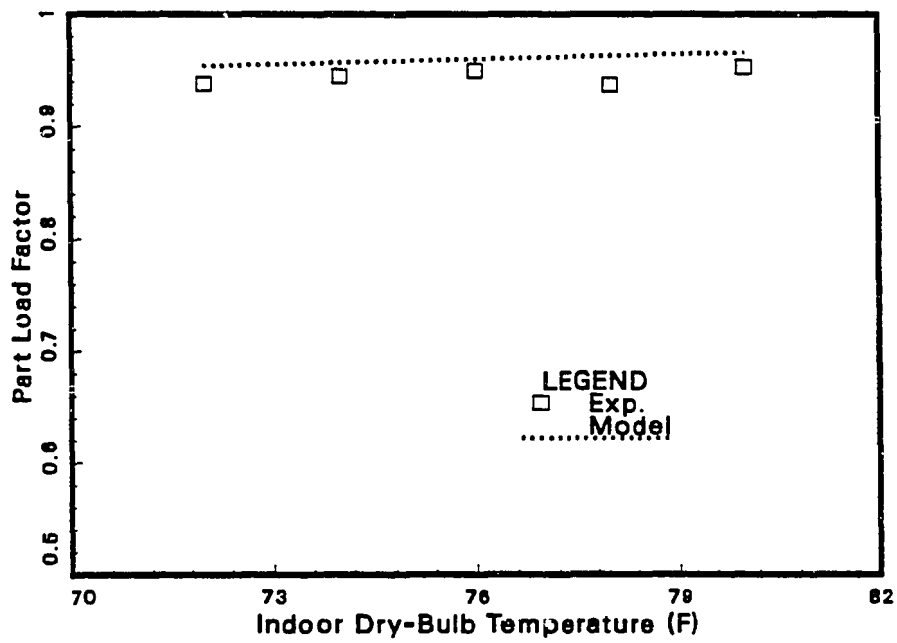

Figure 8.15 - Comparison of Part Load Factors at Various Indoor Dry-Bulb Temperatures, 50 % Rh and 80 Percent ON-Time.

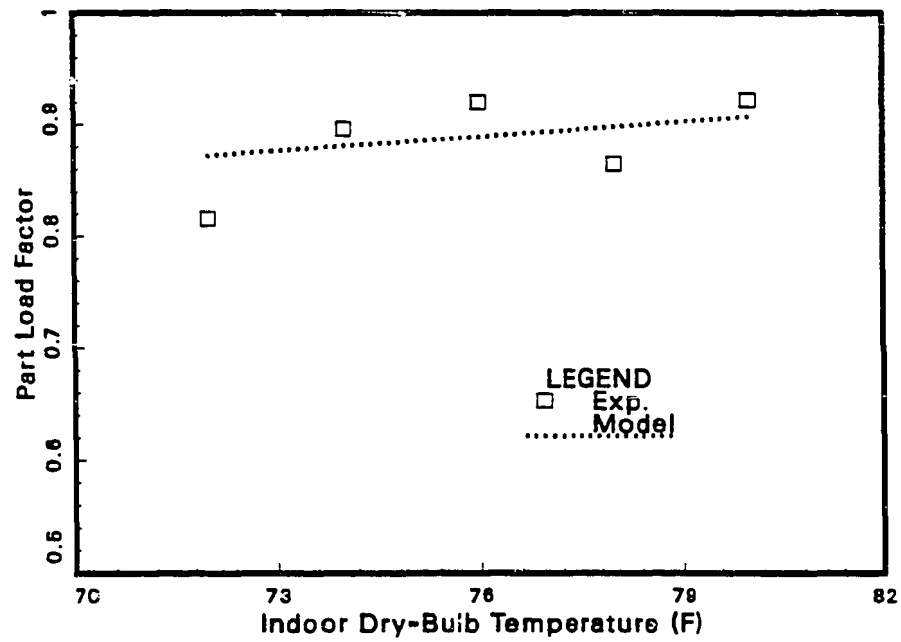

Figure 8.16 - Comparison of Part Load Factors at Various Indoor Dry-Bulb Temperatures, 50 % Rh and 20 Percent ON-Time.

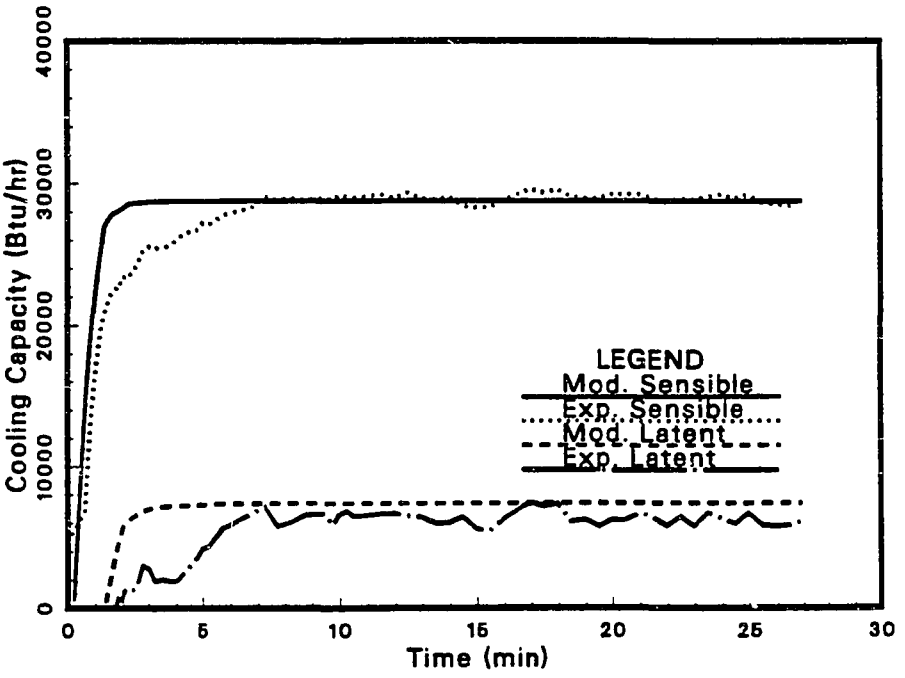

Figure 8.17 – Comparison of Cyclic Sensible and Latent Response at 78 F Indoor Dry-Bulb Temperature and 80 Percent ON-Time.

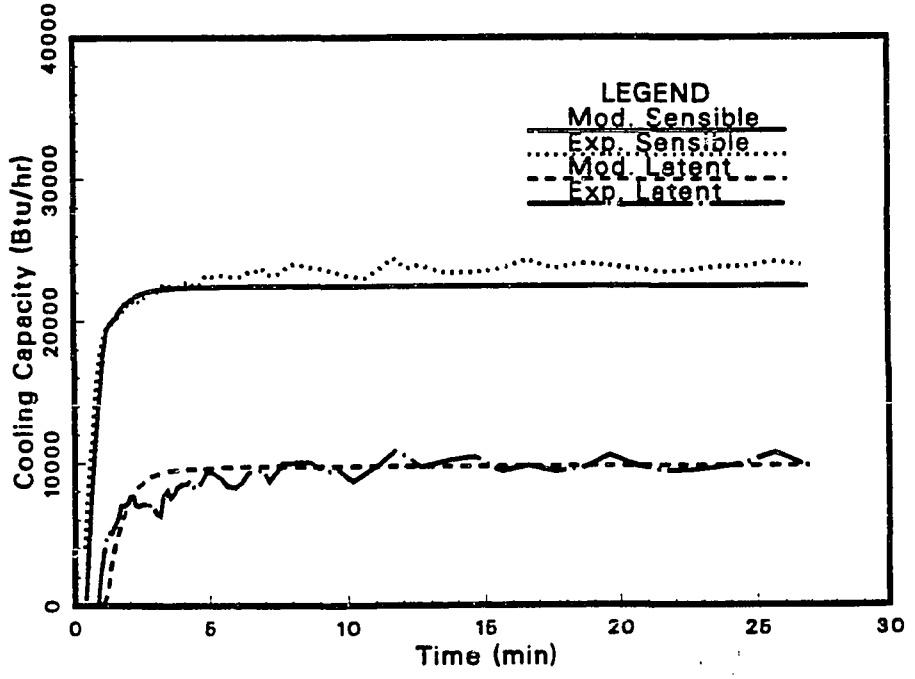

Figure 8.18 – Comparison of Cyclic Sensible and Latent Response at 72 F Indoor Dry-Bulb Temperature and 80 Percent ON-Time.

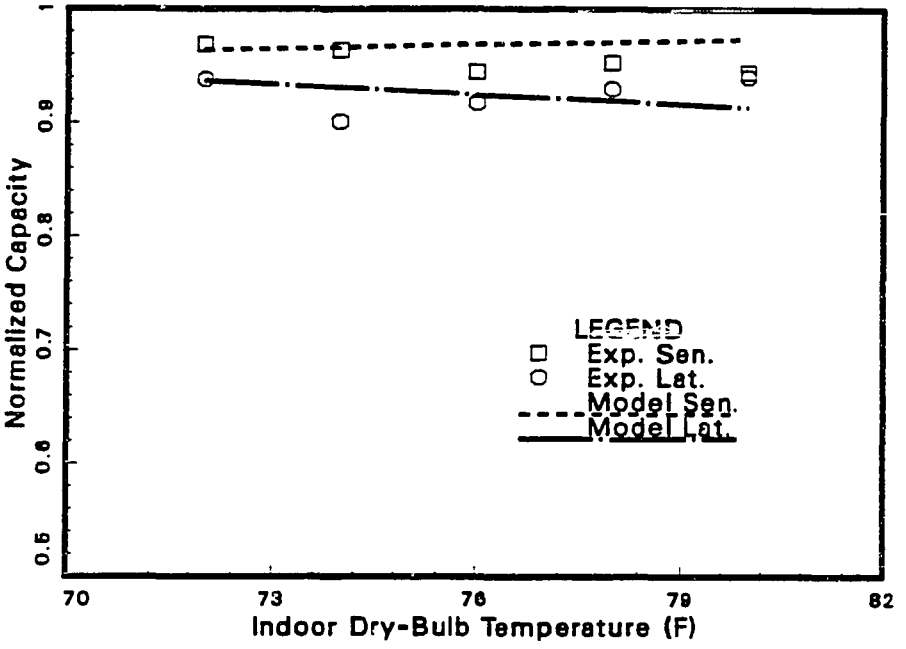

Figure 8.19 - Comparison of Normalized Sensible and Latent Capacities at Various Indoor Temperatures, 58 F Dew-Point and 80 % ON-Time.

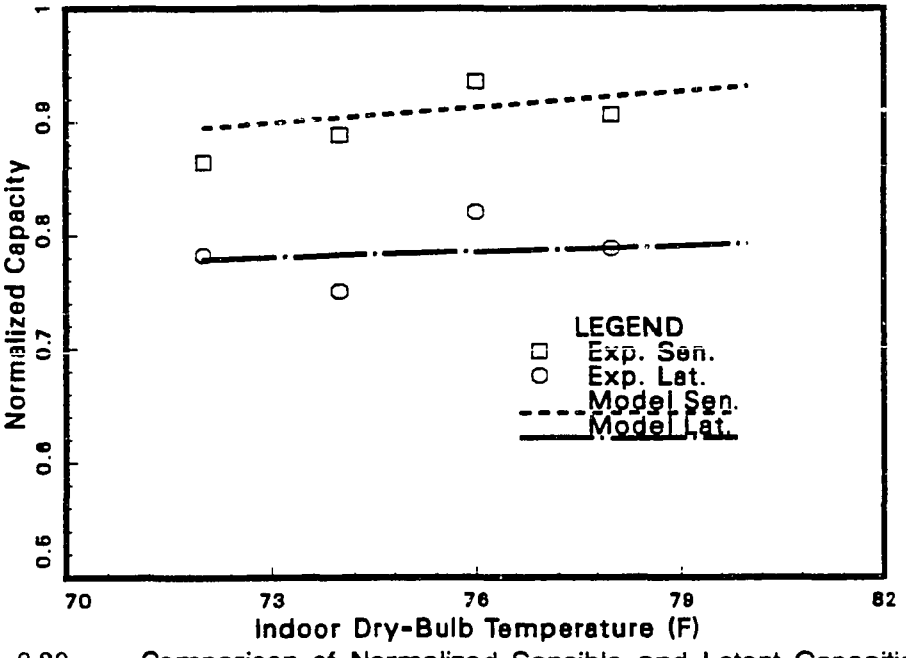

Figure 8.20 - Comparison of Normalized Sensible and Latent Capacities at Various Indoor Temperatures, 58 F Dew-Point and 50 % ON-Time.

COMPARISON OF RESULTS AT VARIOUS OUTDOOR DRY-BULB TEMPERATURES

The comparison of the simulated normalized capacities and simulated PLFs at various outdoor dry-bulb temperatures are shown in Figures 8.21 to 8.24, respectively. The other variables for the simulation are shown in Table 5.5.Since the percent ON-time and the indoor relative humidity were high (50%) the simulated results were in good agreement with the measured ones.

SUMMARY OF COMPARISON OF SIMULATED RESULTS WITH MEASURED RESULTS

The transient simulation results from the present model, which was a modified version of the TRPUMP, were compared with the laboratory results at several ambient conditions. It was found that the model estimates were in good agreement with the laboratory results at high percent ON-times (> 50%) and high relative humidities (> 45%), because at high percent ON-times and high relative humidities, the cycling losses and losses due to off-cycle refrigerant migration into the evaporator became small. Therefore, the model estimates matched well with the laboratory results. Since the model could not handle shut-down, it could not account for all the cyclic losses. Therefore, at low percent ON-times, the estimated results were higher than the laboratory measured results.

The present model needs to be refined to make it a better design tool. The refinements include: (i) Capability to model transient shut-down. (ii) Inventory of refrigerant at start-up and during run-time. (iii) Total accounting

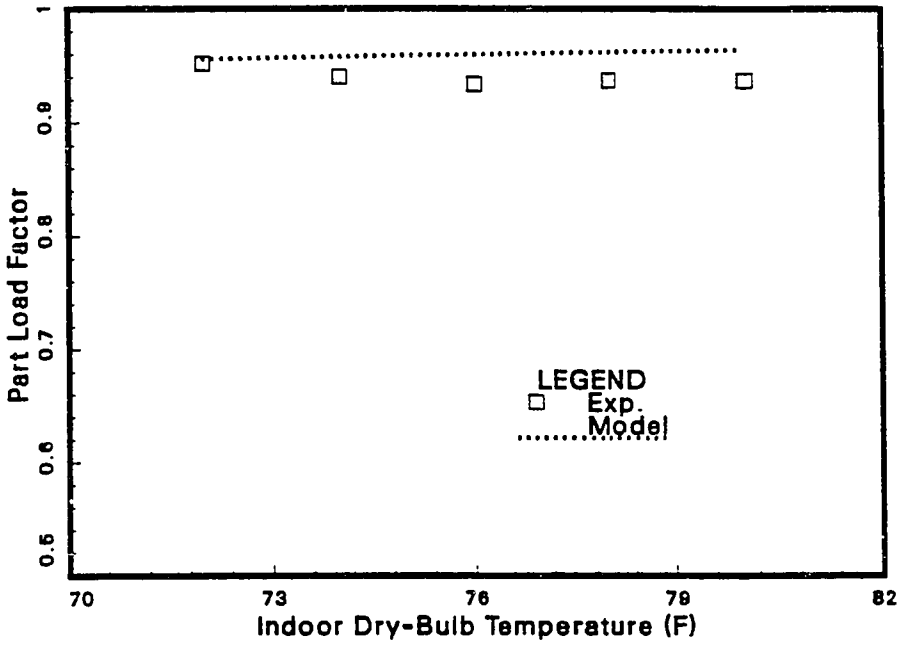

Figure 8.21 – Comparison of Part Load Factors at Various Indoor Dry-Bulb Temperatures, 58 F Dew-Point and 80 Percent ON-Time.

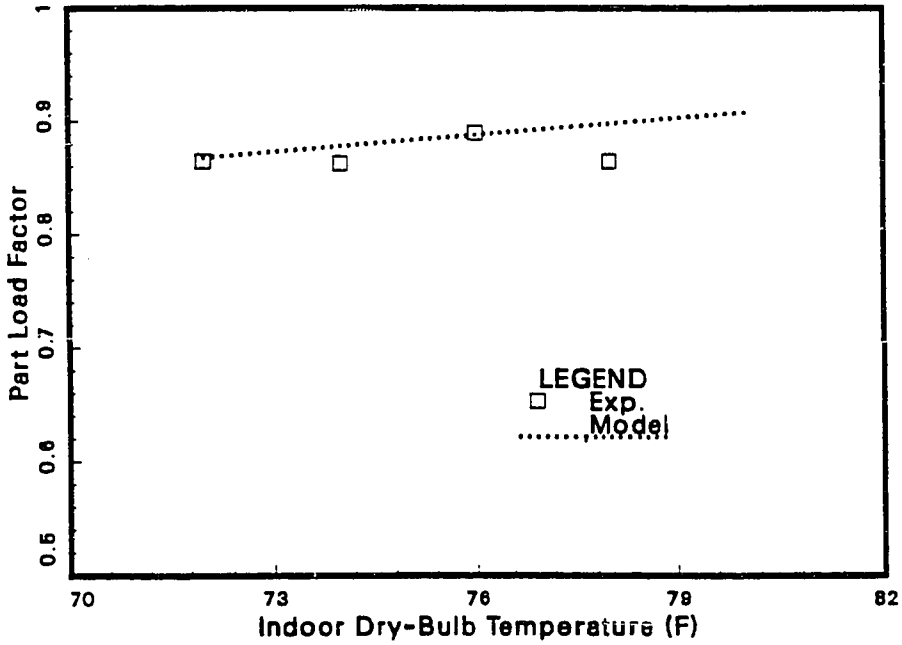

Figure 8.22 – Comparison of Part Load Factors at Various Indoor Dry-Bulb Temperatures, 58 F Dew-Point and 80 Percent ON-Time.

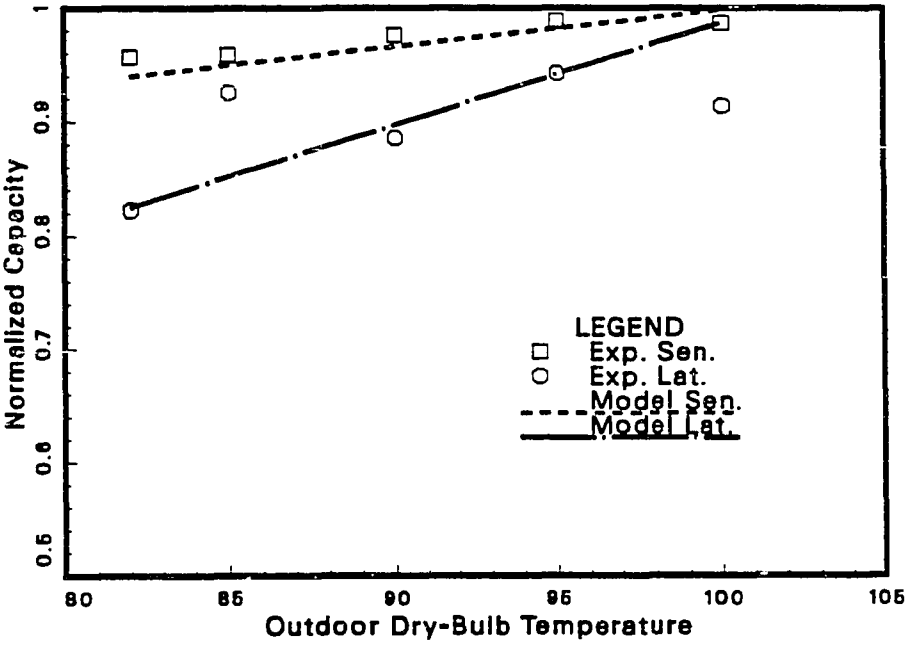

Figure 8.23 – Comparison of Normalized Sensible and Latent Capacities at Various Outdoor Dry-Bulb Temperatures.

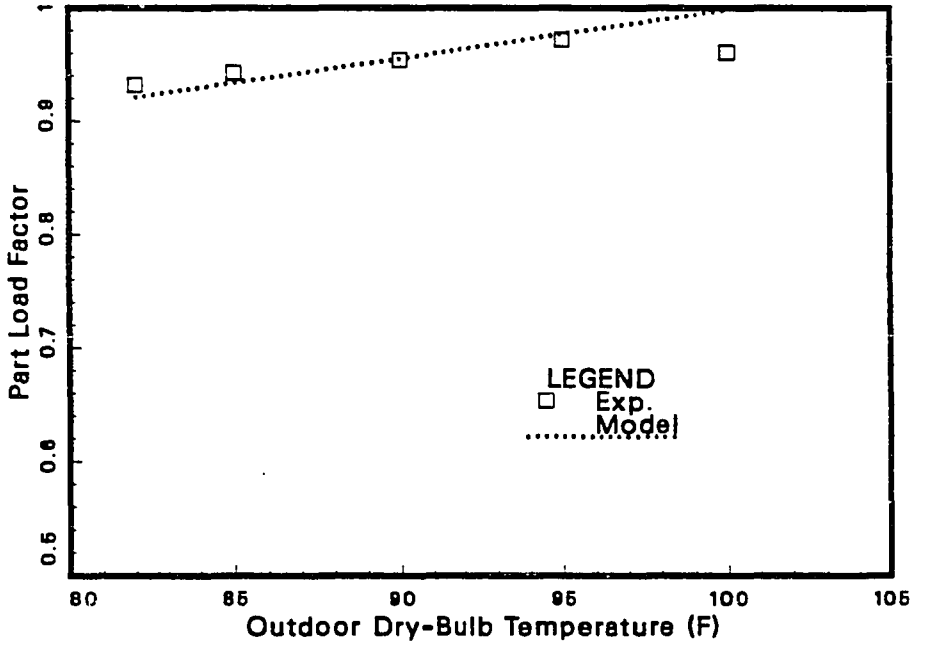

Figure 8.24 – Comparison of Part Load Factors at Various Outdoor Dry-Bulb Temperatures.

of the refrigerant migration into the evaporator and into the accumulator just after start-up. (iv) Finally, verification of the model in heating mode.

CHAPTER IX

CONCLUSIONS AND RECOMMENDATIONS

CONCLUSIONS

To characterize the transient start-up performance of heat pumps in the cooling mode, an experimental and analytical investigation was performed. Five variables were identified as being the most important to characterize the transient behavior: (i) the indoor dry-bulb temperature, (ii) outdoor dry-bulb temperature, (iii) the indoor relative humidity, (iv) cycling rate and (v) percent ON-time. A series of tests were performed at varying operating conditions and the transient performance was characterized.

This study illuminated several trends required to characterize both transient sensible and dehumidification performances of the test heat pump. Some of the general characteristics include:

(1) The suction and discharge pressures approached their steady-state values quickly (75 seconds).

(2) The sensible capacity rose rapidly during the first 75 to 90 seconds after start-up and then gradually reached steady-state between 6 to 15 minutes depending on the ambient conditions.

(3) At start-up, moisture removal was negative, i.e. moisture was actually being put into the air-stream.

(4) There was a considerable build-up of liquid refrigerant in the accumulator just after start-up.

(5) It took almost 10 to 15 minutes for all the refrigerant in the accumulator to vaporize.

(6) After an initial spike, the power consumption dropped and quickly rose when part of the liquid refrigerant entered the compressor shell.

(7) The power consumption reached steady-state 90 to 120 seconds after start-up.

Major conclusions of the dehumidification performance are listed below:

(1) For almost all the tests, moisture was added at start-up and dehumidification began 60 to 150 seconds after start-up depending on the ambient conditions. Therefore, it appears that if the heat pump is ON for less 2 minutes it will add rather than remove moisture from the air.

(2) The latent capacity took 6 to 15 minutes to reach steady-state after start-up. As the ON/OFF cycles increased it took longer for the latent capacity to reach steady-state. Also as the indoor relative humidity decreased the latent capacity took longer to reached steady-state.

(3) The loss in latent capacity was greater than the loss in the sensible capacity with a decrease in the unit's run time and increase in the number of ON/OFF cycles. In an actual residence, if the conditioning unit is over-sized, which is a common practice, the unit will cycle longer. Therefore, the unit's dehumidification performance will be poor and the unit may not meet the comfort criteria.

Major conclusions of the overall performance are listed below:

(1) The cycling losses were maximum at low percent ON-times, low relative humidities and high cycling rates. Low percent ON-time corresponds to over-sizing of the unit. High cycling rate corresponds to small dead band on the thermostat.

(2) It took between 6 to 15 minutes for the system to reach steady-state depending on the ambient conditions. The cyclic energy efficiency is dependent on the time taken by the system to reach steady-state. Therefore, there was a wide variation in energy efficiency ratio. Even for the most favorable conditions, it took almost 6 minutes for the system to reach steady-state.

(3) The combination of high cycling rate and low percent ON-time caused maximum losses in capacity. An oversized unit will only be ON for a small period of time and it will cycle more often. Therefore, the actual seasonal efficiency of the oversized unit will be less than a properly sized unit.

(4) The part load factor (PLF) which is an index of part load efficiency increased with the unit run time and indoor relative humidity. The ASHRAE Standard [1983] assumed that the PLF varied linearly with ON-time. However, from the present investigation it was clearly evident that PLF increased non-linearly with unit run time. The ASHRAE Standard [1983] may have to be re-evaluated.

(5) The relationship between (1-PLF) and (1-CLF) was not linear. Hence, the assumption of a constant slope is not necessarily valid. Since the relationship was non-linear the coefficient of degradation (C_D) at 50

percent ON-time was lower than at 80 or 20 percent ON-times. There was a wide variation in the coefficient of degradation for the operating conditions considered.

(6) Because there was a wide variation in part load performance of the test unit, the seasonal energy efficiency ratio (SEER) based on one single test, as recommended by the ASHRAE Standard [1983], may not reflect the actual seasonal efficiency.

(7) The number of minutes the unit was ON in a given cycle was found to be the single most important variable in determining the cyclic losses. Because most of the cyclic losses occurred during the first few minutes after start-up, the losses magnified as the unit cycled more often.

(8) The outdoor dry-bulb temperature did not have any effect on the transient performance.

One of the major contribution of this investigation was the development of a multiple linear regression model (developed in Chapter VII) to predict the PLF for a wide range of operating conditions. The equation can be used to estimate the SEER of a heat pump more realistically. Because the equation was based on the actual relationship of each of the five independent variable with the PLF.

Finally, a heat pump analysis computer model, which evolved from the previous models by Chi and Didion [1982] and Oak Ridge National Laboratory [1981], was developed in lumped parametric form. The simulated results from the present model were compared with the laboratory results at several ambient conditions. It was found that the model estimates were in good agreement with the laboratory results, especially at high percent ON-times (> 20) and high relative humidities (> 45).

RECOMMENDATIONS

The heat pump test procedure adopted in 1979 called for seasonal rating which would account for the cyclic losses during the part load operation of

the conditioning units. The definition of the seasonal rating was based on several variables, one of which was the PLF. The test procedure prescribed two options for estimating the PLF: (i) from the cyclic dry coil test (Test D) or (ii) assuming C_D as 0.25 and then estimating PLF (from Eq. 5.7). The test procedure assumed that C_D was linear about a single cyclic test point. In reality, as evident from the present study, the C_D is actually non-linear.

Recent modifications [DOE, 1986] to the 1979 test procedures expressed the PLF as an exponential function of CLF. However, the C_D is still estimated at a single test point. The variation in the value C_D with PLF and CLF is very complicated. Therefore, it would probably be better to express PLF in terms of more fundamental variables which influence it. For example, the indoor dry-bulb temperature and relative humidity, percent ON-time and the cycling rate. In the present study, an expression has been developed to estimate PLF which could then be used in the estimation of SEER more accurately. However, further experiments are required to generalize the expression for a variety of heat pump models and to account for the variation in designs between different manufacturers.

The 1979 DOE procedure prescribed a damper method of conducting the cyclic dry coil Test D, while the ASHRAE Standard prescribed a continuous air method. The DOE has recently modified their test procedure to match that of ASHRAE. However, the continuous air method may not reflect the performance observed in the field, because the shut down characteristics are different for the case with and without a continuous air movement. Therefore, a detailed study of the shut down characteristics is recommended. Such an analysis may lead to a development of a factor which could be used to adjust

the PLF estimated from Test D.

Finally, the model developed to simulate the transient performance of heat pumps needs refinement to make it a better design tool. The recommended refinements include: (i) capability to model transient shut-down, (ii) inventory of refrigerant at start-up and during run-time, (iii) better accounting of refrigerant migration into the evaporator and the accumulator just after start-up, and (iv) verification of the model in the heating mode.

REFERENCES

AMCA/ANSI Standard 210–85, "Laboratory Methods of Testing Fans for Rating," 30 West University Dr., Arlington Heights, IL, 1985.

ASHRAE Standard 41.1–74, "Standard Measurement Guide: Section on Temperature Measurements," Atlanta, 1974.

ASHRAE/ANSI Standard 116–1983, "Methods of Testing Seasonal Efficiency of Unitary Air–Conditioners and Heat Pumps," Atlanta, 1983.

Baxter, V.D., and Moyers, J.C., "Field–Measured Cycling, Frosting and Defrosting Losses for a High–Efficiency Air–Source Heat Pump," ASHRAE Transactions, vol. 91, pt. 2B, 1985, pp. 537–554.

Brasz, J.J., and Koenig, K., "Numerical Methods for the Transient Behavior of Two-Phase Flow Heat Transfer in Evaporators and Condensers," Numerical Properties and Methodologies in Heat Transfer: Proceedings of the Second National Symposium, Hemisphere Publishing Co., Washington, D.C., 1983, pp. 461-476.

Bullock, C.E., and Reedy, W.R., "Heat Pump Cyclic Performance and its Influence on Seasonal Operation," Third Annual Conference on Heat Pump Technology, Oklahoma State University, 1978.

Chaddock, J.B., and Noerager, J.A., "Evaporation of Refrigerant 12 in a Horizontal Tube with Constant Wall Heat Flux," ASHRAE Transactions, vol. 92, pt. 1, 1986, pp. 22-54.

Chi, J., and Didion, D.A., "A Simulation of Transient Performance of Heat Pump," International Journal of Refrigeration, vol. 5, no. 3, May 1982, pp. 176–184.

Dhar, M., and Soedel, W., "Transient Analysis of a Vapor Compression Refrigeration System: Part I — The Mathematical Model," XV International Congress of Refrigeration, Venice, Italy, September 1979.

Didion, D.A., and Kelly, G.E., "New Testing Procedure for Seasonal Performance of Heat Pumps," ASHRAE Journal, vol. 21, no. 9, September 1979, pp. 40–44.

DOE Proposed Standard, "Proposed Heat Pump Test Procedure," Docket No. CAS-RM-79-102, Washington, D.C., May 1986.

Goldschmidt, V.W., Hart, G.H., and Reiner, R.C., "A Note on the Transient Performance and Degradation Coefficient of a Field Tested Heat Pump — Cooling Mode," ASHRAE Transactions, vol. 86, pt. 2, 1980, pp. 368–375.

Groff, G.C., and Bullock, C.E., "A Computer Simulation Model for Air Source Heat Pump System Seasonal Performance Study," Second Annual Heat Pump Conference on Heat Pump Technology, Oklahoma State University, October 18–19, 1976.

Hart, G.H., and Goldschmidt, V.W., "Field Measurement of a Mobile Home Unitary Heat Pump," ASHRAE Transactions, vol. 86, pt. 2, 1980, pp. 347–367.

Katipamula, S., O'Neal, D.L., and Somasundaram, S., "Determination of the Transient Dehumidification Characteristics of High Efficiency Central Air-Conditioners," Report # ESL/87-04, Dept. of Mechanical Engineering, Texas A&M University, 1987.

Katipamula, S., O'Neal, D.L., and Somasundaram, S., "Simulation of Dehumidification Characteristics of Residential Air-Conditioners,"

ASHRAE Transactions, vol. 94, pt. 2, 1988, pp. 829 - 849.

Kelly, G.E., and Bean, J., "Dynamic Performance of a Residential Air-to-Air Heat Pump," Second Annual Conference on Heat Pump Technology, Oklahoma State University, October 18-19, 1976.

Kelly, G.E., and Bean, J., "Dynamic Performance of a Residential Air-to-Air Heat Pump," National Bureau of Standards Building Science Series, BSS93, Washington, D.C., March 1977.

Klein, S.A., et al., TRANSYS A Transient Simulation Program, Engineering Experiment Station Report 38-12, Version 12.1, University of Wisconsin, December 1983.

MacArthur, J.W., "Analytical Representation of the Transient Energy Interactions in Vapor Compression Heat Pumps," ASHRAE Transactions, vol. 90, pt. 1, 1984, pp. 982-996.

MacArthur, J.W., and Grald, E.W., "Prediction of Cyclic Heat Pump Performance with a Fully Developed Model and a Comparison with Experimental Data," ASHRAE Transactions, vol. 93, pt. 2, 1987, pp. 1159-1172.

McQuiston, F.C., and Parker, J.D., Heating Ventilating and Air-Conditioning, Third Edition, John Wiley & Sons, New York, NY, 1987.

Miller, W.A., "The Laboratory Evaluation of the Heating Mode Part-Load Operation of an Air-to-Air Heat pump," ASHRAE Transactions, vol. 91, pt. 2B, 1985, pp. 524-536.

Mulroy, W.J., and Didion, D.A., "Refrigerant Migration in a Split-Unit Air Conditioner," ASHRAE Transactions, vol. 91, pt. 1A, 1985, pp. 193-206.

Murphy, W.E., and Goldschmidt, V.W., "The Degradation Coefficient of a Field Tested Self-Contained 3-Ton Air-Conditioner," ASHRAE Transactions, vol. 85, pt. 2, 1979, pp. 396-405.

Murphy, W.E., and Goldschmidt, V.W., "Transient Response of Air Conditioners — A Qualitative Interpretation Through a Sample Case," ASHRAE Transactions, vol. 90, pt. 1B, 1984, pp. 997-1008.

Murphy, W.E., and Goldschmidt, V.W., "Cyclic Characteristics of a Typical Residential Air-Conditioner — Modeling of Start-Up Transients," ASHRAE Transactions, vol. 91, pt. 2A, 1985, pp. 427-444.

Murphy, W.E., and Goldschmidt, V.W., "Cyclic Characteristics of a Residential Air Conditioner — Modeling of Shutdown Transients," ASHRAE Transactions, vol. 92, pt. 1A, 1986, pp. 186-202.

NEMA Standard for Low-Voltage Room Thermostats, Pub. No. DC3-1972, New York, NY, 1972

ORNL Model: (ORNL/CON-80), "A Steady-State Computer Design Model for Air-To-Air Heat Pumps," Energy Division, ORNL, Oak Ridge, TN, December 1981.

Parken, W.H., Beausoliel, R.W., and Kelly, G.E., "Factors Affecting the Performance of a Residential Air-to-Air Heat Pump," ASHRAE Transactions, vol. 83, pt. 1, 1977, pp. 839-849.

Pierre, B., "Flow Reisistance with Boiling Refrigerant," ASHRAE Journal, vol. 6, no. 9, 1964, pp. 58-65.

Sami, S.M., Duong, T.N., Mercadier, Y., and Galanis, N., "Prediction of the Transient Response of Heat Pumps," ASHRAE Transactions, vol. 93, pt.

2, 1987, pp. 1173-1191.

Tanaka, N., Ikeuchi, M., and Yamanaka, G., "Experimental Study on the Dynamic Characteristics of a Heat Pump," ASHRAE Transactions, vol. 88, pt. 2, 1982, pp. 323–331.

Travis D.P., Baron, A.B., and Rohsenow, W.M., "Forced Convection Condensation Inside Tubes: A Heat Transfer Equation for Condenser Design," ASHRAE Transactions, vol. 79, pt. 1, 1973, pp. 157-165.

Tree, D.R., and Weiss, B.W., "Two Time Constant Modeling Approach for Residential Heat Pumps," International Institution of Refrigeration, August 5–8, 1986, pp. 141–148.

APPENDIX A

Critical Constants

T_c = 6.645E+02 P_c = 8.250E-02 v_c = 3.053E-02

a_J = 1.851E-01

Constants for Vapor Pressure Equations

A_g = 2.936E+01 B_g = -3.845E+03 C_g = -7.861E+00

D_g = 2.191E-03 E_g = 4.457E-01 F_g = 6.861E+02

aa = 1.200E+02 bb = 3.880E+02

Constants for Liquid Density Equations

A_l = 3.276E+01 B_l = 5.463E+01 C_l = 3.675E+01

D_l = -2.229E+01 E_l = 2.047E+01 F_l = 0.000E+00

G_l = 0.000E+00 H_l = 0.000E+00 O_l = 0.000E+00

Constants for Equations of State

R = 1.241E-01 b = 2.000E-03 c = 0.000E+00

A_2 = -4.354E+00 B_2 = 2.407E-03 C_2 = -4.407E+01

A_3 = -1.746E-02 B_2 = 7.628E-05 C_3 = 1.484E+00

A_4 = 2.310E-03 B_4 = -3.606E-06 C_4 = 0.000E+00

A_5 = -3.724E-05 B_5 = 5.355E-08 C_5 = -1.845E-04

A_6 = 1.364E+08 B_6 = -1.673E+05 C_6 = 0.000E+00

α = 5.482E+02 A_k = 4.200E+00

Constants for Heat Capacity Equations

a_c = 2.813E-02 b_c = 2.255E-04 c_c = -6.510E-08

d_c = 0.000E+00 e_c = 0.000E+00 f_c = 2.573E+02

Constants X and Y for the Enthalpy and Entropy Equations

X = 6.240E+01 Y = -4.533E-02

Heat Pump System Parameters

Electric motor rated synchronous speed	= 6.000E+01, rps
Electric motor rated torque	= 5.400E+00, lb-ft
Electric motor rated efficiency	= 9.000E-01
Motor shaft moment of inertia	= 1.500E+00, lb-ft^2
Motor shaft mechanical efficiency	= 9.600E-01
Specific heat of compressor material	= 2.140E-01, Btu/lb
Compressor weight	= 1.000E+01, lb
Compressor inside surface area	= 1.000E+00, ft^2
Compressor outside surface area	= 1.300E+00, ft^2
Compressor inside volume	= 1.000E+00, ft^3
Compressor swept volume	= 2.100E-03, ft^3
Compressor polytropic efficiency	= 8.500E-01
Compressor inlet valve P coefficient	= 0.000E+00, psi-sec^2/lb^2
Compressor outlet valve P coefficient	= 1.150E-01, psi-sec^2/lb^2
Compressor leakage fractor	= 9.600E-01
Compressor clearance fraction	= 1.300E-01
Outdoor fan electric input rate	= 2.000E-01, kW
Outdoor fan air flow rate at steady state	= 2.750E+02, lb/min

Outdoor fan time constant	= 5.000E-01, sec
Outdoor coil tube inside diameter	= 2.625E-02, ft
Outdoor coil tube outside diameter	= 3.125E-02, ft
Outdoor coil fin tip diameter	= 9.400E-02, ft
Outdoor coil tube length in refrigerant flow direction	= 4.200E+02, ft
Outdoor coil flow cross-sectional area	= 2.166E-03, ft2
Outdoor coil tube material thermal conductivity	= 1.180E+02, Btu/ft-hr-F
Outdoor coil fin height	= 3.138E-02, ft
Outdoor coil fin thickness	= 4.583E-04, ft
Outdoor coil fin material thermal conductivity	= 1.180E+02, Btu/ft-hr-F
Outdoor coil depth for air flow,	= 1.667E-01, ft
Outdoor coil air flow cross-sectional area,	= 1.750E+01, ft^2
Outdoor coil inside surface area	= 3.436E+01, ft^2
Outdoor coil total outside area	= 8.243E+02, ft^2
Outdoor coil pipe area	= 1.715E+01, ft^2
Outdoor coil fin area	= 8.071E+02, ft^2
Outdoor coil refrigerant side void volume	= 7.500E-01, ft^3
Outdoor coil airside void volume	= 3.163E+00, ft^3
Outdoor coil wall capacitance	= 2.000E+01, Btu/ht-F
Outdoor coil elevation above indoor coil	= 0.000E+00, ft

Oudoor coil α, β, and γ values in airside heat transfer equation

$Nu = \alpha Re^{\beta} r^{\gamma}$ = 1.200E-01,6.810E-01,3.333E-01

Outdoor coil a and b values in airside = 2.160E-01

fraction equation f = aRe^{b} = -3.200E-01

Indoor fan electric input rate = 6.000E-01, kW

Indoor fan air flow rate = 1.050E+02, lbm/min

Indoor fan time constant = 5.000E-01, sec

Indoor coil inside diameter = 2.625E-02, ft

Indoor coil outside diameter = 3.125E-02, ft

Indoor coil fin tip diameter = 8.792E-02, ft

Indoor coil tube length in refrigerant

flow direction = 1.700E+02, ft

Indoor coil flow cross-sectional area = 2.166E-03, ft^2

Indoor coil tube material thermal

conductivity = 1.180E+02, Btu/ft-hf-F

Indoor coil fin height = 2.834E-02, ft

Indoor coil fin thickness = 4.583E-04, ft

Indoor coil fin material thermal

conductivity = 1.180E+02, Btu/ft-hr-F

Indoor coil depth for air flow = 2.917E-01, ft

Indoor coil air flow cross-sectional area = 3.750E+00, ft^2

Indoor coil inside surface area = 1.402E+01, ft^2

Indoor coil total outside area = 3.390E+02, ft^2

Indoor coil pipe area = 1.670E+01, ft^2

Indoor coil fin area = 3.223E+02, ft^2

Indoor coil refrigerant side void volume = 3.000E+00, ft^2

Indoor coil airside void volume	= 2.932E+00, ft^3
Indoor coil wall capacitance	= 2.500E+01, Btu/hr-F
Indoor coil elevation above outside coil	= 0.000E+00, ft
Oudoor coil α, β, and γ	= 1.360E-01
values in airside heat transfer equation	= 6.810E-01
$Nu = \alpha Re^{\beta} r^{\gamma}$	= 3.333E-01
Outdoor coil a and b values in airside	
fraction equation, f, aRe^{b}	= 3.160E-01,-3.200E-01

APPENDIX B

Initial Conditions

Electric motor torque	= 0.000E+00, lb-ft
Electric motor efficiency	= 0.000E+00
Electric motor power input	= 0.000E+00, kW
Electric motor heat	= 0.000E+00, Btu/sec
Shaft speed	= 0.000E+00, rps
Refrigerant specific enthalpy at compressor outlet	= 1.120E+02, Btu/lb
Refrigerant flow rate at compressor outlet	= 0.000E+00, lb/min
Refrigerant pressure at compressor inlet	= 1.620E+02, psia
Specific internal energy of refrigerant inside compressor	= 1.041E+02, Btu/lb
Specific internal energy of refrigerant inside compressor	= 4.000E-01, Btu/lb
Temperature , compressor wall	= 5.590E+02, R
Compressor braking torque	= 0.000E+00, lb-ft
Condenser air source flow rate	= 0.000E+00, lb/min
Condenser air source temperature	= 5.530E+02, R
Condenser air source pressure	= 1.470E+01, psia
Condenser air source humidity ratio	= 1.100E-02
Condenser air source liquid water content	= 0.000E+00
Air flow rate at condenser fan outlet	= 0.000E+00, lb/min
Air temperature at condenser fan outlet	= 5.490E+02, R
Air humidity ratio at condenser fan outlet	= 1.100E-02, lba/lbm

Air water content at condenser inlet	= 0.000E + 00
Air pressure at condenser fan inlet	= 1.470E + 01, psia
Condenser fan electric power input	= 0.000E + 00, kW
Air temperature at condenser outlet	= 5.490E + 02, R
Air flow rate at condenser outlet	= 0.000E + 00
Air humidity ratio at condenser outlet	= 1.100E-02
Air liquid water content at condenser outlet	= 0.000E + 00
Specific enthalpy of refrigerant at condenser outlet	= 1.127E + 02, Btu/lb
Refrigerant flow rate at condenser outlet	= 0.000E + 00, lb/min
Air pressure at condenser inlet	= 1.470E + 01, psia
Refrigerant pressure at condenser inlet	= 1.620E + 02, psia
Specific volume of refrigerant inside condenser	= 3.893E-01 ft^3/lb
Specific internal energy of refrigerant inside condenser	= 1.023E + 02, Btu/lb
Condenser wall temperature	= 5.590E + 02
Liquid refrigerant inside condenser at start	= 0.000E + 00, lb
Specific enthalpy of saturated refrigerant at condenser	= 0.000E + 00, Btu/lb
Air pressure at condenser outlet	= 1.470E + 01, psia
Orifice opening at condenser outlet	= 9.000E-05, ft^2
Evaporator air source flow rate	= 0.000E + 00, ib/min
Evaporator air source temperature	= 5.380E + 02, R
Evaporator air source pressure	= 1.470E + 01, psia
Evaporator air source humidity ratio	= 8.300E-02
Evaporator air source liquid water content	= 0.000E + 00

Air flow rate at evaporator fan outlet	= 0.000E+00, lb/min
Air temperature at evaporator fan outlet	= 5.380E+02, R
Air humidity ratio at evaporator fan outlet	= 8.300E-02, lba/lbm
Air water content at evaporator inlet	= 0.000E+00
Air pressure at evaporator fan inlet	= 1.470E+01, psia
Evaporator fan electric power input	= 0.000E+00, kW
Air temperature at evaporator outlet	= 5.300E+02, R
Air flow rate at evaporator outlet	= 0.000E+00
Air humidity ratio at evaporator outlet	= 8.300E-02
Air liquid water content at evaporator outlet	= 0.000E+00
Specific enthalpy of refrigerant at evaporator outlet	= 1.114E+02, Btu/lb
Refrigerant flow rate at evaporator outlet	= 0.000E+00, lb/min
Air pressure at evaporator inlet	= 1.470E+01, psia
Refrigerant pressure at evaporator inlet	= 1.620E+02, psia
Specific volume of refrigerant inside evaporator	= 3.000E-01 ft^3/lb
Specific internal energy of refrigerant inside evaporator	= 1.012E+02, Btu/lb
Evaporator wall temperature	= 5.400E+02, R
Liquid refrigerant inside evaporator at start	= 7.000E+00, lb
Specific enthalpy of saturated refrigerant at evaporator	= 1.100E+00, Btu/lb
Air pressure at condenser outlet	= 1.470E+01, psia
Orifice opening at condenser outlet	= 6.300E-04, ft^2

APPENDIX C

Experimental data values used in the calculation of moist air thermodynamic properties included dry-bulb and wet-bulb temperatures or dew-point temperatures or relative humidity of the outdoor air as well as the ambient barometric pressure. Data values in the calculation of refrigerant 22 properties at a given location in the refrigerant circuit were the pressure an temperature of the refrigerant at that location. Properties which were calculated were enthalpy an density of the moist air for capacity and flow rate calculations. Procedures that were used in these property calculations are discussed in this appendix

Moist air thermodynamic properties were calculated using FORTRAN subroutines developed from prefect gas relations presented in the ASHRAE Fundamentals, 1985. Capability provided by the subroutines included computation of specific volume of the moist air and enthalpy of the air when given a dry-bulb temperature and wet-bulb temperature or relative humidity.

Refrigerant thermodynamic properties were computed using computer routines developed by Kartsounes and Erth. These routines permitted a state evaluation to allow determination of whether refrigerant at a given pressure and temperature was superheated, sub-cooled, or saturated. For example, for given measured refrigerant pressure, the refrigerant temperature to determine the state. Routines were available to provide superheated refrigerant enthalpy values as well as saturated liquid or saturated vapor refrigerant enthalpy values.

VITA

Srinivas Katipamula was born on December 08, 1960 in Hyderabad, Andhra Pradesh, India, to Indira Devi and Ranga Rao Katipamula. He graduated from Saint Mary's High School in 1976, then joined Aliya Govt. Junior College to do his pre-engineering. Having graduated from Aliya in 1978 he joined College of Engineering, Osmania University, Hyderabad and earned a Bachelor of Engineering degree in Mechanical Engineering in 1983. He was awarded a gold medal for first rank in class of '83. He entered Texas A&M University in Spring of 1984 for the Master of Science Program in Mechanical Engineering. He graduated with a Master of Science in Fall of 1985. He then joined the Doctoral program in Spring of 1986 in Mechanical Engineering.

Mr. Katipamula's permanent address is, H:no: 55–10–19/P, MMTC Colony, Seethamadara, Visakhapatnam–530 022, A.P., India.